A Quantitative Framework Connecting the Critical Factors Determining the Stability of Localized Corrosion

---

A Dissertation

Presented to

the faculty of the School of Engineering and Applied Science

University of Virginia

---

in partial fulfillment

of the requirements for the degree

Doctor of Philosophy

by

Jayendran Srinivasan

December

2016

APPROVAL SHEET

The dissertation

is submitted in partial fulfillment of the requirements

for the degree of

Doctor of Philosophy

Jayendran Srinivasan
AUTHOR

The dissertation has been read and approved by the examining committee:

Robert G. Kelly
Advisor

John R. Scully

Richard P. Gangloff

Gary M. Koenig, Jr.

Raul B. Rebak

Narasi Sridhar

Accepted for the School of Engineering and Applied Science:

Craig H. Benson, Dean, School of Engineering and Applied Science

December

2016

This dissertation is dedicated to my beloved aunt, Hamsa Ravi Mandalam (1959 – 2005). She was a brilliant woman, and I have her to thank for encouraging my interest in chemistry and her unflagging belief that I would succeed in my dreams of higher education and research in the United States. I cannot imagine another person who would have been prouder or happier at my completion of this milestone. I miss her terribly, and would like to think that she still watches over me. Thanks so much, Perima – I hope this dedication makes up in some small part for all the times over the last eleven years I have wanted to tell you how much you mean to me.

Executive Summary

Localized corrosion processes like pitting require the presence of a concentrated solution of cationic chlorides at the highly spatially discrete corroding surface. This chemistry is the consequence of the anodic dissolution of the metal and consequent cation hydrolysis and chloride migration from the bulk, leading to the development of a locally acidic environment that promotes continued corrosion. The minimum aggressive chemistry required to sustain pitting is therefore described in terms of the critical concentration of metal cations and pH. If these minimum conditions are not met, the chemistry in the pit is unfavorable towards continued dissolution and repassivation commences. The electrochemical nature of corrosion processes implies that there are also associated critical values for the dissolution flux and the potential characterizing this transition between stable dissolution and repassivation. These critical values represent threshold conditions for pit propagation and, if known, could be used as inputs for life prediction models based on the maximum damage size that can result from the exposure of a material to a localized corrosion environment. There has been much debate in the literature as to the mechanistic origin and measurement of these critical values. Although it is generally acknowledged that critical dissolution flux, critical solution chemistry, and critical potential all represent aspects of the same phenomenon, studies to date have investigated only one or a few of these factors without developing an integrated, quantitative relationship to connect them.

This dissertation addresses this knowledge gap in the literature by proposing a comprehensive, quantitative, and mechanistic framework relating the critical conditions for localized corrosion with a focus on stainless steels. The framework was structured upon experiments and modeling which employed the artificial pit technique, using 316L in chloride

media as a candidate system. First, the steady state dissolution flux was modeled as a function of one-dimensional (1–D) pit geometry in order to quantify the phenomenology of pit stability with respect to pit depth and bulk electrolyte concentration. These results were utilized in designing 1-D artificial pit experiments to extract estimates of the critical dissolution current density and the critical potential – in terms of the Galvele pit stability product ($i \cdot x$) and the repassivation potential E_{rp} – at various pit depths. Mass transport modeling was then employed to determine the surface concentration at which repassivation commenced in the pit. The critical surface concentration of 50% saturation so obtained was observed to be in agreement with independent kinetics measurements which displayed a distinct transition from dissolution to repassivation at this value. The contribution of the local cathodic reaction towards pit stability was also studied using cation hydrolysis calculations which indicated that the critical pH was a key factor in inducing repassivation via oxide nucleation. The critical pH value for 316L was estimated in this manner to be 2.65, which was consistent with the effects of the individual anodic and cathodic kinetics at the estimated critical surface concentration. Mixed potential theory was utilized to rationalize these results in terms of the electrochemical processes accompanying repassivation. This study therefore demonstrated the development of a general, unified framework to quantitatively relate the critical factors controlling localized corrosion. The utility of such a framework lies in its extension to any system susceptible to localized corrosion, with particular value in its application towards predictive structural integrity analyses and corrosion inhibition strategies.

Acknowledgments

I owe a debt of gratitude to my advisor, Prof. Robert Kelly. In a manner that would make the ancient Indian sages of my heritage proud, he has been both a *Guru* (Sanskrit for teacher; literally, one who reveals the light, a guide) and an *Acharya* (also Sanskrit for teacher; literally, one who instructs by example of personal conduct and character). Thank you, sir, for your encouragement, insight, advice, and support. I will always hold dear what you have taught me, and it is truly an honor and privilege to have been your student – indeed, *nanos gigantum humeris insidentes* – if I have been able to look far at all, it has been in large part due to standing on your shoulders.

A great deal of thanks to my dissertation committee – Prof. John Scully (chair), Prof. Richard Gangloff, and Prof. Gary Koenig from the University of Virginia, Dr. Raul Rebak from GE Global Research, Schenectady, NY, and Dr. Narasi Sridhar from DNV-GL, Dublin, OH.

I am grateful for the financial support provided by the Office of the Undersecretary of Defense through the Technical Corrosion Collaboration program, the Center for Surface Technology, Rolls Royce Corporation, Indianapolis, IN, and the Commonwealth Center for Advanced Manufacturing at the University of Virginia.

My present and former colleagues at the Center for Electrochemical Science and Engineering, and the Department of Materials Science and Engineering – it has been a pleasure knowing and working with each one of you. There are a few people I want to mention in particular – they brought much joy and character to my life here:

> Merrill Tayler, Zach Harris, Mary Lyn Lim, Gilbert Liu, Noelle Co, R. J. Santucci, Ryan Donahue, Balaji Kannan, and Gopal Ramalingam;
>
> The undergraduate students I have worked with: Rebecca Burkley, Christine Rooney, Mike McGrath, and Lark Washington;
>
> The staff of the Department of Materials Science and Engineering, especially Ashley Duke, Barry Baber, Peter Schare, Tanner Fitzgerald, Kim Fitzhugh-Higgins, and Richard White.

Old friends, from near and far – Akshaya Vijayalakshmi, Arun Sethuraman, David Sorge, Utsav Biswas, Nilanjana Bhattacharyya and Rachit Parekh, Krishna Chandran, Hema Sukumar, Deepti Bharthur, and Suchismita Chattopadhyay – thank you for giving me a place to sleep during my travels and a patient ear whenever I needed to rant about the travails of the PhD.

Saving my favorites for the last, to my parents, for having had the patience to raise an insufferably precocious only child and over the past twelve years only sporadically getting to see him – I cannot imagine where to begin thanking you for putting up with my idiosyncrasies, thirty years now and counting. Trust me, you are two people I would pick to be on my side in any battle, any time. I did tell you: *kālénātmani vindati*, and yes, now it is finally done.

Bibliography

The publications that have resulted/will result from this dissertation are listed below:

- Chapter 1

1. M. T. Woldemedhin, **J. Srinivasan**, and R. G. Kelly. *Effects of Environmental Factors on Key Kinetic Parameters Relevant to Pitting Corrosion*. ***Journal of Solid State Electrochemistry*** 19 (2015): pp. 3449-3461.
2. **J. Srinivasan**, M. J. McGrath, and R. G. Kelly. *A High-Throughput Artificial Pit Technique to Measure Kinetic Parameters for Pitting Stability*. ***Journal of The Electrochemical Society*** 162, 14 (2015): pp. C725-C731.
3. **J. Srinivasan** and R. G. Kelly. *Experimental and Modeling Studies on Mass Transport and Electrochemical Factors Influencing Stainless Steel Pitting and Repassivation*. ***Corrosion*** 70, 12 (2014): pp.1172-1174.
4. **J. Srinivasan**, M. J. McGrath, and R. G. Kelly: *Mass Transport and Electrochemical Factors Influencing Stainless Steel Pitting and Repassivation in Neutral Chloride Media*. ***ECS Transactions*** 58 (2014) pp. 1-11 – Proceedings of the 224th ECS Meeting, San Francisco, CA, October 27 – November 1, 2013.
5. **J. Srinivasan** and R. G. Kelly: *Overview of a Recent Quantitative Framework Utilizing the Galvele Stability Product to Examine the Critical Electrochemical Factors for Localized Corrosion*. ***Corrosion*** (submitted November 2016).

- Chapter 2

  1. **J. Srinivasan**, C. Liu, and R. G. Kelly: *Geometric Evolution of Flux from a Corroding One-dimensional Pit and its Implications on the Evaluation of Kinetic Parameters for Pit Stability*. ***Journal of The Electrochemical Society*** 163, 10 (2016): pp. C694-C703.

- Chapter 3

  1. **J. Srinivasan** and R. G. Kelly: *One-Dimensional Pit Experiments and Modeling to Determine Critical Factors for Pitting Stability and Repassivation*. ***Journal of The Electrochemical Society*** 163, 13 (2016): pp. C759-767.

- Chapter 4

  1. **J. Srinivasan** and R. G. Kelly: *Evaluating the Critical Chemistry for Repassivation at the Corroding Surface using Mass Transport Model-based Artificial Pit Experiments*. ***Journal of The Electrochemical Society*** 163, 13 (2016): pp. C768-C777.

- Chapter 5

  1. **J. Srinivasan** and R. G. Kelly: *Overview of a Recent Quantitative Framework Utilizing the Galvele Stability Product to Examine the Critical Electrochemical Factors for Localized Corrosion*. ***Corrosion*** (submitted November 2016).

Contents

List of Figures and Tables

Chapter 1

1.1. Overview

This chapter establishes the scientific basis for the work in this dissertation, expanding upon the introduction provided by the preceding summary. An outline of the current status of the literature on the critical factors for pitting is reviewed in order to examine the knowledge gaps that necessitate the development of the quantitative framework that forms the core of this study. The motivation for accurately determining the critical electrochemical conditions is presented in terms of their utility in damage prediction models. With this background, the scope of the dissertation is then defined, introducing the electrochemical technique employed and the phenomenological response of the critical parameters. This information provides the foundation for the arguments presented in the subsequent chapters which detail a unified, general, quantitative, and mechanistic framework for pitting stability and repassivation.

Elements of this chapter have been published in the following journals/proceedings:

1. M. T. Woldemedhin, **J. Srinivasan**, and R. G. Kelly. *Effects of Environmental Factors on Key Kinetic Parameters Relevant to Pitting Corrosion*. ***Journal of Solid State Electrochemistry*** 19 (2015): pp. 3449-3461.

Respective contribution of authors:
Srinivasan: Manuscript co-author, experimental technique development, NaCl data collection and analysis, development of explanation based on diffusion transport for pit stability phenomenology and rationale based on alloy composition for pit stability and repassivation phenomenology.

Woldemedhin: Manuscript co-author, $FeCl_3$ and acidified LiCl data collection and analysis.

2. **J. Srinivasan**, M. J. McGrath, and R. G. Kelly. *A High-Throughput Artificial Pit Technique to Measure Kinetic Parameters for Pitting Stability*. ***Journal of The Electrochemical Society*** 162, 14 (2015): pp. C725-C731.

   Respective contribution of authors:
   Srinivasan: Manuscript co-author, non-cyclic tests data collection, development of high-throughput experimental technique, data analysis and interpretation, development of pit depth-based rationale flux phenomenology.

   McGrath: Manuscript co-author, Replicate and high-throughput data collection, Matlab scripting and implementation for automation.

3. **J. Srinivasan** and R. G. Kelly. *Experimental and Modeling Studies on Mass Transport and Electrochemical Factors Influencing Stainless Steel Pitting and Repassivation.* ***Corrosion*** 70, 12 (2014): pp.1172-1174.

4. **J. Srinivasan**, M. J. McGrath, and R. G. Kelly: *Mass Transport and Electrochemical Factors Influencing Stainless Steel Pitting and Repassivation in Neutral Chloride Media.* ***ECS Transactions*** 58 (2014) pp. 1-11 – Proceedings of the 224th ECS Meeting, San Francisco, CA, October 27 – November 1, 2013.

   Respective contribution of authors:
   Srinivasan: Manuscript author, data collection, analysis, and interpretation, development of analytical mass transport model to relate pit stability and repassivation.

   McGrath: Replicate data collection.

5. A manuscript entitled *Overview of a Recent Quantitative Framework Utilizing the Galvele Stability Product to Examine the Critical Electrochemical Factors for Localized Corrosion* authored by **J. Srinivasan** and R. G. Kelly, based on parts of this chapter has been submitted to Corrosion as an Invited Review for a Special Issue in memoriam of Prof. José R. Galvele to be published in March 2017.

1.2. Electrochemistry of Pitting

The high driving force for metallic dissolution in aqueous solution is mitigated for some alloys by the spontaneous formation and the dynamic maintenance of a protective oxide film, rendering them passive[1,2]. Localized corrosion results from the breakdown of this passive film at discrete regions which then proceed to actively corrode.[3,4] The presence of anions like chloride permits the maintenance of high dissolution rates due to their participation in the stabilization of low pH in the pit via cation hydrolysis,[5–14] resulting in the chemistry inside a pit being substantially different from the surface. This difference in chemistry leads to galvanic separation between the localized anode of the pit and the cathode of the otherwise passive metal surface. The passive surface serves as a reservoir of cathodic current, supporting very high anodic current densities owing to the large cathode-to-anode area ratio.[7,15,16] In this manner, the electrochemical character of localized corrosion processes necessitates the introduction of potential and current density as parameters to describe the relative tendency of metals to corrode or passivate.[2,3,17–21] Consequently, the minimum electrochemical conditions at the corroding surface that permit pitting to stably proceed, or due to their absence cause repassivation,[22–25] can be characterized in terms of critical values of potential, current density, concentration of metal cations, and pH. The sections that follow in this chapter will critique the current literature with regard to these critical factors, thereby defining the aims of this dissertation to identify and resolve selected issues that remain debated.

1.3. Critical Dissolution Flux and the Pit Stability Product

The stable propagation of pitting once initiation has taken place is contingent upon maintaining a sufficiently concentrated solution of metal ions whose hydrolysis results in acidification at the base of the pit.[2,7,10,19,26] Hisamatsu[27] originally stated that a critical concentration of ions were necessary for pit growth and that failure to maintain this level would result in repassivation. A quantitative methodology to determine this critical value in terms of a measurable estimate like the current density was formulated by Galvele,[11,13,28] who proposed the one-dimensional pit model (Figure 1.1). This model considered dissolution to occur only at the base of the pit, with the walls inert, thus resulting in unidirectional mass transport. Galvele incorporated the idea of competitive dissolution and diffusion espoused by Epelboin *et al*.[29,30] to describe a steady state flux condition between mass transport of the dissolution products out of the pit and active corrosion inside the pit, which resulted in the maintenance of a critical concentration for continued dissolution. Although developed in order to explain the dependence of pitting initiation and pitting potential on the pit solution chemistry, the mass transport arguments developed in the model can be easily extended to describe the critical solution chemistry required inside the pit for stable pitting propagation, once pits of certain depths have already grown, as has been commented upon in the literature.[31–33] The dissolution flux was described in terms of the following reactions comprising metal dissolution and subsequent cation hydrolysis which was assumed to rapidly attain equilibrium:

$$Me \rightarrow Me^{+z} + ze^{-}$$

$$Me^{+z} + H_2O \leftrightarrow Me(OH)^{+(z-1)} + H^{+}$$

Species fluxes were equated in accordance with Fick's first law, with relationships among the unknown concentrations specified by the dissolution current density, general material balance, hydrolysis equilibrium constants, and values of diffusivities taken from the literature. Such an analysis resulted in the formulation of the parameter ($i \cdot x$) – the product of the dissolution current density and the pit depth, later termed the pit stability product[34,35] – as a descriptor of the concentration of metal ions and consequently, the pH, inside the pit for continued steady-state dissolution. Therefore, given a critical surface concentration at the corroding surface, a critical pit stability product can be calculated that describes the required levels of acidification to sustain pitting.

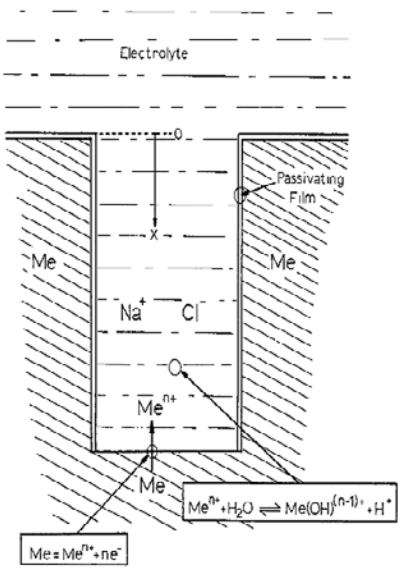

Figure 1.1. One dimensional pit model considered for development of pit stability criteria.[11]

Work towards determining this critical surface concentration has progressed since the development of Galvele's model, with authors reporting that levels of metal chloride

approaching saturation are necessary to maintain the low pH required for continued pitting.[10,27,36] Some researchers have shown that the high anodic current densities associated with pitting result in the formation of a film of the saturated metal chloride salt on the base of the pit.[19,37–41] The high chloride concentration so obtained was considered to be responsible for increasing the activity of H^+ from cation hydrolysis and lowering the pH below calculated values.[36,42,43] Experimental methods to study the conditions described by Galvele's model often involve the utilization of the artificial pit electrode – a metallic wire cast in an inert material like epoxy – to serve as the one-dimensional corroding pit with inactive walls.[44–47] The application of anodic potentials resulted in the active dissolution of the wire with sufficiently high anodic potentials generating a salt film on the corroding surface which provided a quasi-steady state configuration under conditions of diffusion-limited dissolution (Figure 1.2).[35,45–52]

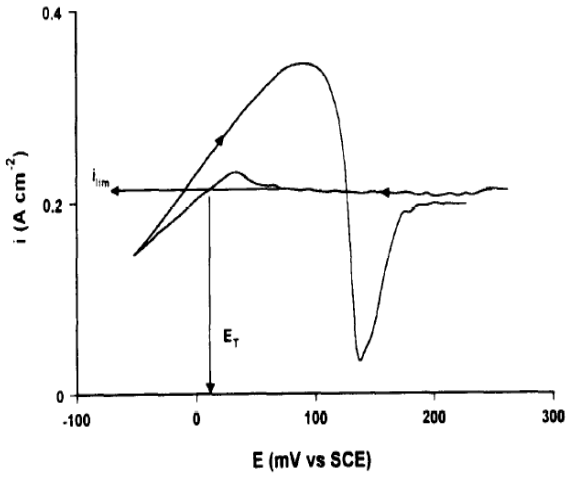

Figure 1.2. Salt film formation at high anodic potentials.[52]

Estimates of the pit stability product for such a surface condition can then be experimentally obtained, and as a result, some authors have considered the presence of a salt film

as a necessity for stable pitting at steady state.[34,35,52–55] However, pitting has been observed to proceed stably at potentials far below those required for a salt film to be stable.[39,47,56] This observation indicates that full saturation is not a critical surface condition for stable pitting. It then follows that the critical surface concentration C_s for stable pitting is some fraction f of the concentration at saturation C_{sat},[57] and the corresponding critical pit stability product $(i{\cdot}x)_{crit}$, the same fraction f of $(i{\cdot}x)_{saltfilm}$, the pit stability product under a salt film:

$$C_s = f \cdot C_{sat}$$

$$(i \cdot x)_{crit} = f \cdot (i \cdot x)_{saltfilm} \quad \ldots\ldots. (1.1)$$

Under such salt film-free surfaces, dissolution at the base no longer occurs under diffusion-limited conditions but instead proceeds under mixed control of ohmic and activation processes.[46,47] The development of a critical surface concentration under such conditions (once the solution resistance within the pit is corrected for) would depend on the products of corrosion transported out of the pit at the same rate at which they are produced by dissolution – the mathematics of which can be formulated in terms of Galvele's original model. The existence of an intermediate steady state where the rates of dissolution and diffusion fluxes are equal was proposed by Epelboin *et al.*[29] Isaacs and coworkers[46,47,58] have studied such configurations experimentally for stainless steel and nickel alloys in aqueous chloride solutions. Curves of current density decay versus time were obtained on switching the applied potential from a high value where the salt film had just dissolved to a low value where repassivation was expected to take place. Such curves obtained on switching to successively lower potentials and at various depths were corrected for the solution resistance within the pit to obtain isopotential lines of current density which could be empirically related to the surface concentration using the solution

of the time-dependent diffusion equation. These curves describing the decay of current density with the corresponding surface concentration were overlaid upon the diffusion rate which was represented as a straight line on this plot, as depicted in Figure 1.3 (a). The existence of intermediate steady states would then be denoted by the points of intersection of the isopotential curves with the diffusion flux line. These points would represent the steady state surface concentrations which would be maintained by diffusion out of the pit at the same rate as dissolution. The stability of such intermediate steady states for 302 stainless steel remained between 60 and 80% of saturation.[47] When model Fe-Cr alloys were considered, the range of this surface concentration grew wider to between 20 and 80% of saturation (Figure 1.3 (b)).[58]

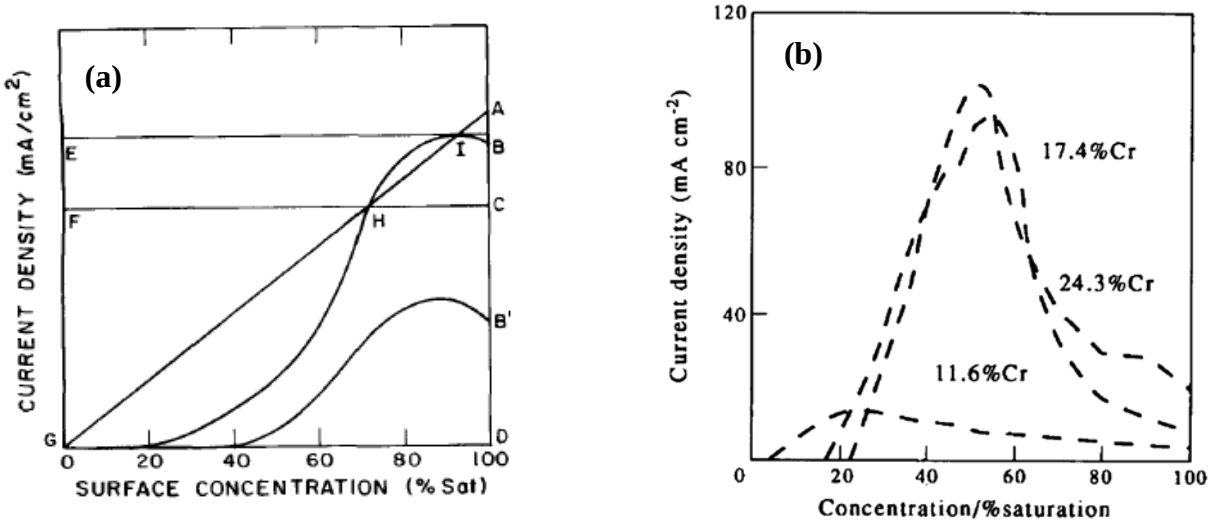

Figure 1.3. Development of multiple steady states following dissolution after loss of salt film for (a) 302 stainless steel[47] and (b) model Fe-Cr alloys.[58]

Tester and Isaacs[45] recognized the effect that the external hemispherical boundary layer might produce on the mass transport from an experimental one-dimensional pit corroding in

solution by accounting for a length parameter, in addition to the pit depth, in their work on the diffusional effects observed in localized corrosion.[45] Gaudet *et al.*[47] also acknowledged the influence of this external boundary layer on the pit stability data from one-dimensional pits. Alkire and coworkers[51,59,60] have examined the impact of geometrical parameters on the mass transport from hemispherical pits in terms of how fluid flow in solution affects diffusional characteristics.

Work on determining the critical dissolution flux has primarily focused on the measurement of the current density parameter and relating it to the surface concentration via mass transport.[11,45–47,52,57,58] Defining the critical surface concentration as that under a salt film allows facile experimentation and analysis due to the observable quasi-steady state conditions, but their utility is questionable when viewed against the evidence that stable pitting proceeds under much lower potentials.[39,56,61] Studies of intermediate steady states obtained on equating time-dependent fluxes to diffusive transport currently result in multiple estimates of film-free critical dissolution conditions without a clear quantitative rationale to select one over the other.[47,58]

This lack of consensus has hampered the estimation of an associated critical potential corresponding to conditions that describe the transition from active dissolution to repassivation. Furthermore, the effect of geometry on mass transport from one-dimensional artificial pits has not been systematically examined with a view to evaluate if the measurements truly correspond to 1–D characteristics. This requirement is essential for the purposes of applying the calculus of Galvele's formulation towards relating the experimentally measured dissolution flux to the chemistry at the corroding surface. Finally, a quantitative connection between the measured

critical current density and the physical cause of repassivation resulting from the loss of critical chemistry at the dissolving surface has not been provided in these studies.

1.4. Critical Potential

Various approaches have been undertaken till date towards the definition, measurement, and interpretation of the critical potential that characterizes the minimum aggressive conditions required for stable pitting. The susceptibility of various alloys to localized corrosion has been examined primarily in terms of two potentials – the breakdown or the pitting potential (E_{pit}) and the repassivation potential (E_{rp}).[2,21] E_{pit} is often characterized as the potential above which pits can nucleate and grow stably[62–68] whereas E_{rp}, following the notion of a protection potential, is defined as the potential below which new pits cannot nucleate and existing pits cannot grow.[11,68–71]

Measurements of these two potentials frequently use the results of cyclic potentiodynamic polarization (CPP) experiments[72,73] with E_{pit} indicated on the forward scan as the potential where a sudden current increase is seen and E_{rp} as the potential on the backward scan where a sudden drop in current occurs (Figure 1.4). Some authors hold that the two potentials are in fact the same, and the difference arises due to a difference in measurement technique.[66,74–76] In this vein, Thompson and Syrett[76] defined a unique potential E_u from their tests which showed that the E_{rp} (termed E_{prot} in their work) as measured by CPP scans following short periods of prior pit growth were approximately equal to the most active values of E_{pit} measured using CPP tests at slow scan rates (Figure 1.5).

The dependence on scan rate of E_{pit} and E_{rp} from CPP scans casts doubt on their utility as critical potentials if measured in this manner. E_{pit} behavior has also exhibited wide scatter depending on the surface finish of the alloy[61,67,68,72,77]. Furthermore, its validity with respect to defining critical conditions for pit stability has been tenuous due to a difference in opinion over the surface conditions it actually describes, having been associated with salt film formation[52] as well as pit

metastability.[55,61] In any case, pitting has been observed to proceed stably at potentials well below E_{pit},[34,56,78,79] and hence it is not useful as a parameter in defining critical conditions for pit stability. E_{rp} estimated from CPP scans appears to be highly dependent on the scan rate and unsuitable as a material parameter, with slow scan rates registering a lower E_{rp}.[68,72,80] Moreover, Rebak and coworkers[81,82] have shown from their work on nickel alloy crevice corrosion that the use of a slow scan rate can also lead to transpassive dissolution due to the charge densities passed at high potentials and current densities.

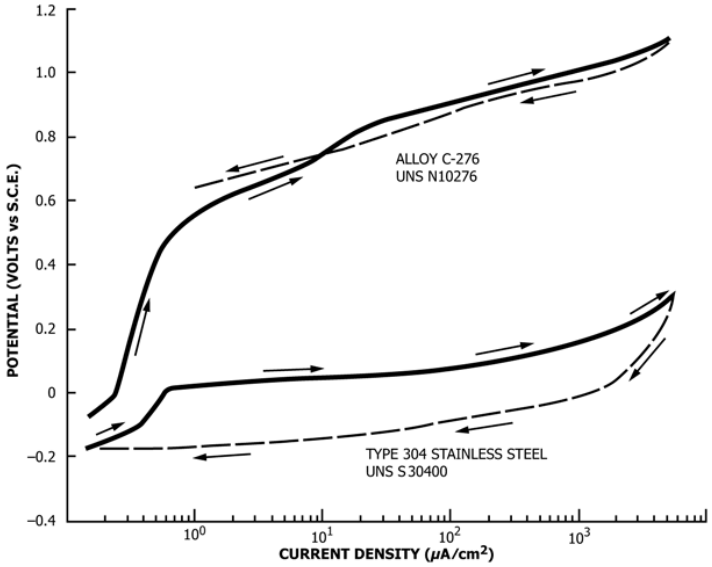

Figure 1.4. Cyclic potentiodynamic polarization technique to determine E_{pit} and E_{rp}.[73]

In their investigations of a critical potential for use as a conservative lower-bound parameter for long-term prediction of localized corrosion, Sridhar and coworkers[83–85] introduced an alternative method of defining and measuring E_{rp}. Their method utilized a pit initiation step, followed by propagation at high anodic potentials to various depths, followed by a stepwise scan

to low current densities. This work followed a method of measuring repassivation potentials similar to that reported for crevices by Tsujikawa and coworkers,[86–88] which was adopted as an ASTM standard.[89] E_{rp} was found to initially decrease with pit depth for shallow pits, but remained quite independent of pit depth for deep pits (Figure 1.6).[83,84] This result was related to the long-term corrosion potential (E_{corr}) measurement of stainless steels and nickel alloys,[85] with localized corrosion resulting when E_{corr} rose above E_{rp}. By calculating the current densities that were passed in the experimental portion of studies on E_{rp} by other authors, Sridhar and coworkers[83–85] were able to compare their results with the E_{rp} values obtained from the CPP scans previously published in the literature (Figure 1.7). The apparent scan rate dependence of E_{rp} was shown to be a result of low charge densities passed in these tests, and therefore insufficient pit depths attained for the E_{rp} to become independent of depth. The measured E_{rp} at deep pits was also seen to be lower when the scan rate of the stepwise scan used was rapid as opposed to more noble values for slow scan rates. This observation was attributed to fast scan rates not providing time for sufficient mass transport out of the pits in order to attain the critical concentration to induce repassivation. Anderko *et al*.[32,33] have indicated that these measurements may result in an overly conservative estimate of E_{rp}.

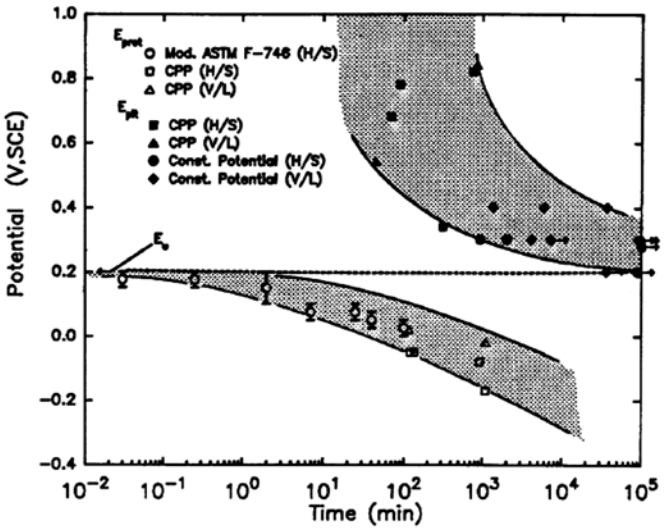

Figure 1.5. Results showing most active values of E_{pit} being approximately equal to the most noble values of E_{rp}.[76]

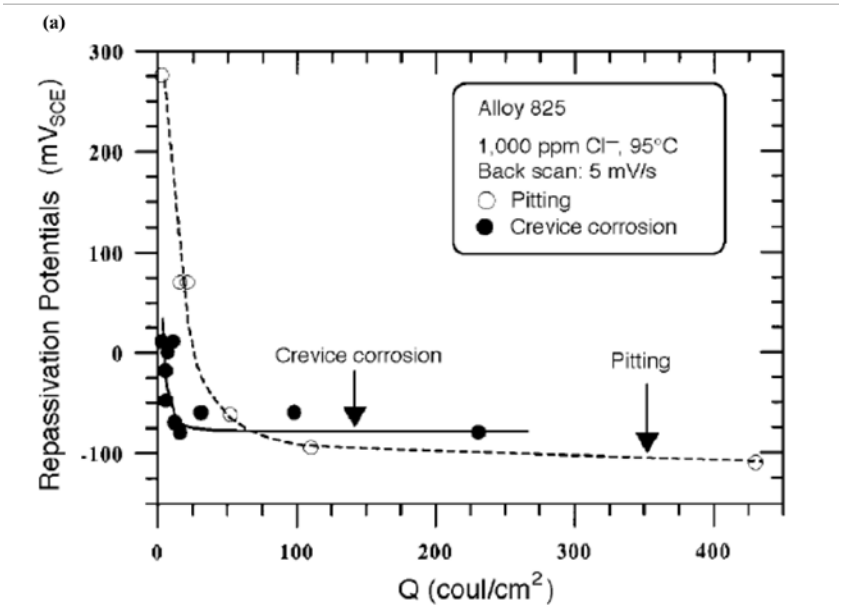

Figure 1.6. Plateau in E_{rp} seen for deep pits.[84]

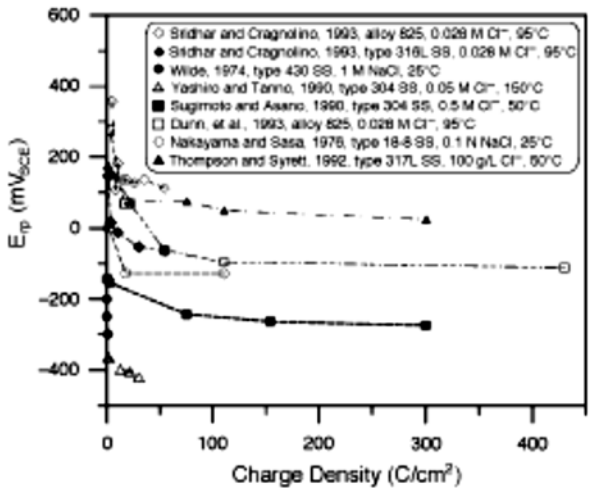

Figure 1.7. Comparison of various studies of E_{rp} variation with charge density/pit depth.[83]

Various hypotheses to explain the effects of experimental and environmental variables on E_{rp} have been presented in the literature. Galvele offered an explanation for the existence of a single repassivation potential[11] based on his pit stability product argument, wherein deeper pits, requiring a lower current density to grow, could accommodate lower potentials until the corrosion potential was reached in the pit solution. Pickering and coworkers[90–92] have advanced an alternative ohmic drop-based view of pit stability based on the observation of film-free dissolution, H_2 gas evolution in pits, and *in situ* potential measurements. Dunn *et al.*[85] attempted to qualitatively synthesize these two positions by arguing that the effects of pit depth on E_{rp} were a result of the high IR drop at shallow pits due to the high current densities required to maintain the pit stability product. As pit depth increased, the current density to maintain the pit stability product (a result of solution modification) decreased, resulting in a negligible increase in the IR drop, manifesting as the relative independence of measured E_{rp} on pit depth for deep pits. Laycock and Newman[52] quantitatively advanced a similar notion for the potential at which the salt film disappears (the transition potential, or E_t) as the critical parameter based on the assumption that the presence of the salt film was necessary for stable pitting. According to this

view, the ohmic drop at all pit depths was constant because the limiting current density (i_L = I_L/area = $zFDC_{sat}/d$) was inversely proportional to the pit depth whereas the resistance was linear with pit depth (= ρ·depth/area); therefore one would cancel the effect of the other.

Generalized models have been developed to predict the effect of environmental variables like electrolyte composition and pH on the repassivation potential of alloys used in industrial practice. Notable examples in this regard include an empirical model based on multiple regression analysis of alloy performance[93,94] and a thermodynamics-based model[32,33,95–97] which utilizes the idea of repassivation as proceeding from oxide nucleation under a hydrous metal halide.[98]

In toto, the critical potential describing the transition from active dissolution to repassivation spans a range of definition and associated methods of measurement. The ASTM standard CPP technique[73] has been shown to be problematic in determining a consistent, conservative value for both the pitting and repassivation potential.[68,72,80] It has also been shown to result in transpassive dissolution, given the high coulombic load passed.[82] The methods of Tsujikawa *et al.*[86–89] and Sridhar *et al.*[83–85] provide a conservative value that is confirmed by long-term testing but its implementation using large-area samples imply that the conversion from charge density to pit depth is inaccurate. This shortcoming impedes its integration into the pit stability model and consequent relation to a critical dissolution flux and solution chemistry. Moreover, given the multiple pits that initiate and grow in the samples used, it is not clear over what area the current densities defined in these experiments are calculated. Arguments for the corrosion potential in the critical pit solution as the critical factor face the criticism that such circumstances would not result in sufficiently aggressive conditions (low pH) for stable dissolution. Furthermore, the Galvele pit stability product would vanish at the corrosion

potential, as the measured current density would be zero. On the other hand, a solely ohmic drop-based critical potential does not account for the fact that once below the corrosion potential in the pit solution, the pit becomes a net cathode and therefore would no longer actively dissolve. Moreover, a purely IR-based critical potential when applied in the context of the Galvele pit stability product implies that pits can grow to extremely large depths, with the associated current density appropriately diminishing in value; this is an outcome that is quite unrealistic given the absence of pits of such size in nature.[16,99,100]

It may be most prudent to reconcile these views using an approach analogous to the opinion of Laycock and Newman[52] who considered a constant ohmic drop with pit depth emerging from the diffusion-limited current density and the resistance in the pit. However, instead of a salt film and the accompanying i_L, a film-free surface condition corresponding to a fraction of saturation may be more appropriate as a critical condition. The corresponding current density would also be at steady state (as it would have to satisfy the Galvele pit stability criterion). Associating this value with the critical potential for repassivation would imply a small ohmic drop, consistent with the expectations of Dunn *et al.*[84,85] who recorded low current densities (≈10 to100 μA/cm^2) for their measurements of E_{rp}. In any case, such efforts necessitate the study of pit stability in the context of repassivation, with a quantitative framework that connects these parameters to the actual chemistry of the corroding surface.

Finally, a mechanistic understanding of the critical factors is required in which the conditions that are described by the critical factors do indeed correspond to a physical cause for repassivation. Towards this end, the work of Anderko *et al.*[32,33,97] is promising as it evaluates E_{rp} in terms of repassivation as a result of oxide nucleation following the view of Okada,[98] but these studies do not quantitatively associate the measured critical potential with a critical surface

concentration. An arbitrary specification of the current density at repassivation also impedes the implementation of these studies within an overarching quantitative framework.

1.5. Critical Chemistry at the Corroding Surface – Cation Concentration and pH

Efforts to determine the critical dissolution flux have also investigated the associated critical surface chemistry, which has been characterized in terms of the concentration of the metal cations produced during dissolution and the pH.[10,36,43,101] Several methods to determine the critical surface concentration for pitting have been described in the literature, as noted by Turnbull in his comprehensive review[102] of the solution chemistry in occluded geometries. These methods include *in situ* probe techniques,[36,103–105] electrochemical measurement in simulated pit solutions,[10,36,40,106] as well as artificial pit experiments of the kind used to estimate the critical dissolution flux.[44–46,50] As has been discussed previously, the primary point of contention among the latter studies has been whether a precipitated salt film describes the critical stable pitting condition. Consequently, estimates of the critical surface concentration have varied from 100% saturation to lower fractions.[47,52,57,58]

Measurement of the pH in pit solutions have been complicated by this disagreement over the critical chemistry. Typical investigations to determine the pH employ direct methods of interrogation or simulated pit solutions, both of which have shortcomings. The use of *in situ* probes necessarily causes solution perturbation which results in transport effects that are difficult to evaluate.[102,107] The lack of agreement on the critical surface concentration means that the pit solutions in which these measurements are performed are simulated chemistries prepared from polarization of metal at high anodic potentials[9,106] or chemical dissolution of cationic chlorides,[108] neither of which are realistic when considered in the context of real pitting conditions near repassivation. Empirical estimates of the pH at high cationic chloride

concentrations have been formulated, and these vary over three orders of magnitude of H^+ activity, depending on the solution chemistry.[43]

Although it has been noted that the local cathodic reaction in the pit plays a role in the elevation of the pH to induce repassivation,[109] these effects have not been examined in the context of critical factors for pit stability. Work on stainless steel crevices[110] and crack tip electrochemistry[111,112] has considered the increased impact of local cathodic reactions at the surface as potentials close to repassivation are approached in terms of their contribution towards satisfying the anodic demand. When hydrogen evolution is considered to be the local cathodic reaction, this contribution can be expressed in terms of the equilibrium availability of OH^-, and consequently, the pH. This treatment can then be investigated in terms of a critical condition and related to the oxide nucleation basis for repassivation that was introduced in the section on critical potential. In this manner, a critical pH condition that corresponds to a physical cause for repassivation can be set up, and under this constraint, the other critical factors of dissolution flux and potential can be quantitatively related. Describing pit stability and repassivation in terms of individual anodic and cathodic processes in this manner would also facilitate a mixed potential-based[113,114] mechanistic rationale for the process.

The current status of understanding of pitting stability and repassivation can therefore be summarized as i) work that has focused on the dissolution flux and solution composition at the corroding interface and ii) work that has focused on the potential measured at this interface referred at the pit mouth. This classification highlights the paradox of the present view of pit stability and repassivation: although it is universally accepted that both the local chemistry and the local potential are key, there is no unified framework that explicitly considers both. The work on solution composition provides little quantitative information to the potential at the interface

whereas the work on the potential measurement yields no direct insights into the local chemistry of the corroding surface. The need for a quantitative framework that considers the various critical factors for stable pitting synergistically is therefore reiterated based on building a fundamental mechanistic basis for general pitting and repassivation phenomena. The utility of a comprehensive, quantitative relationship among the various critical factors can also be appreciated from an engineering perspective when their application in damage prediction models is considered. In this respect, a brief overview of predictive pitting damage estimation modeling based on critical stability criteria is described in the next section.

1.6. Application of Critical Factors to Damage Prediction

Damage prediction models are highly useful as design tools in structural integrity analyses of metallic components that undergo exposure to corrosive environments during service.[115,116] These models are also useful to determine container wall thicknesses for high-level radioactive waste storage.[117,118] Kelly and coworkers[16,99,100] developed a maximum pit size model that could be used to provide input data for such analyses, based on charge conservation considerations, that in natural conditions (*i.e.*, without experimental external polarization) under an electrolyte thin film, an actively dissolving pit anode could grow only as large as long as the current supplied by the surrounding cathode would support it. The individual constraints on the anode and the cathode are set by the respective stability criteria that correspond to the minimum anodic current demand and the maximum cathodic current capacity. This system is schematically depicted in Figure 1.8.

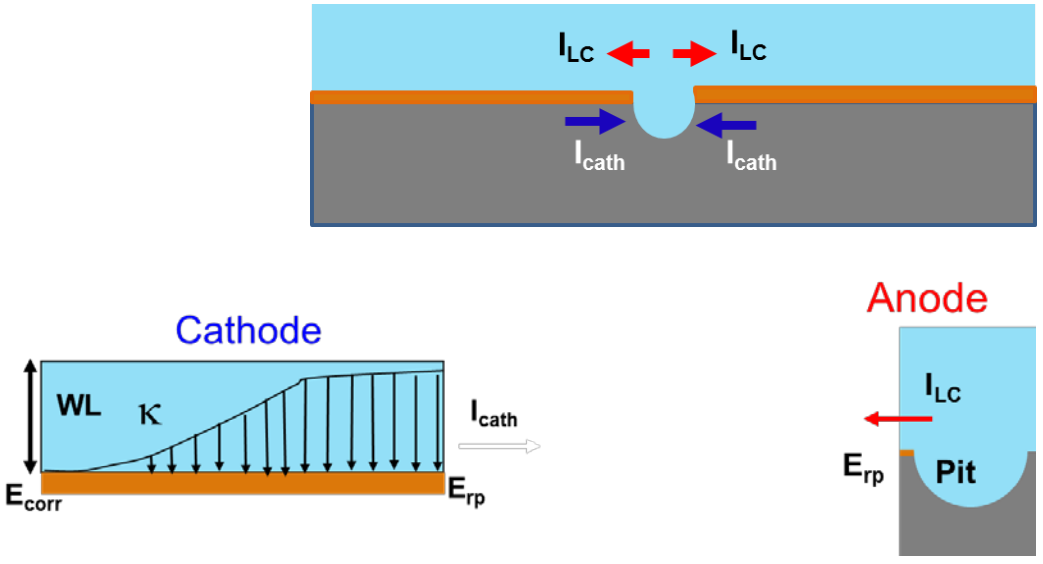

Figure 1.8. Galvanic separation of the cathode and pit anode to evaluate individual currents in terms of respective critical stability criteria.[99]

When expressed in terms of a common geometric dimension, such as the pit radius, a limiting damage size can be estimated when the charge conservation principle is applied. The individual stability criteria can be expressed in terms of the pit radius as discussed below:

Anode – the minimum anodic current demand is a linear relationship with pit radius when considered in terms of an equivalent critical hemispherical pit stability product $(I/r)_{\text{crit}}$, where I is the anodic current and r is the pit radius. Woldemedhin *et al.*[119] have shown that this value is three times the Galvele pit stability product, *i.e.*,

$$I_{anode,\,\min} = \left(\frac{I}{r}\right)_{crit} \cdot r_{pit} = 3\left(i \cdot x\right)_{crit} \cdot r_{pit} = 3f \cdot \left(i \cdot x\right)_{saltfilm} \cdot r_{pit} \quad \ldots\ldots \text{(1.2)}$$

Cathode – the maximum cathode capacity is calculated upon converting the non-uniform current density distribution of the real cathode into an equivalent uniform current density supplied by a cathode of finite length. This uniform current density is also supplied across the potential differential $\Delta E = (E_{\text{OCP}} - E_{\text{rp}})$ which originally exists across the length of the real cathode. However, this potential drop for the equivalent cathode occurs across an equivalent cathode length measured from the pit mouth (at E_{rp}) to a finite distance away on the bulk surface (at E_{OCP}) depending on the ohmic resistance of the medium. The current supplied across this potential gradient is then calculated from the cathodic kinetics corresponding to this value of ΔE. This geometry is illustrated in Figure 1.9. The resulting expression for cathodic current in terms of pit radius is:

$$\ln I_{cathode,\,\max} = \frac{4\pi\kappa \cdot WL \cdot \Delta E}{I_{cathode,\,\max}} + \ln\left(\frac{\pi \cdot e \cdot r_{pit}^2}{\Delta E}\int_{E_{OCP}}^{E_{rp}}\left(i_c - i_p\right)dE\right) \quad \ldots\ldots \text{(1.3)}$$

where κ is the electrical conductivity and WL is the water layer thickness of the electrolyte thin film.

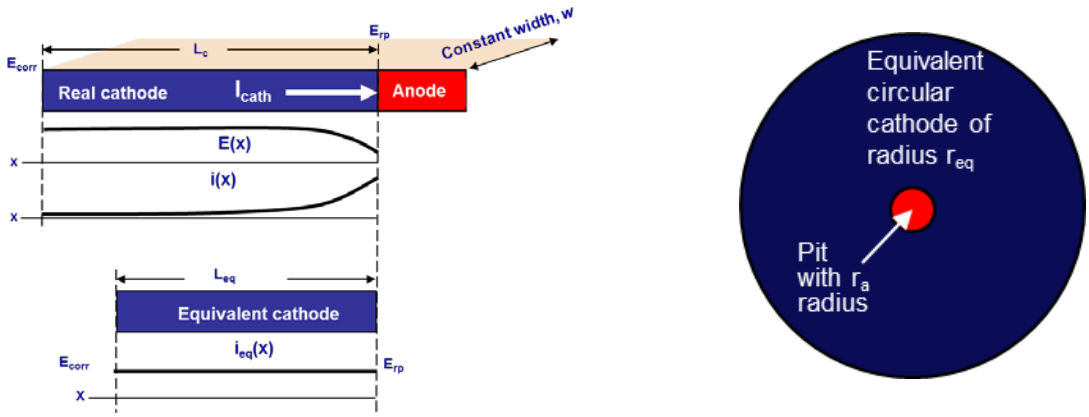

Figure 1.9. Treatment of the real cathode as an equivalent cathode of length L_{eq} or radius r_{eq} with uniform current density distribution across potential gradient ($E_{OCP} - E_{rp}$).[99, 100] Note: E_{OCP} is denoted as E_{corr} in this figure – the two potentials are equivalent in this treatment.

This expression for cathodic current can be numerically solved, and in conjunction with the linear relationship with the pit radius obtained for the anodic current, results in a plot of the type shown in Figure 1.10. The point of intersection of the cathodic curve and the anodic line provides an estimate of the limiting pit size. Figure 10 shows calculations using two different values for the critical pit stability product which, as has been discussed previously, indicate different values for the critical surface concentration. It is observed that a change in critical degree of saturation from 100% (salt film) to 50% results in a variation of a factor of more than 2 in the estimated maximum damage size. Therefore, in order to avoid incorrectly estimating the damage size that may be attained on a metallic surface in a corrosive environment, it is vital to accurately know the critical surface concentration for anodic stability. Similarly, in order to evaluate the cathodic current that can be supplied to support pit growth, the repassivation

potential E_{rp} has to be related to the critical surface concentration, necessitating the development of a quantitative framework to connect the various critical factors.

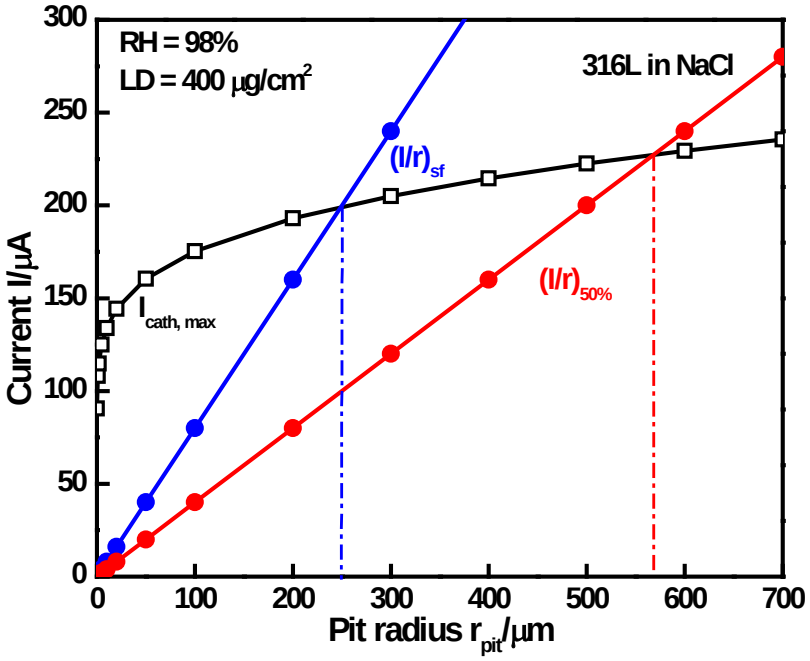

Figure 1.10. Effect of the critical surface concentration on anodic stability criteria and maximum pit size estimation.[120]

1.7. Scope of Dissertation

The goal of this work is to develop a unified framework that describes both pitting stability *and* repassivation. Such an objective necessitates that the field of survey be restricted to some extent in order to preserve focus. This dissertation considers in the design of the framework, factors that sustain pitting rather than those responsible for its nucleation. In this regard, the study employs as its candidate system, the stainless steel alloy 316L corroding in 0.6 M NaCl at ambient conditions of 25 °C at 1 atm. This section is divided into four parts: the first briefly lists the justification for focusing on these particular conditions and the aspects of pit stability and repassivation which are excluded from this study. Notes on pit initiation, metastability, temperature effects, alloys other than 316L, and finally empirical estimates of the effects of alloying constituents on pitting susceptibility are included. The next three parts detail in order, the organization of the research topics throughout the dissertation, the general advantages of using the lead-in-pencil artificial pit architecture, and select phenomenological studies that provide insight into pit stability fundamentals which will be expanded upon in the chapters that follow.

1.7.1. *Topics Excluded from Investigation*

Pit initiation. Early reviews on pitting and related electrochemical conditions tended to focus on the topic of passive film breakdown and the conditions for initiation.[15,26] However, more recent appraisals[61,121,122] hold the view that conditions for growth rather than initiation are more representative. Conditions for initiation of localized corrosion are not always reproducible and are highly dependent on the cleanliness of the alloy surface and the presence of defects in the oxide film.[123–125] Consequently, induction times associated with the onset of pitting also vary considerably even among samples of the same alloy in an environment conducive to localized corrosion.[123] Crevice formation can also accelerate pit initiation, resulting in further variation in corrosion behavior among cases studied.[126,127] Finally, in circumstances where prior pit growth has already taken place,[83–85] issues pertaining to critical conditions describing repassivation are not resolved by considering initiation.

Metastability. Another issue that the literature has focused on while discussing conditions for pitting is metastability.[2] Metastable pitting has been studied by several authors[34,35,128,129] by analyzing the transient current response to applied potential. These studies hypothesized that metastable pits grew into stable ones once they attained conditions permitting the aggressive solution within the pit to be maintained. However, the fate of a nucleating pit is not determined *a priori*, *i.e.*, the pit is not inherently prone to stability or repassivation unless certain critical conditions at its corroding surface are met.[127,130] It is therefore of interest to look at what these critical conditions are, which would be independent of how the pit initiated but crucial in determining whether it continues to propagate. Also, conditions for the inhibition of propagation rather than initiation are more useful in designing strategies for pit repassivation in industrially relevant cases where prior pit growth may already have taken place.[33,83–85,95]

Temperature. Pitting has been reported not to follow the Arrhenius Law expectation of increasing rates in proportionality to the reciprocal absolute temperature, primarily due to the different effects of temperature on the interconnected processes involved.[131] Temperature variations would be expected to have significant effects on the reaction rates at the corroding surface, salt film stability, mass transport characteristics, physicochemical parameters such as viscosity, and the kinetics of oxide nucleation.[2] The critical pitting temperature (CPT) as an empirical criterion for localized corrosion susceptibility was introduced by Brigham and Tozer,[132] and has been expanded upon by Newman and coworkers.[57,133–135] The latter studies reported an irregular variation in E_{pit} with temperature, and these results have been consequently related to their studies on the necessity of the salt film as a stable pitting criterion, concomitant with bulk electrolyte composition. The quantitative framework relating pit stability and repassivation as described in this dissertation is applicable regardless of temperature, as long as its effects are accounted for in the physicochemical parameters that are employed in its implementation. Provided the collection of pit stability and repassivation data is consistent across temperatures, the underlying principles of the framework continue to be viable. Several authors have reported both pit stability[57,135,136] and repassivation potential[83–85,88] parameters as a function of temperature, and these data are seen to behave in a nominally similar manner to those utilized in this study.

Other alloys. Abundant literature exists on the pit stability and the repassivation of alloys other than stainless steels, particularly for aluminum[38,77,78,130,137] and nickel alloys.[49,82,84,138–140] As has been noted in the previous sections, general aspects of pit stability and repassivation phenomena are common to all passivating metals. However, experimental implementation of the artificial pit technique to evaluate the critical factors is not equally viable in the case of every

alloy. For instance, studies with aluminum are complicated by copious hydrogen production inside the pit as well as partial repassivation effects like tunneling.[137] Some of the studies that have been referenced in this document have been applied to nickel alloys.[47,82,84,139,140] The use of 316L stainless steel as a candidate alloy is justified by its ubiquitous use in industry,[141] particularly those relying on damage prediction models based on critical stability criteria.[33,83,97,115–117] Some aspects of extending this study to other stainless steels is discussed in the section on phenomenology to follow. Nonetheless, the framework inherently is applicable qualitatively to all passivating alloys as long as stability criteria can be determined with similar reliability.

PREN. Lorenz and Medawar[142] introduced the Pitting Resistance Equivalence Number (PREN) as an empirical estimate of the localized corrosion susceptibility of stainless steels containing Cr, Mo, and N. These studies were based on experimental fits to E_{pit} measurements for different compositions of the alloying elements. Similar empirical studies have been conducted considering the effects of W and Mn based on E_{pit} measurements in the critical crevice solution. These estimates, apart from being of a heuristic nature, also draw the same criticism that was leveled in earlier sections at the deficiency in the selection of the pitting potential and simulated crevice solutions themselves as critical factors in localized corrosion. Work by Jargelius-Petterson[143] has cautioned against the use of PREN as more than a very approximate estimator of localized corrosion susceptibility, and its utility has been called into question by recent work on duplex stainless steels.[144] Rebak and Crook[145] have also shown that PREN is not a reliable predictor of localized corrosion in nickel alloys. As such, this dissertation will not consider PREN, or similar alternatives, because their application towards constructing quantitative, mechanistic tools of localized corrosion characterization is limited.

1.7.2. *Research Overview and Organization of Dissertation*

The background and the discussion provided in the preceding sections have established the current status of knowledge of critical conditions associated with pitting stability and repassivation. Key gaps in knowledge in the related literature on critical surface concentration and repassivation potential to date have also been identified. These gaps in knowledge include a common method to determine measurable parameters for stability and repassivation criteria, models that investigate critical local chemistry in the context of repassivation, and a physical explanation for the onset of repassivation upon the loss of critical chemistry. These issues pose a barrier to achieving complete mechanistic understanding of the phenomena associated with stable pitting and repassivation.

In order to resolve these issues, the dissertation will follow an approach that will address following topics:

Single experimental method to measure critical parameters. Each following chapter details a specific modified artificial pit technique that is utilized to extract data relevant to both pit stability and repassivation from the same experiment. A high-throughput version of the technique was developed to collect and analyze pit stability and repassivation data across a wide range of pit depths. Key phenomenological insights regarding the effects of pit depth on pit stability data were provided by results from this study, which are included in the remainder of this chapter, and inferences based on these data form the basis of Chapter 2. Separate experiments conducted in a variety of chloride solutions provided data which was analyzed in terms of diffusion-based arguments to rationalize observed dependence of the pit stability parameter on the bulk electrolyte which are later expanded upon in the light of the results obtained using the quantitative framework discussed in Chapter 3.

Geometry effects on one-dimensional (1-D) mass transport. A systematic evaluation of the influence of the effects of pit geometry on the flux characteristics emerging from lead-in-pencil artificial pits is conducted in Chapter 2. Results from this study inform selection of experimental parameters in order to accurately simulate 1-D mass transport characteristics for the application of the Galvele pit stability model as well as provide a quantitative rationale for the observed of repassivation potential behavior with pit depth.

Quantitative framework relating critical factors for pit stability and repassivation. Artificial pit experiments based on the work described in Chapter 2 provide information for a mass transport-based model which quantitatively relates the dissolution flux, repassivation potential, and surface concentration in terms of pit depth, forming the focus of Chapter 3. The surface concentration at the transition from active dissolution to repassivation is estimated as a critical factor, quantitatively connecting pit stability and repassivation. The impact of this critical value on atmospheric pitting is also discussed in the context of the bulk electrolyte effects on pit stability introduced in Chapter 1.

Physical explanation for the onset of repassivation. Chapter 4 demonstrates efforts to build anodic kinetics experiments based on calculations from the mass transport model described in Chapter 3 in order to validate the estimates of the critical surface concentration. These estimates are quantitatively associated with a physical cause of repassivation by way of the minimum pH required to precipitate an oxide in the critical pit solution. Cation hydrolysis calculations are employed to relate the influence of the local cathodic reaction to the pH of the corroding surface at repassivation, and consequently provide data towards a mixed-potential analysis for a mechanistic evaluation of the quantitative framework discussed throughout the dissertation.

1.8. The Artificial Pit Electrode

This section outlines the advantages of the artificial pit configuration that were employed in the study. The first part describes the construction and preparation of the lead-in-pencil artificial pit electrode samples. The second part describes the specific advantages of directly assessing kinetic data in terms of a single variable – the pit depth – that this configuration permits. Details of the experimental techniques themselves are provided in Chapter 3, as well as in the papers by Srinivasan *et al*.[120,146,147]

General sample preparation and architecture. The lead-in-pencil artificial pit electrode used for all studies in this dissertation is shown schematically in Figure 1.11. The standard sample consisted of a 316L stainless steel wire of diameter 50.8 μm cast in epoxy. Electrical conductivity was ensured by winding one end of the stainless steel wire to a length of insulated tin-coated copper electrical wire secured using conductive silver paste, prior to casting in epoxy – this served as the working electrode. Sufficient length (2 to 5 cm) of the stainless steel wire was embedded in the epoxy so that this junction would not be exposed to solution (the deepest pit grown was on the order of 1 mm). The top surface of the artificial pit samples were polished to 320 grit, which resulted in an exposed circular area of 2.03×10^{-5} cm^2 when placed upright in solution.

As has been outlined in previous sections, such a configuration enables the experimental realization of a system that would have a single corroding surface with inert walls. Electrochemical parameters can then be studied in terms of their dependence on the pit depth variable, which is controlled depending upon the charge density passed. Transport out of this artificial pit would approximate conditions of one-dimensional diffusion once sufficient depths had been attained.

Artificial pit electrodes were constructed similarly from wires of 304L, 17-4 PH, 430, and 17-7 PH stainless steels were for use in phenomenology studies. The 304L wire had a similar diameter as the 316L wire whereas the other wire samples had a diameter of 88.9 μm, resulting in an exposed circular area of 6.21×10^{-5} cm^2. The metallurgical composition of all alloy samples used in the study is shown in Table 1.1.

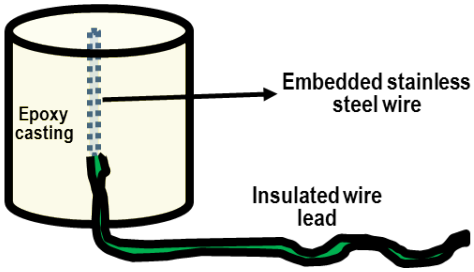

Figure 1.11. The artificial pit electrode sample.[146]

Advantages in employing the lead-in-pencil electrode. A lead-in-pencil artificial pit afforded advantages both in simplicity of construction as well as analysis of data. Electrochemical experiments were run that permitted the extraction of both pit stability as well as repassivation data from the same experiment. These experiments are illustrated in Figure 1.12 and described in detail by Srinivasan *et al.*[120,148] and in Chapter 3. The advantages afforded by the lead-in-pencil electrode are summarized below:[146]

1. Both parameters of interest – $(i \cdot x)_{saltfilm}$ and E_{rp} could be estimated from the same experiment, providing measurable estimates of the critical parameters.
2. A single corroding surface obviated the necessity to correct for activated surface area for charge density calculation. The charge density measured could be directly converted to pit depth using Faraday's law, enabling the evaluation of E_{rp} directly

in terms of pit depth and consequently, diffusive transport. These results are visited in the discussion on the validation of the technique later below.

3. The low volume of corrosion products resulting from the small size of the wire ensured that the bulk chemistry remained virtually unchanged throughout the duration of the experiment, which would not have been possible if a sample of large area were used.
4. Multiple experiments could be carried out using the same sample without having to correct for new pits initiating or old pits growing. Successive charge density and pit depth calculations are simply additive in the case of the artificial pit.

In order to validate the artificial pit method to measure E_{rp}, similar electrochemical experiments were carried out using samples of exposed area ≈ 1 cm^2, which correspond to sample sizes similar to those employed by Sridhar *et al.*[83–85] The charge density calculated for these experiments was normalized over the area of the deepest pit observed using multifocal stitching from three-dimensional digital image microscopy. The E_{rp} values observed at low charge densities for the 1 cm^2 samples were more active than those observed at similar charge densities for the artificial pit sample due to the fact that crevice corrosion was noticed on the large-area samples at the interface between the metal edge and the epoxy. The presence of crevices suggests a longer effective diffusion path, which would not be visible through the microscope, given the plane of observation. A similar observation was reported by Dunn *et al.*[84] in studies on crevice repassivation in stainless steels. The results shown in Figure 1.13 indicate that the measured values of E_{rp} and its behavior on increasing charge density agree well with those reported in the literature. The same results were also expressed in terms of *q* calculated

over the nominal area (1 cm^2). These latter results show good agreement with reported E_{rp} versus q data.[83]

Stainless steel type	Elemental composition (wt%)														
	Fe	Cr	Ni	Mo	Mn	Cu	Si	C	S	N	P	Nb	Ta	Co	Al
430 (wire)	81.79	17.18	-	-	0.49	-	0.45	0.06	0.005	-	0.028	-	-	-	
304L (wire)	70.26	18.48	9.2	-	1.59	-	0.27	0.03	0.001	0.001	0.036	0.001	0.001	0.13	
316L (wire)	67.98	17.07	10.66	2.16	1.36	0.23	0.41	0.019	0.029	0.05	0.03	-	-	-	
17-4 PH (wire)	75.17	15.26	4.58	0.42	0.78	3.25	0.49	0.03	0.002	-	0.022	-	-	-	
17-7 PH (wire)	73.01	16.90	7.22	0.34	0.78	0.16	0.28	0.07	0.001	-	0.018	-	-	-	1.17
316L (coupon)	68.81	16.72	10.06	2.03	1.89	-	0.39	0.021	0.0004	0.05	0.03	-	-	-	

Table 1.1. Composition of stainless steel wire used (all values in weight percent). Composition provided by vendor was confirmed by quantitative speciation using inductively coupled plasma optical emission spectroscopy (ICP-OES).

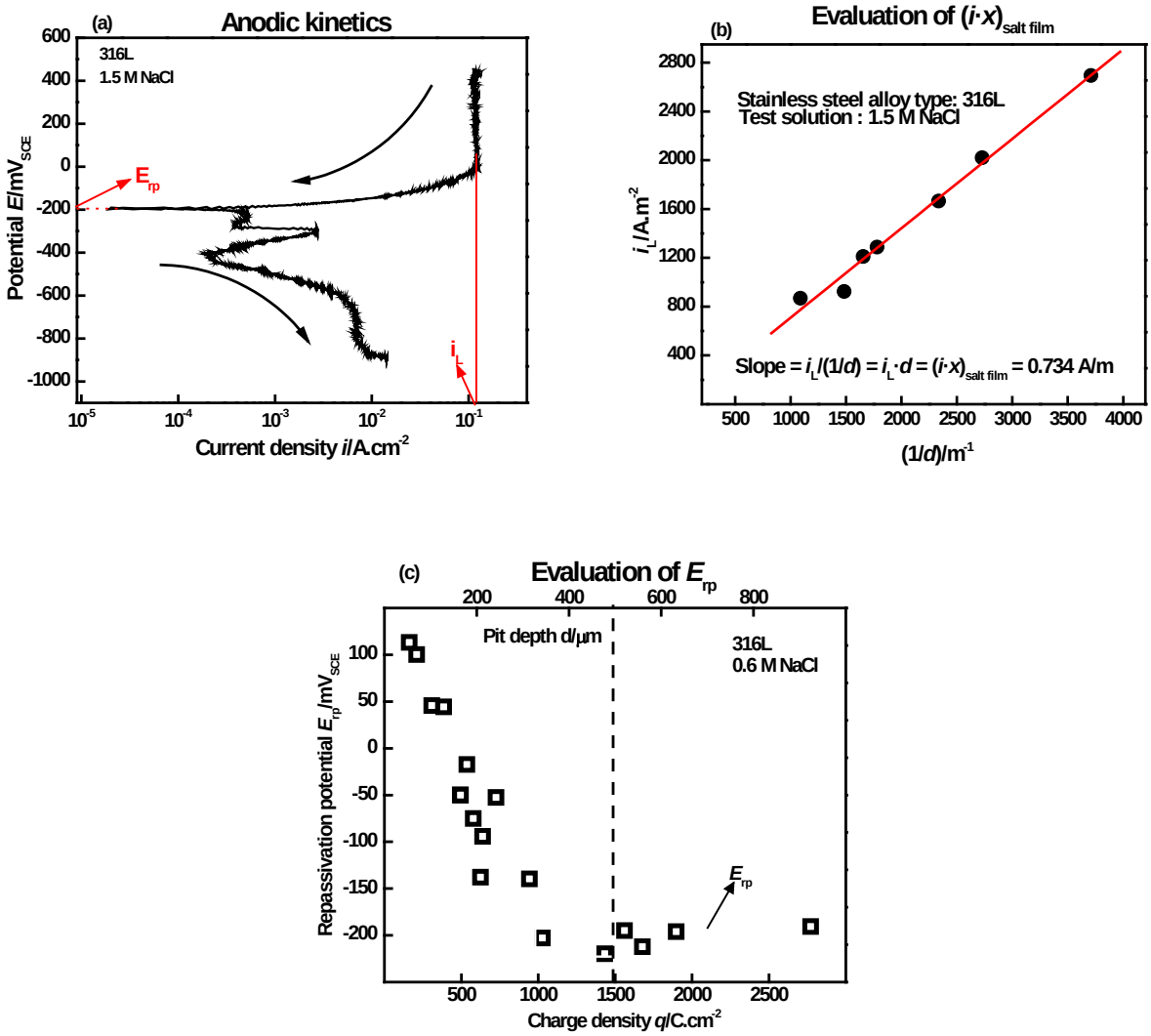

Figure 1.12. Extraction of pit stability and repassivation parameters from the same experiment. (a) Typical data from electrochemical experiments to measure both critical parameters.[120] (b) Plot of i_L from the kinetics data in (a) versus the reciprocal of pit depth. The linear fit to the plot provides the value of $(i \cdot x)_{saltfilm}$. (c) From the same experiment, E_{rp} is extracted as shown in (a). Plotted versus charge density, a plot similar to that obtained by Sridhar *et al.*[83,84] is obtained with the E_{rp} approaching a plateau for high charge density (which can be directly expressed in terms of pit depth for these experiments).

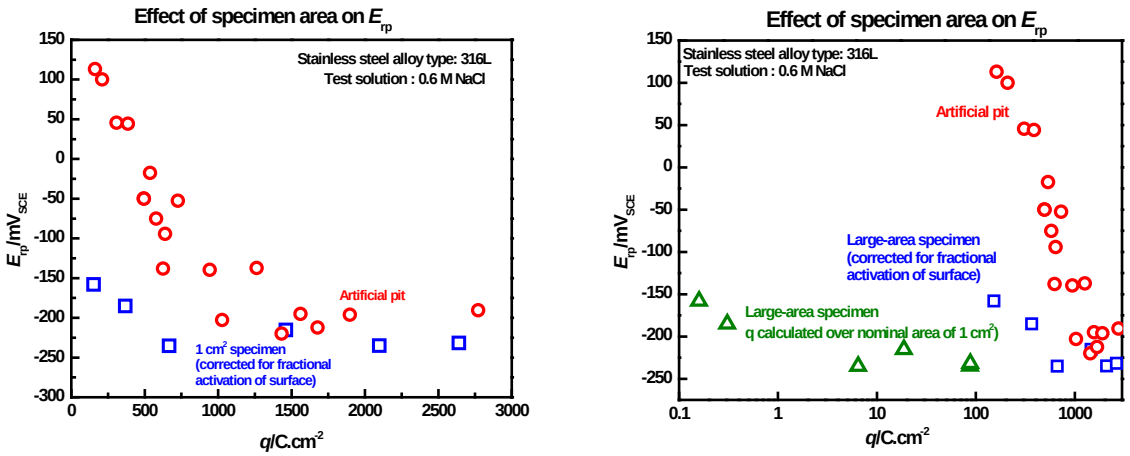

Figure 1.13. Validation of artificial pit methodology as a technique for E_{rp} measurement. The plot on the right is drawn on a semi-log scale to display the lower charge density values that result when the nominal area is used to calculate charge density.[146]

1.9. Pit Stability and Repassivation Phenomenology

This section describes selected phenomenology observed during electrochemical experiments performed with the artificial pit electrode to investigate pit stability and repassivation parameters. Alloy chemistry, bulk chloride concentration, and pit depth are the variables considered. The observed effects due to alloying microconstituents on the repassivation potential serve to account for interfering redox reactions while extending the measurement techniques to other stainless steel alloys. The phenomenology associated with the bulk chloride concentration and the pit depth is seen to affect pit stability kinetics. These results form the basis of the treatment of pit stability data collection and interpretation and its impact on atmospheric corrosion detailed in Chapters 2 and 3.

Alloy Chemistry

Artificial pit experiments similar to those outlined in Srinivasan *et al.*[120,148] and described in Figure 1.12 as well as the Experimental section of Chapter 3 were performed on 304L, 17-4 PH, and 430 stainless steel wires to examine the effects of alloy chemistry on $(i \cdot x)_{\text{saltfilm}}$ and E_{rp}. Results from experiments run on these wires in 0.6 M [Cl^-] are shown in Figure 1.14. The measured value of $(i \cdot x)_{\text{saltfilm}}$ was within experimental scatter of the same value of 0.8 A/m for all alloys examined (Figure 1.14 (a)) which agreed well with values reported in the literature.[34,35] Error bars for E_{rp} in Figure 1.14 were obtained by averaging the values at which measured E_{rp} remained relatively independent of pit depth after passing sufficient charge density, while those for $(i \cdot x)_{\text{saltfilm}}$ were obtained by averaging over the values from the slope of the linear fit of the plot of dissolution-limited current density and inverse of the pit depth for deep pits, as described in Chapter 3 and the literature.[120,146–148]

The measured E_{rp} on the other hand showed significant variation across the stainless steels (Figure 1.14 (b)). 304L followed the same trend as 316L, but with slightly more active values. This difference could be attributed to the presence of the molybdenum in 316L, which tends to provide some ennobling action to the alloy, as reported by Newman.[149] Type 430, a low-alloy ferritic stainless steel, displayed E_{rp} values much lower than 316L, around –450 mV_{SCE}. However, the trend of decreasing E_{rp} with increasing charge density as seen in 316L was reversed in the case of 430, with E_{rp} rising from more active values to reach a plateau at higher values as charge density increased. A similar trend observed for 316L at rapid scan rates is discussed in detail in Chapter 3. Finally, the repassivation potential for 17-4 PH remains constant and slightly higher than that of 316L across all charge densities. This last result is particularly surprising because 17-4 PH is less resistant to localized corrosion than 316L in service,[141] as evidenced by the lower OCP of 17-4 PH coupons in long-term tests (Figure 1.15 (a)).

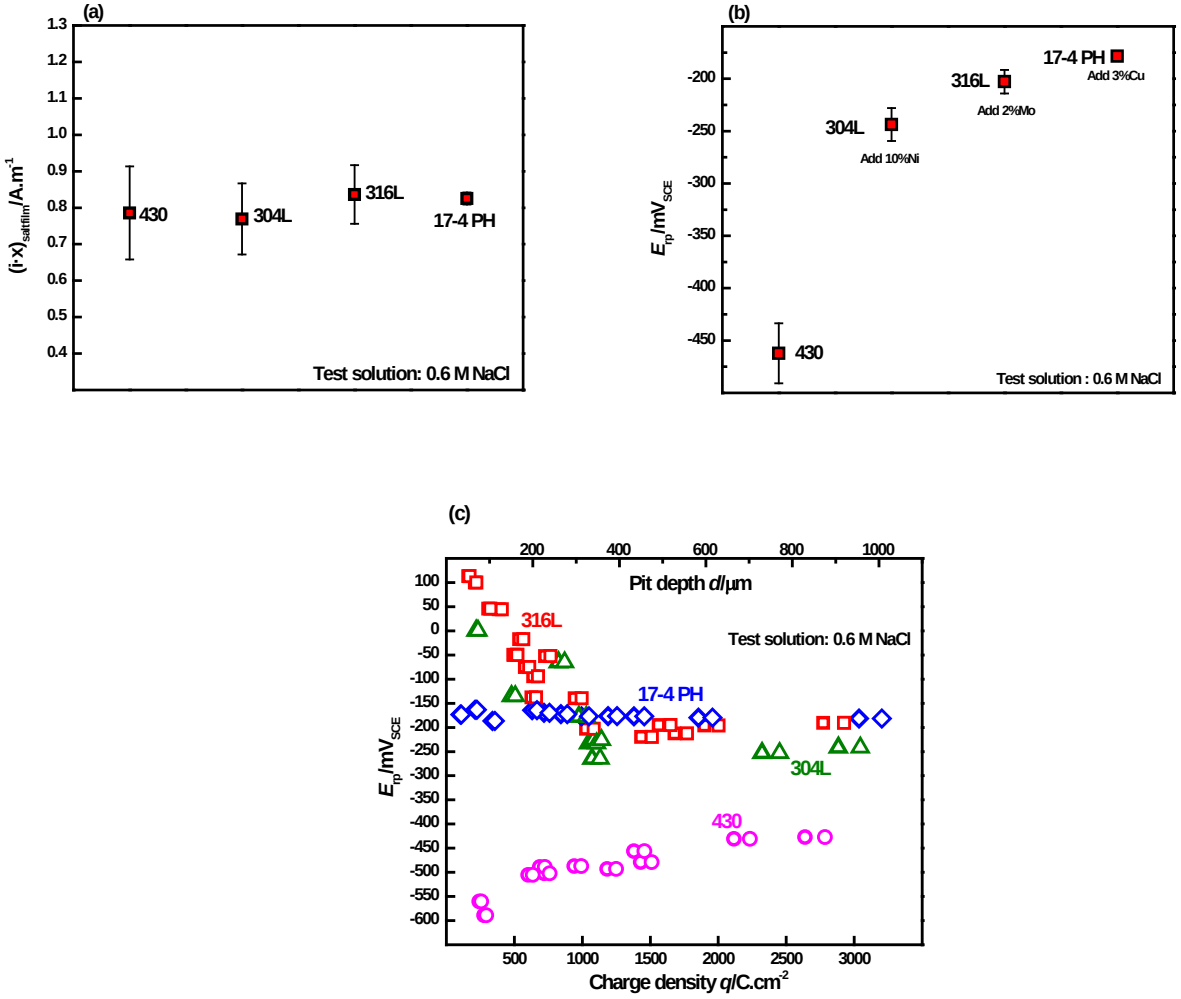

Figure 1.14. Pit stability and repassivation phenomenology across stainless steel alloys studied.[120]

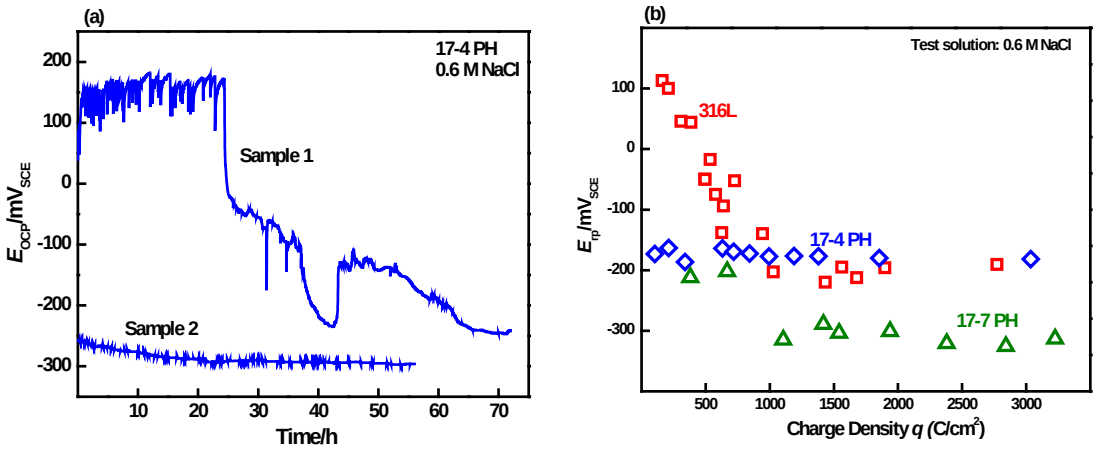

Figure 1.15. Evidence for electroactive copper species interference with 17-4 PH E_{rp} measurement.[120] (a) Long-term OCP measurements of 17-4 PH approach much lower values than measured E_{rp}. (b) E_{rp} measurements on 17-7 PH which is similar to 17-4 PH except that it contains a much lower Cu content, show values close to the long-term OCP values seen for 17-4 PH.

This result where the measured E_{rp} of 17-4 PH was more noble than that of 316L, despite the latter being the more corrosion-resistant alloy, was examined in the context of the electroactive alloying elements. Cu in 17-4 PH could interfere with the measurement of E_{rp} due to redox reactions that take place in the vicinity of the same potential was considered. Newman and Isaacs have observed similar results in polarization curves on 304 stainless steel in chloride solutions.[149,150] Evidence from the literature on the dealloying of brasses[151] indicates that the redox reactions exhibited by some copper species in chloride solution fall within the range of potentials sampled while measuring E_{rp} in this work.

E_{rp} measurements were performed on 17-7 PH, an alloy similar to 17-4 PH in composition, except that its copper content is much lower, as is indicated in Table 1.1. The E_{rp} values of 17-7 PH stabilized at around –300 mV_{SCE} as shown in Figure 1.15 (b), which agrees well with the long-term OCP values approached by the 17-4 PH coupons (Figure 1.15 (a)).

Any interference in E_{rp} measurement originating due to electroactive copper species can be analyzed using a technique similar to the one used in cyclic voltammetry to identify redox species via current peaks observed in the polarization scan.[152] Current peaks were observed in the potential range where the redox reactions corresponding to copper were expected and the current density corresponding to these peaks correlates with the copper content of the alloy. Analysis of these current peaks for the different alloys in 0.6 M [Cl^-] at 5 mV/s was performed once comparable pit depths were achieved. As shown in Figure 1.16, the peak for 17-4 PH appeared at much higher current densities than that for 316L. The reported copper content of 17-4 PH was nearly 10 to 12 times that of 316L and 17-7 PH (Table 1.1). The ratio of the peak current density values approached this ratio, lending credence to the hypothesis that electroactive alloying constituents may interfere with E_{rp} measurement. The elemental analysis of the 17-7 PH wire indicated a copper content comparable to that of 316L. However, despite the similar copper content of 17-7 PH and 316L, the latter showed a current peak of significantly higher value. This difference could point towards some microstructural effect on electrochemical parameters, because 316L is fully austenitic whereas 17-7 PH is a semi-austenitic precipitation-hardened steel, containing both martensite and residual untransformed austenite.[141] This dissimilarity may also arise from the fact that the measurement range for the repassivation potentials of 17-7 PH is more active than for 316L,[151] implying that the Cu replating effect may be superseded by other cathodic reactions.

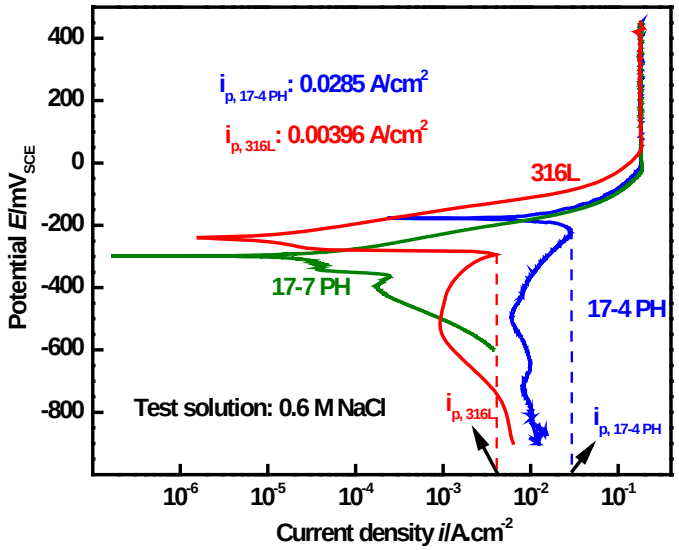

Figure 1.16. Investigation of Cu replating evidence for the observed noble E_{rp} of 17-4 PH.[120]

Bulk Chloride Concentration[147]

Artificial pit experiments performed in a similar manner to those illustrated in Figure 1.12 were performed on 316L wires in bulk NaCl concentrations at low levels (between 0.6 M and 2.8 M) to evaluate the effect of bulk electrolyte on $(i \cdot x)_{saltfilm}$. These experiments resulted in a plot that displayed a clear linear dependence of $(i \cdot x)_{saltfilm}$ on bulk chloride levels, similar to those obtained by Woldemedhin *et al.*[147] for 304L and 316L in $FeCl_3$ and LiCl, as shown in Figure 1.17. These results implied that there was little effect of pH or the nature of the cation in the supporting electrolyte on the pit stability parameter. As has been identified by Tester and Isaacs,[45] dissolution kinetics of stainless steels in chloride solutions up to 3 M [Cl^-] are practically identical, with no particular effects of viscosity. Therefore, a diffusion-based rationalization of the observed phenomenology of pit stability data with respect to bulk chloride concentration could be performed, which provided valuable information regarding the

physicochemical parameters employed. The salient results of this analysis are reproduced below, the development of which is provided in detail in the Appendix section of this dissertation. The linear dependence of the pit stability data on the bulk chloride concentration was explained in terms of an alternative expression of the relationship between the diffusion fluxes of the metal cation and the chloride ion under steady-state conditions:

$$\begin{aligned}(i \cdot x)_{saltfilm} &= FD_{Cl} z C_{sat,\,m} - FD_{Cl} C_{bulk,\,Cl} \\ (i \cdot x)_{saltfilm} &= FD_{Cl} z C_{sat,\,m} - FD_{Cl}[Cl^-] \quad \ldots\ldots (1.4) \\ (i \cdot x)_{saltfilm} &= A - B[Cl^-]\end{aligned}$$

These calculations yielded an estimate for the diffusion coefficient (D) and concentration at saturation ($C_{sat,\,m}$) of the metal ion as 9.2×10^{-6} cm^2/s and 3.72 M. This estimate for D is agrees well with those utilized in several artificial pit studies, but underestimates the value for C_{sat} (typically 4 to 5 M).[46,47,52,136,153] The impact of bulk electrolyte composition on the pit stability data as higher chloride concentrations are approached is discussed in greater detail in Chapter 2 with particular reference to its implications on modeling true 1–D behavior and in Chapter 3 with regard to applications to atmospheric corrosion.

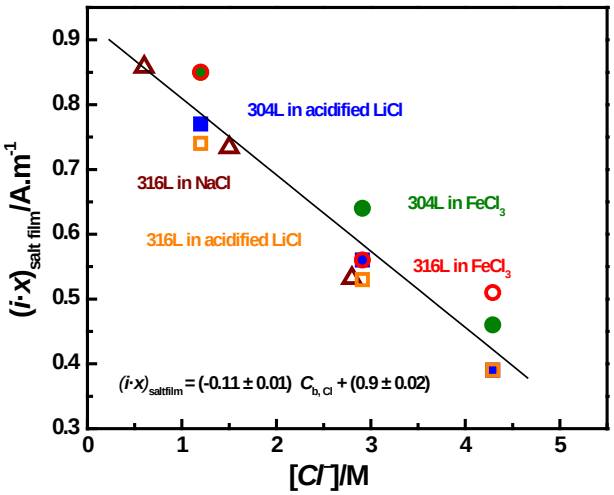

Figure 1.17. Linear dependence of pit stability product on bulk [Cl^-]. Data replotted from Woldemedhin *et al.*[147]

Pit Depth[146]

A high-throughput version of the artificial pit experimental technique described in Figure 1.12 was employed by Srinivasan *et al.*[146] to obtain a large volume of pit stability and repassivation data. The pit stability product under a salt film evaluated by including data accessed from deep pits using this technique compares well with literature values of $(i{\cdot}x)_{saltfilm}$ for 316L.[35,136,147] This modification to the original technique avoids sampling only shallow pit depths where one-dimensional diffusion does not capture the complete mass transport behavior of the system due to the hemispherical boundary layer at the pit mouth imparting some three-dimensional characteristics.[47,51] On the other hand, for sufficiently deep pits, the diffusion length is effectively the same as the pit depth, permitting better approximation of the mass transport behavior of the system by one-dimensional diffusion.

Figure 1.18 compares the experimental flux obtained from the technique to the theoretical flux as a function of the reciprocal of the pit depth expected based on cation transport for 316L and 17-4 PH. Values for physicochemical parameters of the metal cation were assumed to be those of Fe^{+2} (for instance, the cation diffusion coefficient was approximated by $D_{\text{ferrous ion}} = 8.24 \times 10^{-}6$ cm^2/s, and C_{sat} = 4.2 M) as considered by literature studies[47,57,105,147] that had also considered mass transport in corroding one-dimensional stainless steel pits. The $(i \cdot x)_{\text{saltfilm}}$ value of 0.836 A/m obtained for 316L was consistent with the results reported by Woldemedhin *et al.*[147] for austenitic stainless steels in chloride solutions. In the case of 17-4 PH, the $(i \cdot x)_{\text{saltfilm}}$ value of 0.763 A/m was lower than that of 316L. Figure 1.18 (b) shows that the data for 17-4 PH follows the theoretical calculation based on Fe^{+2} diffusion closely. A lower $(i \cdot x)_{\text{saltfilm}}$ value corresponds to a lower diffusion flux, a result that can be rationalized based on the fact that 17-4 PH has a lower Ni content than 316L. Furthermore, based on the *in situ* X-ray work of Isaacs *et al.*,[105] Ni is also depleted in the saturated solution, resulting in a further decrease in the concentration gradient. As a result, the cation transport behavior in the 17-4 PH system would be expected to be closer to the case approximated by ferrous ion diffusion. Conversely for 316L, a higher Ni content in the alloy implies that the concentration gradient is not as depleted as the 17-4 PH case, resulting in a higher diffusion flux. Furthermore, it is likely that the value of C_{sat} used was not appropriate for 316L, given the higher Ni content produced by dissolution. The value suggested by Isaacs *et al.*[105] (5.02 M) from *in situ* X-ray studies may be more suitable. These analyses illustrate the utility of the proposed technique in obtaining statistical data from pits of various depths, from which kinetic information can be extracted. These results are systematically evaluated in greater detail in Chapter 2, in the light of the dimensionality of flux emanating from a 1–D pit modeled as a function of geometry. This analysis provides an understanding of the pit

depths to access in order to obtain data truly representative of 1-D cation transport isolated from the effects of the bulk electrolyte.

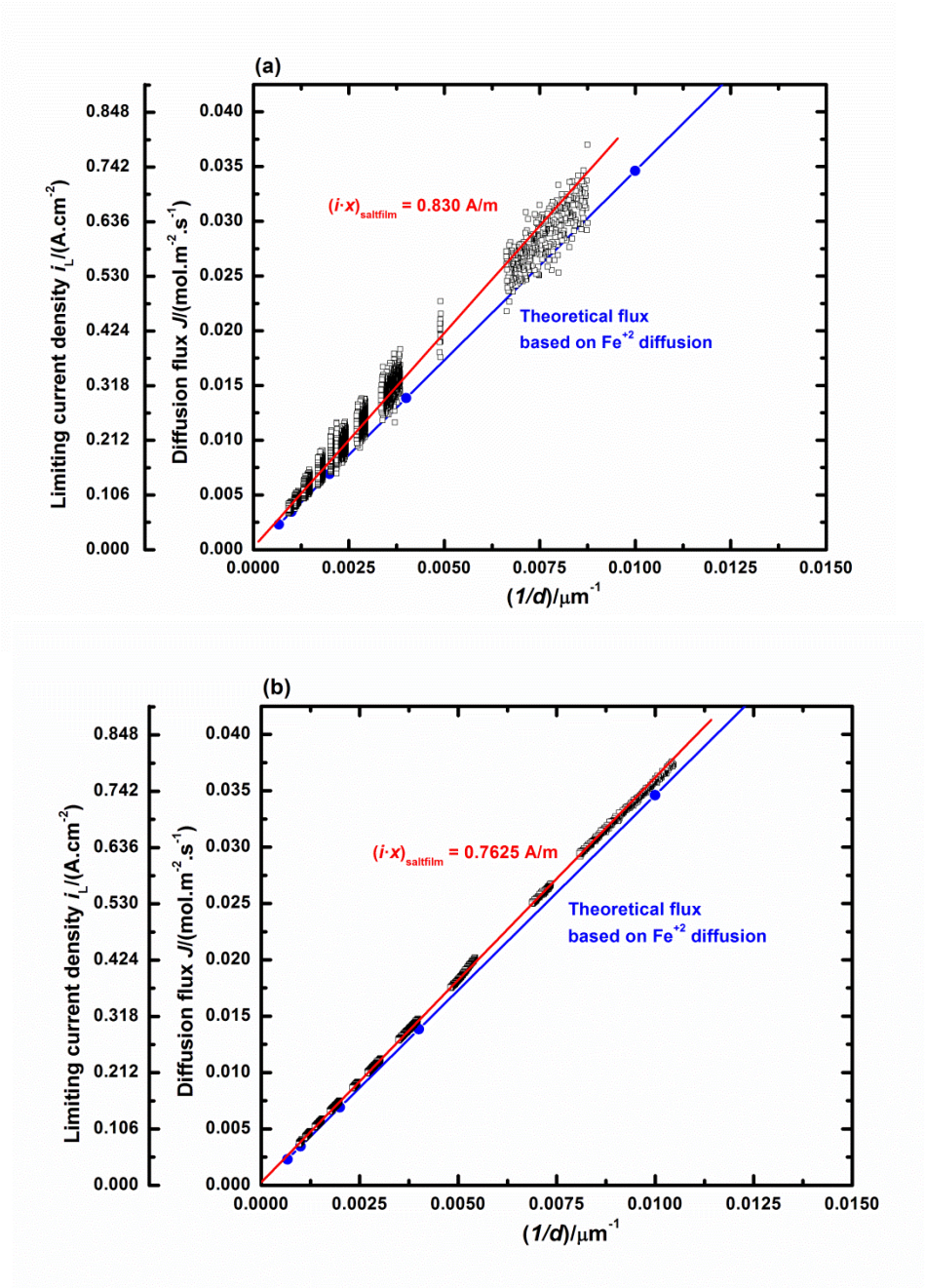

Figure 1.18. Comparison of experimental flux with theoretical one-dimensional diffusion flux based on Fe^{+2} as a function of the reciprocal of the pit depth for (a) 316L (b) 17-4 PH.[146]

1.10. Summary

Despite their dependence on the same processes happening at the corroding surface, pit stability and repassivation have not been investigated in concert using a quantitative mechanistic framework. This chapter introduces the work of this dissertation, which is focused on developing such a unified framework that connects the critical factors describing both pit stability and repassivation. The current literature is reviewed and topics that require further investigation in the light of this framework are identified. The necessity of a synergistic consideration of critical factors is reinforced in terms of a fundamental electrochemical standpoint as well as an engineering design perspective. Finally, an overview of the dissertation is provided with respect to the general experimental approach adopted and the phenomenological aspects of pit stability and repassivation that will be rationalized using the quantitative framework are briefly discussed.

1.11. References

1. U. R. Evans, *Journal of the Chemical Society*, 1020–1040 (1927).

2. Z. Szklarska-Smialowska, *Pitting and Crevice Corrosion*, NACE International, Houston, TX, (2005).

3. U. R. Evans, *Journal of the Chemical Society*, 92–110 (1929).

4. U. R. Evans, *Journal of the Chemical Society*, 478–492 (1930).

5. C. Edeleanu and U. R. Evans, *Trans. Faraday Soc.*, **47**, 1121–1135 (1951).

6. N. D. Greene and G. Judd, *Corrosion*, **21**, 15–18 (1965).

7. T. P. Hoar, *Corrosion Science*, **7**, 341–355 (1967).

8. W. D. France and N. D. Greene, *Corrosion*, **26**, 1–4 (1970).

9. J. A. Smith, M. H. Peterson, and B. F. Brown, *Corrosion*, **26**, 539–542 (1970).

10. J. Mankowski and Z. Szklarska-Smialowska, *Corrosion Science*, **15**, 493–501 (1975).

11. J. R. Galvele, *Journal of The Electrochemical Society*, **123**, 464–474 (1976).

12. I. L. Rosenfeld, I. S. Danilov, and R. N. Oranskaya, *Journal of The Electrochemical Society*, **125**, 1729–1735 (1978).

13. J. R. Galvele, *Corrosion Science*, **21**, 551–579 (1981).

14. H. S. Isaacs, *Corrosion Science*, **29**, 313–323 (1989).

15. J. M. Kolotyrkin, *Corrosion*, **19**, 261t–268t (1963).

16. F. Cui, F. J. Presuel-Moreno, and R. G. Kelly, *Corrosion Science*, **47**, 2987–3005 (2005).

17. T. P. Hoar and U. R. Evans, *J. Electrochem. Soc.*, **99**, 212–218 (1952).

18. W. Schwenk, *Corrosion*, **20**, 129t–137t (1964).

19. T. P. Hoar, D. C. Mears, and G. P. Rothwell, *Corrosion Science*, **5**, 279–289 (1965).

20. P. Marcus, Ed., *Corrosion Mechanisms in Theory and Practice*, Second., Marcel Dekker, Inc., New York, NY, (2002).

21. R. G. Kelly, J. R. Scully, D. W. Shoesmith, and R. G. Buchheit, *Electrochemical Techniques in Corrosion Science and Engineering*, CRC Press, Boca Raton, FL, (2003).

22. J. R. Ambrose and J. Kruger, *Corrosion*, **28**, 30–35 (1972).

23. W. J. Rudd and J. C. Scully, *Corrosion Science*, **20**, 611–631 (1980).

24. R. M. Carranza and J. R. Galvele, *Corrosion Science*, **28**, 233–249 (1988).

25. J. R. Galvele, R. M. Torresi, and R. M. Carranza, *Corrosion Science*, **31**, 563–571 (1990).

26. Z. Szklarska-Smialowska, *Corrosion*, **27**, 223–233 (1971).

27. Y. Hisamatsu, *Pitting Corrosion of Stainless Steels in Chloride Solution* R. W. Staehle and H. Okada, Editors, p. 99, NACE, Houston, TX, (1976).

28. S. M. Gravano and J. R. Galvele, *Corrosion Science*, **24**, 517–534 (1984).

29. I. Epelboin, C. Gabrielli, M. Keddam, and H. Takenouti, *Zeitschrift für physikalische Chemie (Neue Folge)*, **98**, 215–232 (1975).

30. I. Epelboin, C. Gabrielli, and M. Keddam, *Corrosion Science*, **15**, 155–171 (1975).

31. R. C. Newman, M. A. A. Ajjawi, H. Ezuber, and S. Turgoose, *Corrosion Science*, **28**, 471–477 (1988).

32. A. Anderko, N. Sridhar, and D. S. Dunn, *Corrosion Science*, **46**, 1583–1612 (2004).

33. A. Anderko, F. Gui, L. Cao, N. Sridhar, and G. R. Engelhardt, *Corrosion*, **71**, 1197–1212 (2015).

34. G. S. Frankel, L. Stockert, F. Hunkeler, and H. Boehni, *Corrosion*, **43**, 429–436 (1987).

35. P. C. Pistorius and G. T. Burstein, *Philosophical Transactions: Physical Sciences and Engineering*, **341**, 531–559 (1992).

36. T. Suzuki, M. Yamabe, and Y. Kitamura, *Corrosion*, **29**, 18–22 (1973).

37. T. R. Beck, *Journal of The Electrochemical Society*, **126**, 1662 (1979).

38. T. R. Beck, *Electrochimica Acta*, **29**, 485–491 (1984).

39. N. Sato, *Journal of The Electrochemical Society*, **129**, 260–264 (1982).

40. T. Hakkarainen, in *Corrosion Chemistry within Pits, Crevices and Cracks*, A. Turnbull, Editor, p. 17–26, Her Majesty's Stationery Office, London, United Kingdom (1987).

41. R.-D. Grimm and D. Landolt, *Corrosion Science*, **36**, 1847–1868 (1994).

42. P. R. Rhodes, *Corrosion*, **25**, 462–472 (1969).

43. J. W. Oldfield and W. H. Sutton, *British Corrosion Journal*, **13**, 104–111 (1978).

44. T. R. Beck, *Journal of The Electrochemical Society*, **120**, 1317–1324 (1973).

45. J. W. Tester and H. S. Isaacs, *Journal of The Electrochemical Society*, **122**, 1438–1445 (1975).

46. R. C. Newman and H. S. Isaacs, *Journal of The Electrochemical Society*, **130**, 1621–1624 (1983).

47. G. T. Gaudet et al., *AIChE J.*, **32**, 949–958 (1986).

48. H. S. Isaacs, *J. Electrochem. Soc.*, **120**, 1456–1462 (1973).

49. F. Hunkeler, A. Krolikowski, and H. Böhni, *Electrochimica Acta*, **32**, 615–620 (1987).

50. R. C. Alkire and K. P. Wong, *Corrosion Science*, **28**, 411–421 (1988).

51. J. N. Harb and R. C. Alkire, *J. Electrochem. Soc.*, **138**, 2594–2600 (1991).

52. N. J. Laycock and R. C. Newman, *Corrosion Science*, **39**, 1771–1790 (1997).

53. K. J. Vetter and H. H. Strehblow, in *Localized Corrosion*, R. W. Staehle, B. F. Brown, J. Kruger, and A. Agrawal, Editors, p. 240, NACE, Houston (1974).

54. H.-H. Strehblow and M. B. Ives, *Corrosion Science*, **16**, 317–321 (1976).

55. G. T. Burstein, P. C. Pistorius, and S. P. Mattin, *Corrosion Science*, **35**, 57–62 (1993).

56. R. C. Newman and E. M. Franz, *Corrosion*, **40**, 325–330 (1984).

57. P. Ernst and R. C. Newman, *Corrosion Science*, **49**, 3705–3715 (2007).

58. U. Steinsmo and H. S. Isaacs, *Corrosion Science*, **35**, 83–88 (1993).

59. J. N. Harb and R. C. Alkire, *Corrosion Science*, **29**, 31–43 (1989).

60. J. N. Harb and R. C. Alkire, *J. Electrochem. Soc.*, **138**, 3568–3575 (1991).

61. G. S. Frankel, *J. Electrochem. Soc.*, **145**, 2186–2198 (1998).

62. S. Brennert, *Journal of the Iron and Steel Institute*, **35**, 101 (1937).

63. H. P. Leckie and H. H. Uhlig, *Journal of The Electrochemical Society*, **113**, 1262–1267 (1966).

64. J. Horvath and H. H. Uhlig, *Journal of The Electrochemical Society*, **115**, 791 (1968).

65. H. P. Leckie, *Journal of The Electrochemical Society*, **117**, 1152 (1970).

66. Z. Szklarska-Smialowska and M. Janik-Czachor, *Corrosion Science*, **11**, 901–914 (1971).

67. N. Pessall and C. Liu, *Electrochimica Acta*, **16**, 1987–2003 (1971).

68. B. E. Wilde, in *Localized Corrosion*, R. W. Staehle, B. F. Brown, J. Kruger, and A. Agarwal, Editors, p. 342–352, NACE, Houston, TX (1974).

69. M. Pourbaix, *Corrosion*, **26**, 431–438 (1970).

70. K. K. Starr, E. D. Verink, and M. Pourbaix, *Corrosion*, **32**, 47–51 (1976).

71. R. C. Newman, *Corrosion Science*, **23**, 1045–1046 (1983).

72. B. E. Wilde and E. Williams, *Electrochimica Acta*, **16**, 1971–1985 (1971).

73. *ASTM G61-86 Standard Test Method for Conducting Cyclic Potentiodynamic Polarization Measurements for Localized Corrosion Susceptibility of Iron-, Nickel-, or Cobalt-Based Alloys*, ASTM International, West Conshohocken, PA, (2009).

74. Z. Smialowska and M. Janik-Czachor, *British Corrosion Journal*, **4**, 138–145 (1969).

75. G. Herbsleb and W. Schwenk, *Corrosion Science*, **13**, 739–746 (1973).

76. N. G. Thompson and B. C. Syrett, *Corrosion*, **48**, 649–659 (1992).

77. G. S. Frankel, J. R. Scully, and C. V. Jahnes, *Journal of The Electrochemical Society*, **143**, 1834–1840 (1996).

78. D. W. Buzza and R. C. Alkire, *Journal of The Electrochemical Society*, **142**, 1104–1111 (1995).

79. B. A. Kehler, G. O. Ilevbare, and J. R. Scully, *Corrosion*, **57**, 1042–1065 (2001).

80. B. E. Wilde, *Corrosion*, **28**, 283–291 (1972).

81. K. J. Evans, L. L. Wong, and R. B. Rebak, in *ASME Pressure Vessels and Piping Conference*,, p. 137–149, The American Society of Mechanical Engineers, San Diego, CA (2004).

82. K. J. Evans et al., *JOM*, **57**, 56–61 (2005).

83. N. Sridhar and G. A. Cragnolino, *Corrosion*, **49**, 885–894 (1993).

84. D. S. Dunn, N. Sridhar, and G. A. Cragnolino, *Corrosion*, **52**, 115–124 (1996).

85. D. S. Dunn, G. A. Cragnolino, and N. Sridhar, *Corrosion*, **56**, 90–104 (2000).

86. S. Tsujikawa and Y. Hisamatsu, *Boshoku Gijutsu - Corrosion Engineering*, **29**, 37–40 (1980).

87. S. Tsujikawa and Y. Hisamatsu, in *Improvement of Corrosion Resistance of Structural Materials in Aggressive Media*, J. M. Kolotyrkin, Editor, Nauka Publishers, Moscow, Russia (1984).

88. S. Tsujikawa and S. Okayama, *Corrosion Science*, **31**, 441–446 (1990).

89. *ASTM G192-08 Standard Test Method for Determining the Crevice Repassivation Potential of Corrosion-Resistant Alloys Using a Potentiodynamic-Galvanostatic-Potentiostatic Technique*, ASTM International, West Conshohocken, PA, (2008).

90. H. W. Pickering and R. P. Frankenthal, *Journal of The Electrochemical Society*, **119**, 1297–1304 (1972).

91. H. W. Pickering, *Corrosion Science*, **29**, 325–341 (1989).

92. H. W. Pickering, *Journal of The Electrochemical Society*, **150**, K1 (2003).

93. S. Okayama, Y. Uesugi, and S. Tsujikawa, *Boshoku Gijutsu - Corrosion Engineering*, **36**, 157–167 (1987).

94. S. Okayama, S. Tsujikawa, and K. Kikuchi, *Boshoku Gijutsu - Corrosion Engineering*, **36**, 631–638 (1987).

95. G. Tormoen, N. Sridhar, and A. Anderko, *Corrosion Engineering, Science and Technology*, **45**, 155–162 (2010).

96. A. Anderko, N. Sridhar, and G. Tormoen, *Corrosion Engineering, Science and Technology*, **45**, 204–223 (2010).

97. L. Cao, A. Anderko, F. Gui, and N. Sridhar, *Corrosion*, 636–654 (2016).

98. T. Okada, *Journal of The Electrochemical Society*, **131**, 1026–1032 (1984).

99. Z. Y. Chen, F. Cui, and R. G. Kelly, *Journal of The Electrochemical Society*, **155**, C360–C368 (2008).

100. Z. Y. Chen and R. G. Kelly, *Journal of The Electrochemical Society*, **157**, C69–C78 (2010).

101. N. D. Greene and M. G. Fontana, *Corrosion*, **15**, 41–47 (1959).

102. A. Turnbull, *Corrosion Science*, **23**, 833–870 (1983).

103. G. Butler, H. C. K. Ison, and A. D. Mercer, *British Corrosion Journal*, **6**, 31–38 (1971).

104. M. Marek and R. F. Hochman, *Corrosion*, **30**, 208–210 (1974).

105. H. S. Isaacs, J.-H. Cho, M. L. Rivers, and S. R. Sutton, *Journal of The Electrochemical Society*, **142**, 1111–1118 (1995).

106. S. Brennert and G. Eklund, *Scandinavian Journal of Metallurgy*, **2**, 269–272 (1973).

107. G. Sandoz, C. T. Fujii, and B. F. Brown, *Corrosion Science*, **10**, 839 (1970).

108. D. A. Jones and B. E. Wilde, *Corrosion Science*, **18**, 631–643 (1978).

109. T. Suzuki and Y. Kitamura, *Corrosion*, **28**, 1–6 (1972).

110. K. C. Stewart, thesis, University of Virginia, Charlottesville, VA (1999).

111. A. Turnbull, *British Corrosion Journal*, **32**, 283–290 (1997).

112. K. R. Cooper, thesis, University of Virginia, Charlottesville, VA (2001).

113. C. Wagner and W. Traud, *Zeitschrift für Elektrochemie und angewandte physikalische Chemie*, **44**, 391–402 (1938).

114. U. R. Evans, *The Corrosion and Oxidation of Metals: Scientific Principles and Practical Applications,* 1st ed., Edward Arnold (Publishers) Limited, London, United Kingdom, (1960).

115. Y. Kondo, *Corrosion*, **45**, 7–11 (1989).

116. T. Mills, S. Prost-Domasky, K. Honeycutt, and C. Brooks, in *Corrosion Control in the Aerospace Industry*, S. Benavides, Editor, CRC Press LLC, Boca Raton, FL (2009).

117. D. W. Shoesmith, in *Electrochemical Techniques in Corrosion Science and Engineering*,, CRC Press, Boca Raton, FL (2003).

118. J. Smith, Z. Qin, F. King, L. Werme, and D. W. Shoesmith, *Corrosion*, **63**, 135–144 (2007).

119. M. T. Woldemedhin, M. E. Shedd, and R. G. Kelly, *Journal of the Electrochemical Society*, **161**, E3216–E3224 (2014).

120. J. Srinivasan, M. J. McGrath, and R. G. Kelly, *ECS Transactions*, **58**, 1–11 (2014).

121. S. M. Sharland, *Corrosion Science*, **27**, 289–323 (1987).

122. J. Soltis, *Corrosion Science*, **90**, 5–22 (2015).

123. T. Shibata and T. Takeyama, *Corrosion*, **33**, 243–251 (1977).

124. G. T. Burstein and P. C. Pistorius, *Corrosion*, **51**, 380–385 (1995).

125. G. T. Burstein and S. P. Vines, *J. Electrochem. Soc.*, **148**, B504–B516 (2001).

126. I. L. Rosenfeld and I. S. Danilov, *Corrosion Science*, **7**, 129–142 (1967).

127. N. Sridhar and D. S. Dunn, *Corrosion*, **50**, 857–872 (1994).

128. P. C. Pistorius and G. T. Burstein, *Corrosion Science*, **36**, 525–538 (1994).

129. D. E. Williams, J. Stewart, and P. H. Balkwill, *Corrosion Science*, **36**, 1213–1235 (1994).

130. S. T. Pride, J. R. Scully, and J. L. Hudson, *J. Electrochem. Soc.*, **141**, 3028–3040 (1994).

131. C. J. Semino, P. Pedeferri, G. T. Burstein, and T. P. Hoar, *Corrosion Science*, **19**, 1069–1078 (1979).

132. R. J. Brigham and E. W. Tozer, *Corrosion*, **29**, 33–36 (1973).

133. N. J. Laycock, M. H. Moayed, and R. C. Newman, *Journal of The Electrochemical Society*, **145**, 2622–2628 (1998).

134. N. J. Laycock and R. C. Newman, *Corrosion Science*, **40**, 887–902 (1998).

135. M. H. Moayed and R. C. Newman, *Journal of The Electrochemical Society*, **153**, B330–B335 (2006).

136. P. Ernst and R. C. Newman, *Corrosion Science*, **44**, 943–954 (2002).

137. A. B. Cook et al., *ECS Trans.*, **41**, 121–132 (2012).

138. H. H. Strehblow and J. Wenners, *Electrochimica Acta*, **22**, 421–427 (1977).

139. N. Sridhar and D. S. Dunn, *J. Electrochem. Soc.*, **144**, 4243–4253 (1997).

140. N. S. Zadorozne, C. M. Giordano, M. A. Rodríguez, R. M. Carranza, and R. B. Rebak, *Electrochimica Acta*, **76**, 94–101 (2012).

141. A. J. Sedriks, *Corrosion of Stainless Steels*, 2nd ed., John Wiley & Sons, Inc., New York, NY, (1996).

142. K. Lorenz and G. Medawar, *Thyssen Forschung*, **1**, 97–108 (1969).

143. R. F. A. Jargelius-Pettersson, *Corrosion*, **54**, 162–168 (1998).

144. L. F. Garfias-Mesias, J. M. Sykes, and C. D. S. Tuck, *Corrosion Science*, **38**, 1319–1330 (1996).

145. R. Rebak and P. Crook, in, p. 289–302 (1999).

146. J. Srinivasan, M. J. McGrath, and R. G. Kelly, *J. Electrochem. Soc.*, **162**, C725–C731 (2015).

147. M. T. Woldemedhin, J. Srinivasan, and R. G. Kelly, *Journal of Solid State Electrochemistry*, **19**, 3449–3461 (2015).

148. J. Srinivasan and R. G. Kelly, *Corrosion*, **70**, 1172–1174 (2014).

149. R. C. Newman, *Corrosion Science*, **25**, 341–350 (1985).

150. R. C. Newman and H. S. Isaacs, in *Passivity of Metals and Semiconductors: Proceedings of the Fifth International Symposium on Passivity, Bombannes, France*, M. Froment, Editor, Elsevier Science Publishing Company Inc., New York, NY (1983).

151. R. H. Heidersbach and E. D. Verink, *Corrosion*, **28**, 397–418 (1972).

152. W. R. Heineman and P. T. Kissinger, *Laboratory Techniques in Electroanalytical Chemistry* P. T. Kissinger and W. R. Heineman, Editors, Marcel Dekker, Inc., New York, NY, (1984).

153. J. Jun, G. S. Frankel, and N. Sridhar, *J Solid State Electrochem*, **19**, 3439–3447 (2015).

Chapter 2

2.1. Overview

This chapter describes the mass transport characteristics of flux emanating from one-dimensional (1-D) pits with particular focus on the effects of pit depth and bulk electrolyte concentration. The results emerging from high-throughput artificial pit techniques that outlined the utility in accessing a wide range of pit depths so that pit stability data truly representative of 1-D transport may be obtained (described briefly in the introductory chapter) are expanded upon. This chapter quantitatively determines the minimum pit depth (normalized over pit diameter) that has to be attained for data to correspond to 1-D flux isolated from the effects of the bulk electrolyte and therefore characteristic of the cation concentration gradient within the pit. Finally, these results provide insight into explaining the observed behavior of repassivation potential with pit depth, which is employed in the development of the quantitative framework relating pit stability and repassivation described in detail in Chapter 3.

An original research article based on this chapter has been published in the Journal of The Electrochemical Society, and can be accessed by the following description:

J. Srinivasan, C. Liu, and R. G. Kelly, *Geometric Evolution of Flux from a Corroding One-dimensional Pit and its Implications on the Evaluation of Kinetic Parameters for Pit Stability.* ***Journal of The Electrochemical Society*** 163, 10 (2016): pp. C694-C703.

Respective author contributions:
Srinivasan: Manuscript author, experimental data collection, analysis, and interpretation of pit depth and bulk electrolyte dependence of pit stability phenomenology, development of diffusive transport rationale for repassivation phenomenology with pit depth.

Liu: FEM model setup, geometry construction, simulation implementation and data collection.

2.2. Abstract

The flux from a one-dimensional (1-D) artificial pit electrode corroding under a salt film was examined using experimental and modeling techniques. Finite element simulations showed that the flux at shallow depths was consistently lower than theoretical calculations for 1-D diffusion. This deviation was due to a substantial contribution of the external hemispherical boundary layer to the overall diffusion length. Increasing the pit diameter resulted in a larger boundary layer, which in turn affected the flux characteristics to greater depths. Data from experiments and simulation converged with the theoretical 1-D calculations only when pit depths approached nearly ten times the pit diameter. The experimental data from this study as well as data from related published work were observed to span the range bounded by the simulated and the theoretical flux predictions. Comparison with published pit stability phenomenology showed that only deep pits provided kinetic data based on the cation concentration gradient unadulterated by bulk chloride effects. Finally, this work also provided insight into the origin of the dependence of the measured repassivation potential with pit depth, contributing towards a quantitative framework relating the various critical factors governing pitting.

2.3. Introduction

The stable growth of corrosion pits requires the presence of aggressive chemistry at the corroding surface as characterized by a high metal chloride concentration and low pH[1,2]. The conditions leading to the maintenance of such chemistry were mathematically considered by Galvele[3] through an investigation of the steady state relationship between metal dissolution and mass transport[4,5] out of a one-dimensional (1-D) pit. For the case of a 1-D pit, it was theoretically demonstrated that a minimum critical value of cation flux – expressed as the product of the current density and the pit depth, ($i \cdot x$) – was necessary for the pit to maintain a critical chemistry and thus stably corrode. As such, should the product of the current density and the pit depth fall below this critical value, repassivation would set in. Subsequent studies on stainless steel pitting referred to this parameter and equivalent relationships for other pit geometries as the pit stability product[6,7]. This critical pit stability product (denoted $(i \cdot x)_{crit}$) has been employed as the anodic stability parameter to determine the maximum pit size that can be attained on a particular metal surface in a given corrosive environment[8–11].

Experimental results obtained using the artificial pit or lead-in-pencil electrode[12–17] can be directly used to study 1-D dissolution kinetics because the construction of this electrode results in inert walls surrounding a single active surface[13,14,16] corroding under a precipitated salt film[18–24] upon the application of high anodic potential in corrosive solution. The presence of the salt film results in diffusion-limited dissolution conditions that permit the study of the corroding system in a quasi-steady state. The pit stability product under a salt film, $(i \cdot x)_{saltfilm}$ can then be extracted[13,14,25–28] from measuring the diffusion-limited current density at different depths. The critical pit stability product can then be expressed as a fraction of this measured pit stability parameter $(i \cdot x)_{saltfilm}$.[29,30]

Pit stability data collected from experiments at shallow pit depths may possess three-dimensional characteristics due to the influence of the external hemispherical boundary layer at the pit mouth[14,31]. The value of high-throughput artificial pit techniques in accessing a wide range of pit depths to obtain kinetic data and therefore avoid this problem has been previously reported[28]. It is necessary however to consider in detail, the dependence of flux on geometric variables in order to ensure that pit stability data extracted from artificial pit experiments does indeed correspond to true 1-D transport. An analysis of this nature would assist in judicious selection of the experimental parameter space (pit diameter, pit depth, concentration of bulk electrolyte) within which pit stability data can be properly collected and interpreted.

The utilization of finite element modeling permitted the rapid generation of flux characteristics by varying specific geometric parameters of a 1-D pit, similar in approach to the work performed on hemispherical pits conducted by Harb and Alkire[31]. A systematic treatment of the flux response to pit geometry in this manner evaluated the minimum depth that had to be attained in order to obtain artificial pit data truly representative of 1-D mass transport. Furthermore, the data from deep pits reflected pit stability kinetics isolated from effects of the bulk chloride environment, thus affording better agreement of experimental measurements with the theoretical basis of the Galvele anodic criteria. Finally, the results of this study provide a scientifically defendable rationale for the empirical observation of a plateau in the measured repassivation potential for deep pits,[27,28,32,33]thereby assisting in the development of a quantitative framework[30,34] that connects electrochemical parameters critical to both pit stability and repassivation.

2.4. Experimental

Mass Transport Modeling

In order to evaluate the flux characteristics in terms of pit geometry, diffusion kinetics of an artificial pit electrode were modeled based on a two-dimensional pit geometry using the COMSOL Multiphysics® v5.2 (COMSOL, Inc., Burlington, MA) software. Figure 2.1 illustrates this model for the following conditions under which the steady state mass transport of the system was allowed to evolve.

- The flux in the system was considered to be axisymmetrical with respect to the z-axis as shown.

- The initial concentration at the bottom of the pit C (z = 0, t = 0) = C_{sat} where C_{sat} is the concentration of the '316L cation' at saturation. The value of C_{sat} used was 5.02 M from *in situ* X-ray studies by Isaacs *et al*.[35] on saturated solutions of 18-8 stainless steel in chloride media.

- The concentration far away from the pit mouth (representing bulk solution) was set to zero for all time, i.e., $C(z \to \infty, t) = 0$. This distance from the pit mouth was considered to be 10 cm in the simulations, which was two orders of magnitude larger than the deepest pit simulated.

- An initial linear concentration gradient was considered inside the pit, i.e., $C(z, t = 0) = C_{sat} \frac{z}{d}$.

- The walls of the pit were considered to be inert, i.e., the flux across these boundaries was set to zero for all time.

- A constant diffusion coefficient D was assumed; the value used was 8.24×10^{-6} cm^2/s as employed by Gaudet *et al.*[14] based on $FeCl_2$ diffusion in 1 M HCl. This value is a reasonable approximation because it is within the range of the values of 7×10^{-6} cm^2/s to 1×10^{-5} cm^2/s reported for D in other 1-D pit studies in the literature. [26,27,29,36] Also, the assumption of constant diffusivity has been shown by Gaudet *et al.*[14] to effectively approximate the combined effects of variable diffusivity and electromigration on the cation flux. Finally, accounting for variable D and electromigration would be more representative of actual mass transport conditions, but the effects of these individual variables tend to counter each other, resulting in a situation where their net influence on the flux is approximated within an error of 10% by assuming a constant value for D[14].

The steady-state flux data for this system were extracted by integrating the individual flux elements along the z-direction and dividing by the cross-sectional area of the pit. This provides an average value of the flux across the corroding surface. Simulations were run until differences in calculations from consecutive iterations as determined by the FEM software's built-in *a posteriori* error estimation capability decreased to less than the threshold tolerance of 0.1%.

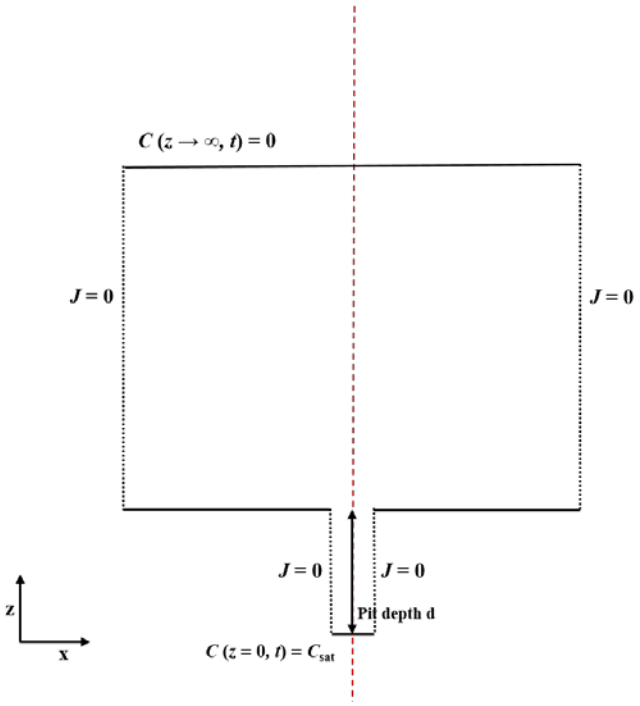

Figure 2.1. Geometry of system considered in this study – the mass transport generated in the pit as a result of continuous steady state dissolution under a salt film is modeled (diagram not to scale). The dotted lines indicate the walls of the pit and the boundaries of the domain across whose areas there is zero (inert boundaries). The boundary far away from the pit mouth ($z \rightarrow \infty$) is set as a finite distance which is 10 times the depth of the deepest pit modeled. The pit mouth is considered to be where the pit meets the bulk domain. The mass transport characteristics are considered along the z-axis (dotted line perpendicular to the pit cross-section), as indicated. The origin (0, 0) is considered to be at the center of the pit base. Mass transport is axisymmetrical around the z-axis.

Artificial pit experiments

The 1-D artificial pit (lead-in-pencil) electrode was constructed using 316L stainless steel wire (California Fine Wire Company, Grover Beach, CA) of diameter 50.8 μm cast in epoxy.

The composition of the wires used is shown in Table 2.1. The electrode surface was polished to a surface finish of 320 grit with SiC abrasive paper and placed upright in a test cell containing unbuffered 0.6 M NaCl solution. The exposed area of the electrode was 2.03×10^{-5} cm^2. A saturated calomel reference electrode (SCE) and a platinum mesh counter electrode were utilized for all the tests. All electrochemical testing was carried out at an average ambient temperature of 22 °C using a Bio-Logic SP-200 (Bio-Logic SAS, Claix, France) potentiostat.

Alloy	C	Mn	P	S	Si	Cr	Ni	Mo	N	Cu	Fe
316L	0.019	1.356	0.030	0.0287	0.406	17.07	10.66	2.16	0.0499	0.232	67.98

Table 2.1. Composition of stainless steel wire used (all values in weight percent). Composition provided by vendor was confirmed by quantitative speciation using inductively coupled plasma optical emission spectroscopy (ICP-OES).

Pitting was initiated by applying a potential of +750 mV_{SCE} for a short duration (2 to 5 minutes) and then propagated to various depths by applying a lower potential of +450 mV_{SCE} for different periods of time. This sequence was followed by a rapid cathodic polarization scan at 5 mV/s to a final potential of −100 mV_{SCE} in order to obtain an estimate of the diffusion-limited dissolution current density i_L. Variants of this procedure to measure i_L have been employed in other pitting studies as well[27,28]. This dissolution current density was converted to a flux value J as shown in Equation 2.1.

$$J = \frac{i_L}{zFD} = \frac{\Delta C}{d} \Rightarrow J \propto \frac{1}{d} \quad \ldots\ldots\ldots\ldots\ldots\ldots\ldots\ldots (2.1)$$

where z is the number of electrons transferred during the oxidation reaction (2.2), D is the diffusion coefficient of the cation species (8.24×10^{-6} cm^2/s), and F is Faraday's constant (96,485 C/mol-equivalent). One-dimensional mass transport with the pit depth as the diffusion length would therefore be indicated as a straight line on a plot of J versus $(1/d)$[14,18,25,28]. These values have been taken from several sources in the literature on stainless steel dissolution in chloride media[14,25,26,28,29,36]. The pit depth d was calculated by converting the charge density passed during the potentiostatic hold and the polarization scan using Faraday's law, as indicated in similar experiments reported in the literature[27,28].

ΔC is the concentration gradient of the cation across the pit depth. *Theoretically*, following the literature on stainless steel pitting, the cation concentration at the pit base is considered to be at the saturation concentration of either a stoichiometric combination of the chlorides of Fe^{+2}, Cr^{+3}, and Ni^{+2}, or only $FeCl_2$; the cation concentration at the pit mouth is considered to be zero[3,13,14,25,29,35].

A separate set of artificial pit experiments as described above were also performed on the sample with the exposed surface facing downward, in both quiescent and stirred 0.6 M NaCl solution. The stirring rates employed were 75 rpm (low) and 300 rpm (high). These configurations were employed to study the effect of boundary layer thickness on the kinetics of the system due to either natural or forced convection[37,38]. The experimental procedure described was also performed on a separate sample with the exposed surface facing upward in quiescent 0.6 M HCl solution (measured pH = 0.58) which would prevent the precipitation of any corrosion product at the pit mouth (as predicted using thermodynamic modeling by the OLI Analyzer Studio 9.2 software (OLI Systems, Inc., Cedar Knolls, NJ)). This latter test served to

observe what effects, if any, the possible deposition of corrosion products at the pit mouth[39] may have had on the mass transport of the system in the neutral, unbuffered chloride solution.

2.5. Results

Figure 2.2 plots the simulated flux as a function of pit depth for two different pit diameters. The slopes of the curves as pit depth increases provide a preliminary idea about the nature of mass transport for the two cases. The decrease in flux is very steep for the 50 µm diameter pit as it approaches 500 µm, indicating that theoretical 1-D mass transport based on the pit depth as the diffusion length is closely approximated beyond this depth. For the 1 mm diameter pit however, there is no such distinct transition, in addition to the overall flux across depths being quite low.

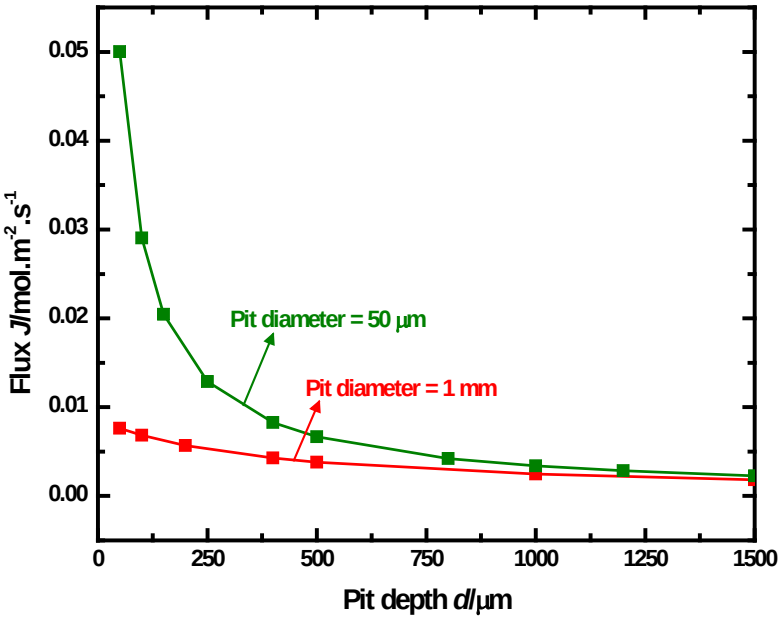

Figure 2.2. Simulated flux results obtained using model geometry for pit diameters of 50 µm and 1 mm, mapped versus the pit depth.

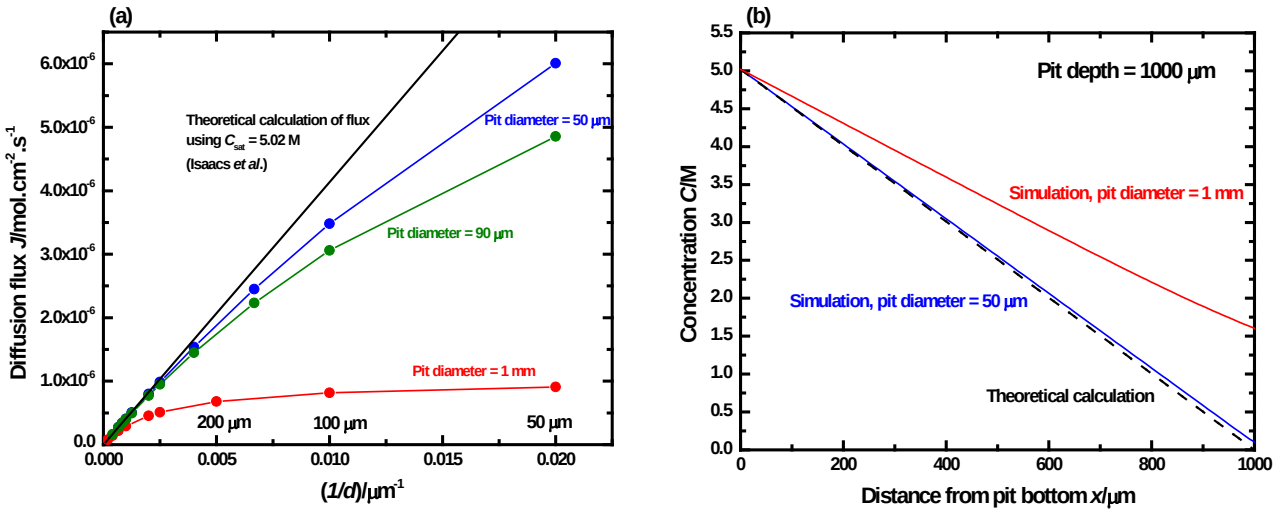

Figure 2.3. Simulated results for different pit diameters in comparison with theoretical calculations. (a) Variation of flux with the reciprocal of pit depth, as an indication of dimensionality of mass transport. Note that the theoretical calculation yields a straight line across the entire range of pit depths. The line is independent of pit diameter as indicated by the expression in Equation 1. The simulated results deviate from the theoretical line at shallow pit depths and clearly show a trend with pit diameter. (b) Concentration profile along the depth for two pits of the same depth but of different diameters. The zero on the abscissa refers to the pit base.

Figure 2.3 (a) shows a plot of the simulated flux results versus the reciprocal of the pit depth for three different pit diameters. These results were obtained by running the simulation on the geometry described previously using values of 5.02 M for C_{sat}[35] and 8.24×10^{-6} cm^2/s for D[13,14]. In Figure 2.3 (a), these simulations are compared with the theoretical expectation of 1-D flux, calculated using the same values for C_{sat} and D. A linear relationship between flux and the reciprocal of the pit depth is expected in the case of 1-D transport, as indicated in Equation 1;

this is the line that describes the theoretical 1-D flux in Figure 2.3 (a). It is evident from the plot that the simulated flux deviates from the theoretical calculation for shallow pits. This deviation decreases as the pit depth increases – pits of diameter 50 μm begin converging with the theoretical 1-D flux for pits deeper than 300 μm and are indistinguishable from the latter once pits of depth close to 1000 μm are attained. A similar trend is observed for a pit diameter of 90 μm – the convergence to the theoretical line begins around depths of 400 μm (equivalent to the steep decline in the slope of the J versus d seen in Figure 2.1) and the simulated and theoretical fluxes coincide for pit depths in the vicinity of 1000 μm. However, for the larger pit diameter of 1 mm, the simulated flux deviates greatly from the theoretical calculations and begins to converge only once depths of nearly 5 mm are attained. Figure 2.3 (b) illustrates this difference even more starkly with the simulated concentration profiles plotted along the pit depth for two 1 mm deep pits of different diameters. The simulated result for the 50 μm diameter pit agrees very well with the theoretical line, with the concentration at the pit mouth approaching zero. However, for the 1 mm diameter pit, the simulated results show that the concentration at the pit mouth has dropped to only around 30% of saturation (≈1.5 M), and therefore deviate from theoretically expected behavior at these depths.

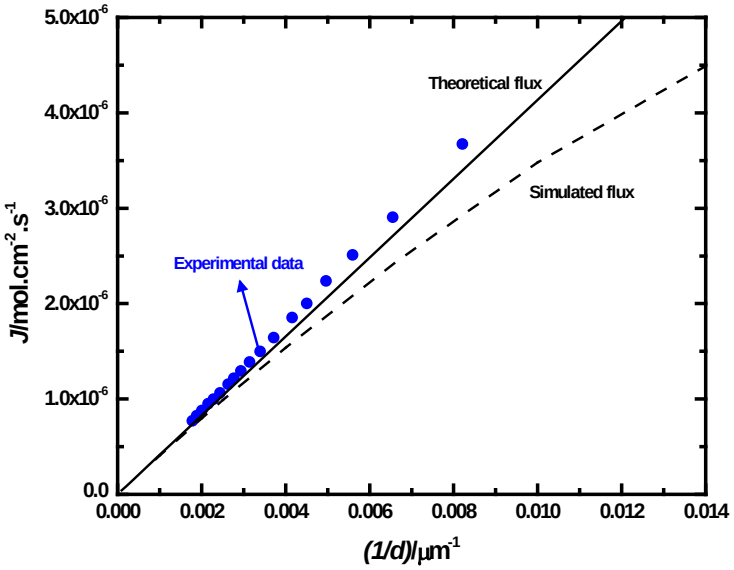

Figure 2.4. Experimental data in comparison with theoretical and simulated flux. Note that the three datasets begin to converge as pit depths approach 500 µm ((1/d) = 0.002 μm^{-1}).

Figure 2.4 shows that the experimental flux obtained from 50 µm diameter artificial pits of up to 500 µm deep match the theoretical expectations closely, even for shallow depths around 100 µm. In order to ensure that experimental conditions did not cause mass transport restrictions, the effect of convection and possible corrosion product deposition on the flux were explored. These results are shown in Figures 2.5 and 2.6, respectively, and indicate that the flux is not affected significantly by either of these modifications to the experimental conditions, with the results bounded by the simulations on the lower end and the theoretical line on the upper end. In each of these experiments, it is observed that as pits grow deeper, the experimentally observed flux converges to the theoretical estimate.

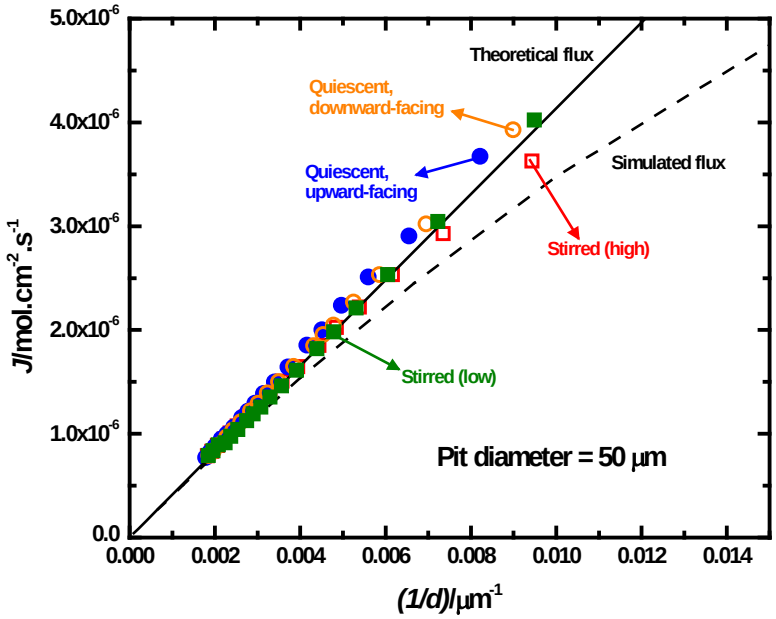

Figure 2.5. Investigation of any possible effects on mass transport by convective transport – natural (via gravity from the downward-facing configuration) and forced (stirring at 75 rpm (low) and 300 rpm (high) in addition to gravity).

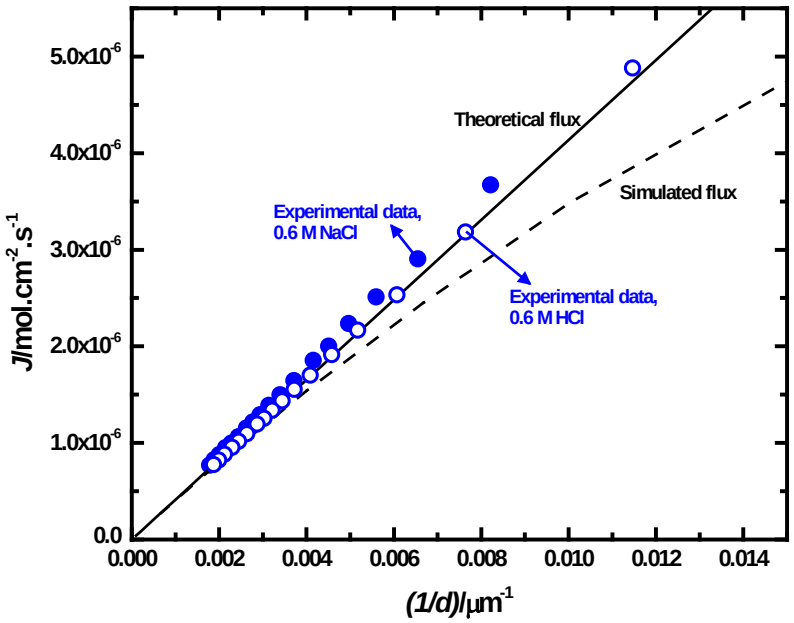

Figure 2.6. Examination of possible effects of corrosion products on mass transport. Note that there is no effect on the flux when an acidified electrolyte is employed, which would dissolve any corrosion products that would form otherwise in the neutral 0.6 M NaCl.

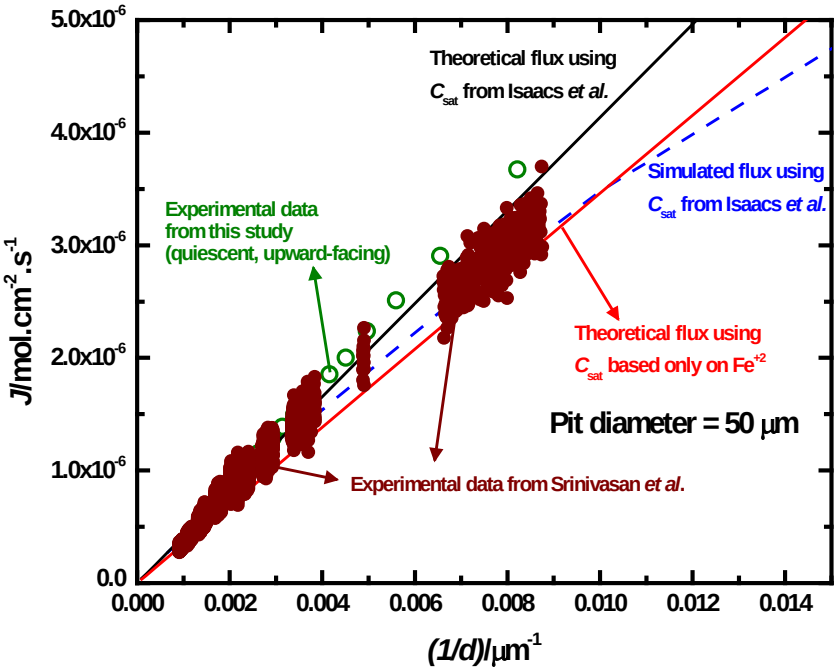

Figure 2.7. Comparison of experimental data from published high-throughput studies[28] with the datasets obtained in this study. Note that the experimental scatter is lower at deeper pits and converges with the theoretical, simulated, and the experimental data from this study, and that the theoretical line that considers only Fe^{+2} does not approximate the experimental data well.

In Figure 2.7, published high-throughput artificial pit experimental data[28] for 50 μm diameter pits are juxtaposed with the simulated flux as well as two theoretically calculated flux lines. The theoretical calculations differ only in terms of the value of C_{sat} used. The line with the higher slope utilizes the value of 5.02 M that results from observations by Isaacs *et al.*[35] based on the stoichiometric dissolution of the individual components of 18-8 stainless steel (Fe^{+2}, Cr^{+3}, and Ni^{+2}), whereas the line with the lower slope adopts 4.2 M as C_{sat} reported by Gaudet *et al.*[14] as well as by Ernst and Newman[29], based on the assumption that saturated $FeCl_2$ approximates the behavior of the concentration at the pit base. The experimental data are observed to span the region between the simulated flux and the theoretical flux based on 5.02 M for shallow pits, and

converge to the theoretical line for deep pits (> 400 μm). It was seen that theoretical calculations using C_{sat} data from stoichiometric dissolution bound the experimental data for 316L stainless steel better than if only $FeCl_2$ were considered. This result concurs with previous work[28] on the dissolution kinetics of 316L and 17-4 PH stainless steel artificial pits, indicating the C_{sat} value used in calculations needs to be based on stoichiometric dissolution. The experimental data obtained in this study from the different configurations considered also were found to be contained within the limits of scatter of the high-throughput data at all depths.

2.6. Discussion

This work presents a combined experimental and computational analysis of the effects of the pit depth on the measurement and evaluation of the pit stability parameter from artificial pit experiments from the perspective of 1–D mass transport. Possible effects of convection and corrosion products on the 1–D flux are taken into account, before parsing the results to elucidate the effects of the external boundary layer on mass transport with pit depth and diameter. Artificial pit data in the literature are considered to rationalize the effect of the effect of bulk [Cl^-] on pit stability in addition to pit depth. Finally, the observed behavior of repassivation potential on pit depth is quantitatively explained in the context of steady state 1–D transport, using the results of this study.

Mass transport is unaffected by bulk convection and corrosion products at pit mouth

The results of artificial pit experiments performed with configurations designed to examine the effects of both natural and forced convective flow, demonstrated that these modifications had no substantial effect on the flux, as shown in Figure 2.5. Work on rescaled crevices by Lee *et al*.[40] was leveraged to ensure that effects due to gravity were countered by capillary forces and did not lead to momentum transfer within the pit (Figure 2.8). The results shown in Figure 2.5 were consistent with the interpretation provided in published hydrodynamic studies on pitting[39,41] that external fluid flow has little effect on narrow cavities as opposed to shallow ones. The possibility of mass transport effects due to corrosion product precipitation (which may be likely in the neutral chloride solution when the cations encounter a higher pH at the pit mouth) can be rejected based on the results shown in Figure 2.6. These results demonstrated that performing the same experiment in media in which the bulk pH would be too low for such corrosion products to precipitate does not lead to a considerable change in flux. On the basis of these results, mass

transport effects observed in the system can therefore be examined solely on the basis of a dependence on pit depth.

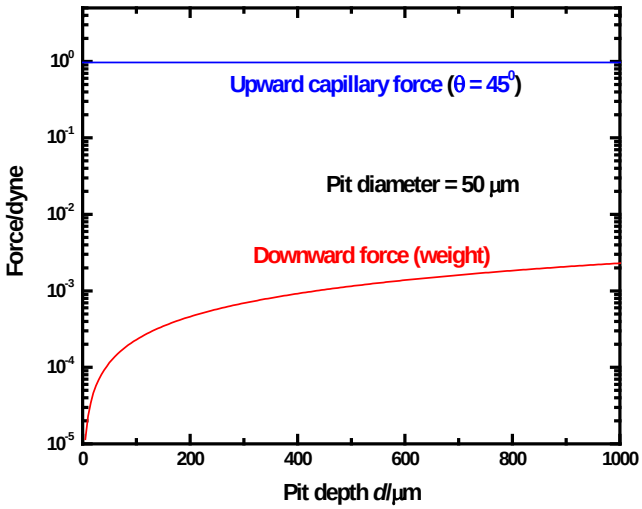

Figure 2.8. Balance of forces within pit cavity for the experiments performed in configurations examining the effects of convection on mass transport, with the sample facing downward. Note that the capillary force (acting upward) are greater than the weight of the solution within the pit (acting downward) by at least three orders of magnitude across all pit depths attained. The capillary force was calculated for a contact angle of 45°.

External hemispherical boundary layer affects mass transport of shallow pits

The deviation from linearity at shallow pit depths displayed by the simulated flux results can be attributed to the effect of the external hemispherical boundary layer on the total diffusion length[31]. The deviation from the theoretical expectation therefore occurs because the pit depth

alone does not approximate the total diffusion length for shallow pits. The hemispherical boundary layer influences the mass transport because the cation concentration outside the pit does not immediately vanish at the pit mouth. Instead, this change in concentration occurs across a finite length; for shallow pits, this additional length is comparable to and sometimes much larger than the pit depth, as shown in Figure 2.9.

The consequence of this effect is that the mass transport follows a behavior expressed in terms of a modified version of Equation 2.1:

$$J = \frac{i_L}{zFD} = \frac{\Delta C}{d+\delta} \Rightarrow J \propto \frac{1}{d+\delta} \quad \ldots\ldots\ldots\ldots\ldots\ldots\ldots\ldots (2.2)$$

where δ represents the effect of the boundary layer on the overall diffusion length. The value of δ can be calculated using Equation 2.2 from the simulated data. As Figure 2.9 (a) indicates, δ is dependent only on the pit diameter and does not change as the pit depth increases. When normalized in terms of the pit diameter, δ assumed relatively constant values equal to approximately 40% of the pit diameter across the range of pit depths studied (Figure 2.9 (b)). Finally in Figure 2.9 (c), when visualized as a fraction of the pit depth, it is abundantly clear that for the larger pit diameter, the effect of the boundary layer is massive for shallow pits. At these depths, δ contributes disproportionately to the overall diffusion length because it is nearly three orders of magnitude greater than the pit depth. Conversely, as pits grow deeper, the effect of δ on the overall diffusion length diminishes greatly, as is made distinctly apparent in the figure. In fact, at pit depths where the simulated flux is seen to converge with the theoretical calculations, δ is less than 2% of the pit depth. Therefore, for deep pits, the relative influence of δ vanishes and utilizing the pit depth alone serves as a good approximation for the overall diffusion length.

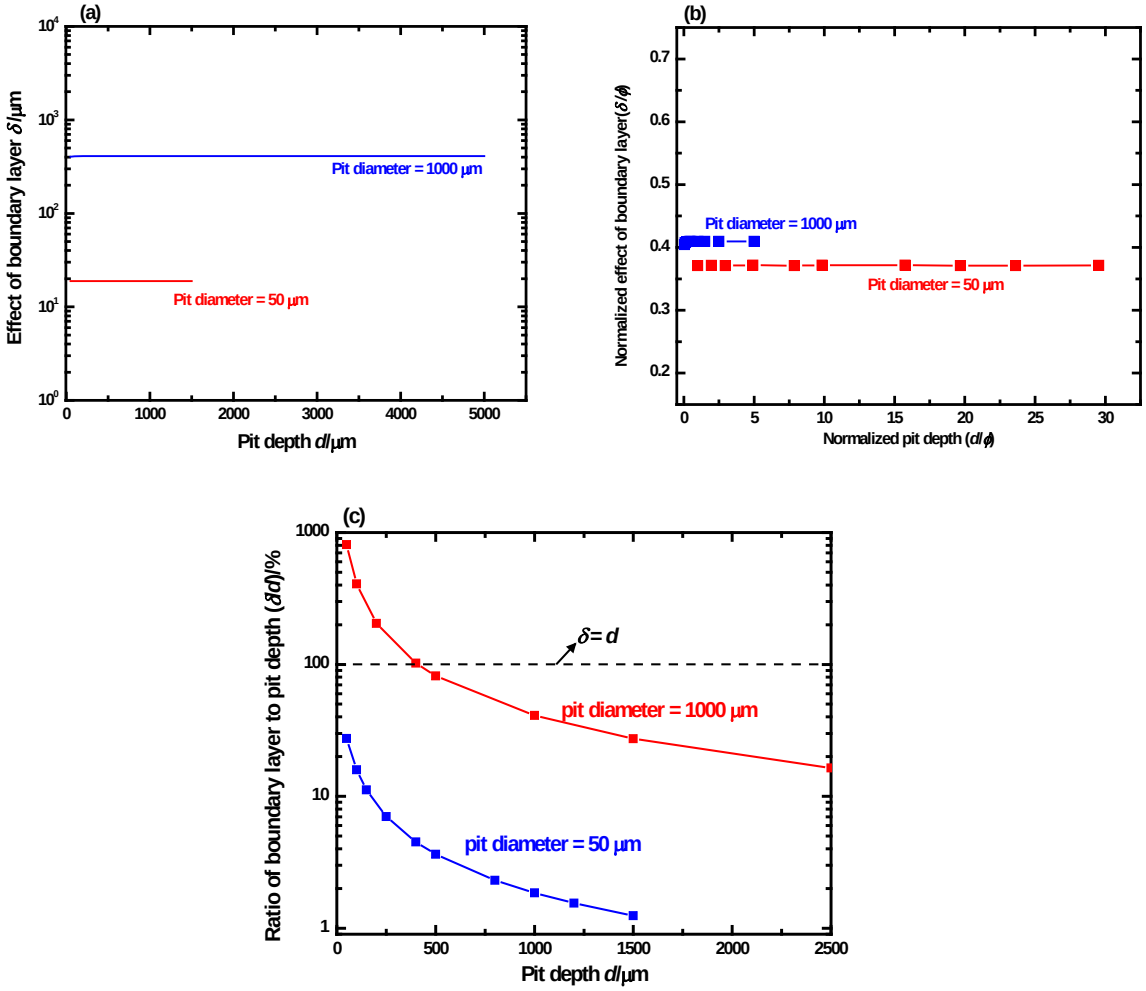

Figure 2.9. Effect of the boundary layer δ on the overall diffusion length across pit depths for pits of different diameters. (a) Absolute value of δ across pit depths. Note the logarithmic scale on the ordinate – the dependence of δ on pit diameter is evident in this comparison. (b) Effect of the boundary layer on the overall diffusion length interpreted in terms of a generalized geometry – δ has been normalized as a ratio of pit depth plotted versus pit depth normalized over diameter. (c) Influence of the boundary layer on affecting the overall diffusion length in relation to the pit depth. Note how the contribution of δ to the overall diffusion length (d + δ) decreases with increasing pit depth.

The effect of δ on the observed mass transport of the system can also be examined in terms of the change in concentration from the pit base to the pit mouth. Figure 2.10 displays the concentration change across the model domain using a set of contour plots as well as concentration profiles (the latter are similar to Figure 2.3 (b)). As is evident upon comparing Figures 2.10 (a) and 2.10 (b), the concentration profile of the pit of smaller diameter is closer to the theoretical basis of $\Delta C = (C_{sat} - 0) = 5.02$ M than that of the pit of larger diameter. This result implies that the concentration gradient for the smaller diameter is steeper than that of the larger diameter because both these pits are of the same depth. In order to interpret these data in terms of a generalized geometry, the cation concentration at the pit mouth as estimated by the simulations is plotted as a fraction of the concentration at the pit base (C_{sat} = 5.02 M) against pit depth normalized by the pit diameter in Figure 2.11. As can be seen in this plot, the data obtained based on different pit diameters collapses on to a single curve, indicating that the concentration of the pit mouth approaches zero (the basis for a 1-D theoretical calculation using the pit depth as the diffusion length) only when pit depths close to 10 times the pit diameter are attained.

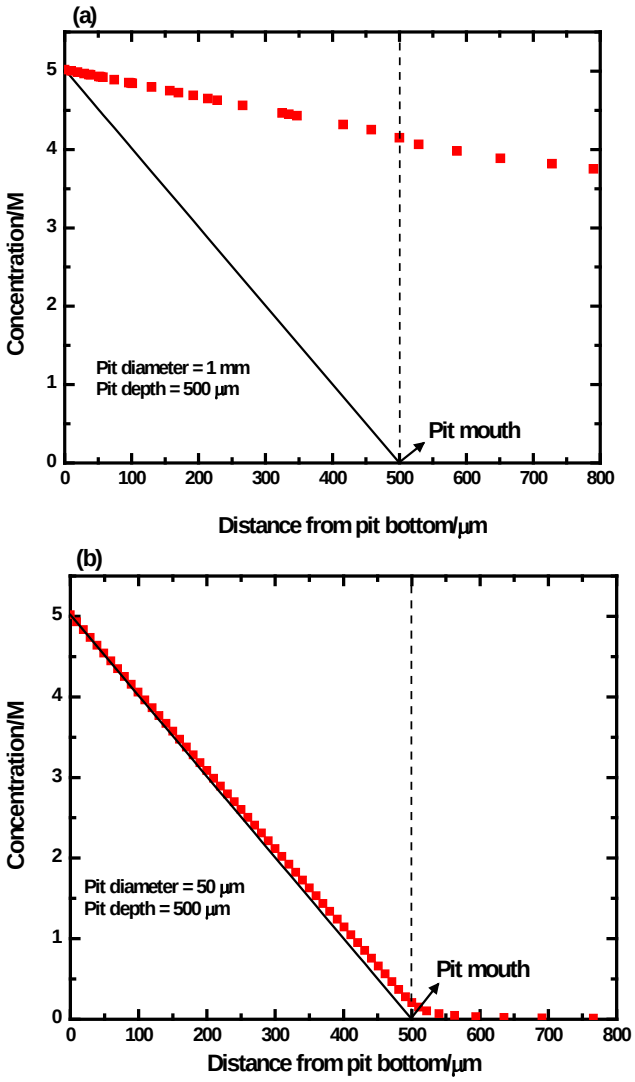

Figure 2.10. Changes in concentration as a function of position in the simulated system domain, compared across pit diameters. Lines indicate the theoretical value and the data points refer to values from the simulation. (a) Concentration gradient along the z-axis for a 500 µm deep pit of 1 mm diameter. (b) Concentration gradient along the z-axis for a 500 µm deep pit of 50 µ m diameter. Note the significant deviation displayed by the pit of larger diameter from the theoretical concentration gradient.

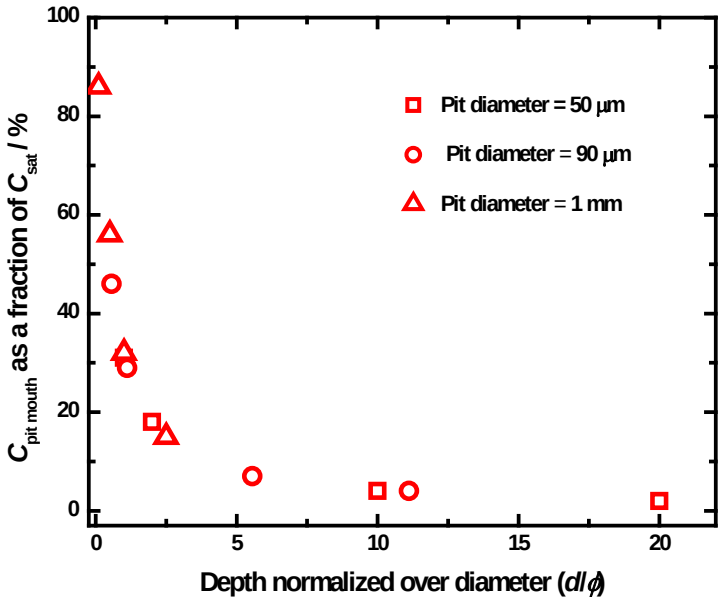

Figure 2.11. Simulated concentration at the pit mouth for a generalized 1-D pit.

Bulk [Cl⁻] affects pit stability product measurement for shallow pits

Prior work has shown that of the pit stability product is affected by bulk electrolyte chemistry[27,29,36,42]. Figure 2.12 (a) reproduces the plot of $(i \cdot x)_{saltfilm}$ versus bulk [Cl^-] from the work of Woldemedhin *et al.*[27] In this plot, the y-intercept provides the value of pit stability product under a salt film isolated from the effects of bulk [Cl^-] (i.e., at a [Cl^-] =0). This value is the true measure of the anodic stability parameter because it reflects a zero cation concentration gradient at the pit mouth, which is the theoretical basis of the Galvele formulation.[3] The resulting expression (Equation 2.3) is similar in form to Equation 2.1 and is also noted similarly in the literature.[25,27,28,34]

$$\frac{i_L}{zFD} = \frac{C_{sat}}{d} \Rightarrow i_L \cdot d = zFDC_{sat} = (i \cdot x)_{saltfilm} \text{ …..…..} \quad (2.3)$$

From Figure 2.12 (b), the slopes of the linear fits for the experimental data obtained at shallow pits are lower than those for the deep pits. Furthermore, the scatter (indicated by the R^2 value) is lower for deep pits than for shallow pits. The $(i{\cdot}x)_{\text{saltfilm}}$ value of 0.9031 obtained for deep pits is in good agreement with the value of $(i{\cdot}x)_{\text{saltfilm}}$ isolated from the effects of bulk $[Cl^-]$ (y-intercept in Figure 2.12 (a)). Figure 2.13 shows the apparent cation concentration at the pit mouth as a fraction of C_{sat} mapped against the bulk $[Cl^-]$, calculated from the experimental $(i{\cdot}x)_{\text{saltfilm}}$ versus bulk $[Cl^-]$ data,[27] assuming a constant value of D. It is evident that as the bulk $[Cl^-]$ increases, the cation concentration of the pit mouth increases. This result therefore implies that as the bulk $[Cl^-]$ rises, the assumption that the cation concentration at the pit mouth is zero breaks down, i.e., ΔC is no longer equal to C_{sat}. This result may be reflective of the fact that viscosity effects on physicochemical parameters play an increasingly important role in determining mass transport as the bulk chemistry becomes more concentrated in chloride, as reported in the literature.[19,29,36,42] Such effects on solution properties may have an impact on both D as well C_{sat}, the latter being influenced by the common ion effect from the bulk electrolyte, as has been discussed in other studies.[29,36,42] *In toto*, the results shown in Figures 2.9 through 2.13 demonstrate that it is imperative to account for the effects of *both* pit depth as well as bulk electrolyte chemistry during measurement and analysis of artificial pit studies to obtain accurate estimates of pit stability parameters.

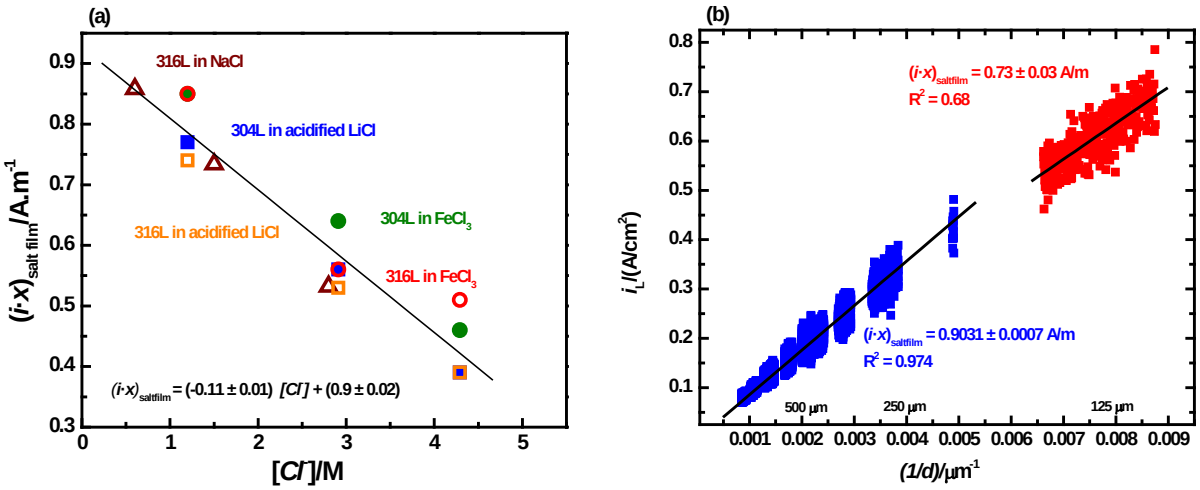

Figure 2.12. Effect of the bulk [Cl^-] on the pit stability data from artificial pit experiments. (a) Replotted data from Woldemedhin *et al*.[27] indicating linear dependence of $(i{\cdot}x)_{saltfilm}$ on bulk [Cl^-]. (b) Data from Srinivasan *et al*.[28] replotted to highlight the difference in slopes at shallow and deep pits.

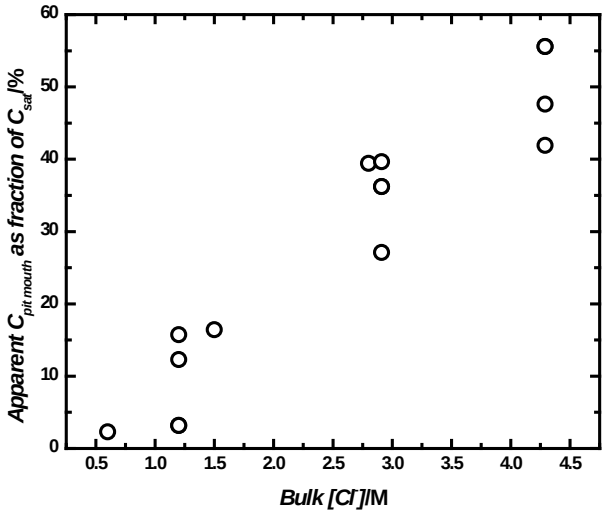

Figure 2.13. Apparent cation concentration at the pit mouth as a function of bulk [Cl^-], calculated from the $(i \cdot x)_{saltfilm}$ data of Woldemedhin *et al.*,[27] assuming a constant value of D.

Saturation based on stoichiometric dissolution correctly represents theoretical flux

The influence of pit depth and bulk electrolyte concentration also impacts the value of C_{sat} considered when calculating the theoretical flux estimate. This point is made particularly evident when the experimental data from Gaudet *et al.*[14] is considered (reproduced in Figure 2.14). At pit depths of ≈400 μm, the experimental values (data points) appear to converge to the theoretical expectation (dashed line) calculated using the saturation concentration of $FeCl_2$ in 1 M HCl (4.2 M)[43]. However, the results from this study show that the experimental data converge with the theoretical calculations with low scatter only when the depth is greater than about 8 times the diameter (Figure 7). Therefore, for a pit diameter of 1 mm, deviation between experiment and theory would be expected to disappear only beyond a depth of 8 mm, in contrast to 400 μm as observed. When 5.02 M, the value obtained from *in situ* X-ray measurement of the stoichiometrically dissolved 18-8 stainless steel in chloride solution,[35] is used for C_{sat} instead, it

is observed that the experimental data now indeed deviate from the theoretical prediction (solid line) at ≈400 μm. It must also be noted that the experimental data of Gaudet *et al.*[14], although convergent at ≈400 μm to the theoretical line assuming a surface concentration of 4.2 M $FeCl_2$, begins to deviate away from that theoretical line towards the line describing a surface concentration of 5.02 M as deeper pits are approached, as can be observed in Figure 2.14.

The observed agreement of the experimental data with the theoretical calculations based on a C_{sat} of 4.2 M can be rationalized with analysis based on the data from Figures 2.12 and 2.13. The experimental data of Gaudet *et al.* were reportedly obtained in a solution with a concentration of approximately 1 M [Cl^-]. Substituting this value for [Cl^-] in Equation 3, a value of 0.79 A/m for $(i \cdot x)_{saltfilm}$ is obtained, which in turn results in a value of 4.52 M for C_{sat}, which is in good agreement with the value of 4.2 M used by Gaudet *et al.*[14], with a relative error of only around 7.6%. This deviation was within the error of the linear regression for $(i \cdot x)_{saltfilm}$ in Figure 2.12 (a). These results reinforce the necessity of data collection from deep pits. The lack of data from sufficiently deep pits ($> d/\phi \approx 8$) indicates that the experimental values in the Gaudet *et al.*[14] obtained are not isolated from the effects of bulk [Cl^-]. The depressed value of $(i \cdot x)_{saltfilm}$ that is obtained as a result yields a C_{sat} estimate which is lower than the actual value for 18-8 stainless steel, but fortuitously agrees with the value for $FeCl_2$ in 1 M HCl. Consequently, the perceived agreement of the Gaudet *et al.*[14] experimental data with the theoretical predictions at depths shallower than expected from this study emerges because a lower value of C_{sat} based on $FeCl_2$ solubility rather than stoichiometric dissolution of the stainless steel was used.

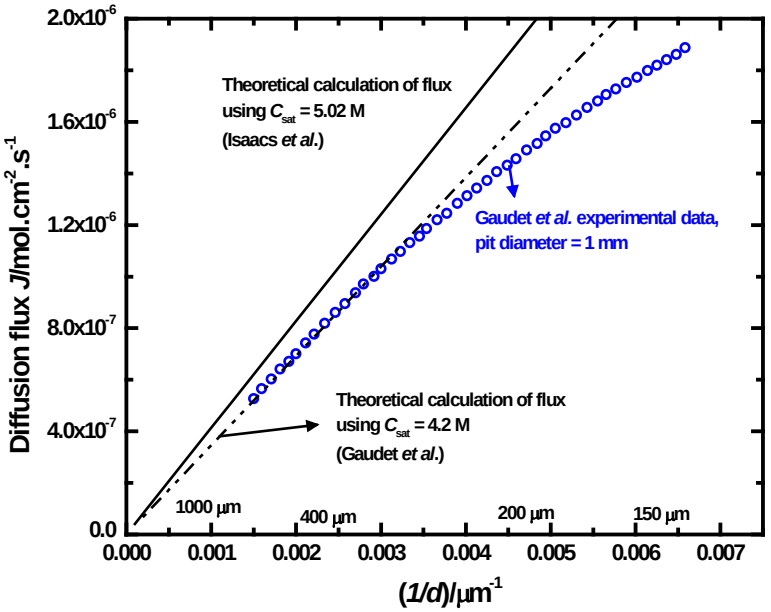

Figure 2.14. Effect of utilizing different values of C_{sat} (based on stoichiometric dissolution of 18-8 stainless steel or only $FeCl_2$) on interpretation of experimental data from 1-D pits of large diameter. Experimental data are replotted from Gaudet *et al*.[14]

Effect of pit depth on 1-D transport rationalizes repassivation behavior

The results in this study can also be used to examine the impact of pit depth on the critical surface concentration associated with repassivation. Several studies have shown that a salt film is not critical for stable pit growth[13,29,44] and that pit stability ought to be examined in the context of repassivation[10,28,30]. This latter idea implies that the minimum critical conditions for stable pit growth also characterize pit repassivation. Figure 2.15 (a) shows that even when the surface concentration at the pit base is diluted to lower fractions of the concentration at saturation, the simulated flux continues to converge towards the theoretical calculations at pit depths which are approximately eight to ten times the pit diameter. Suzuki and Kitamura[45], while

examining stainless steel pits and crevices to determine a critical potential, observed that pits that were about ten times as deep as their diameter were similar in repassivation behavior to activated crevices. This result provides quantitative support to the notion that it is only upon attaining such depths that sufficient mass transport restriction results so that pits are able to sustain the steady state to corrode stably with a film-free surface. At pits of shallower depths, the diffusion out of the pit would overwhelm the rate of metal dissolution, leading to repassivation. The view that restricted mass transport impedes repassivation has been substantiated by Sridhar and Cragnolino[32], as well as Srinivasan *et al*.[28], who have shown that crevice formation in large-area samples can lead to the measurement of more active repassivation potential values even when the charge density passed is low. Finally, studies using artificial pits[27,28,30] have shown that the depth at which the measured repassivation potential approaches a plateau is approximately eight to ten times the pit diameter, as can be seen in the data reproduced in Figure 2.15(b). These latter results lend credence to the proposition that at this pit depth, a critical steady state concentration (lower than saturation)[30,32,34] is attained at the pit base, with equal rates of both metal dissolution and diffusion out of the pit, thus marking the transition between pit stability and repassivation.

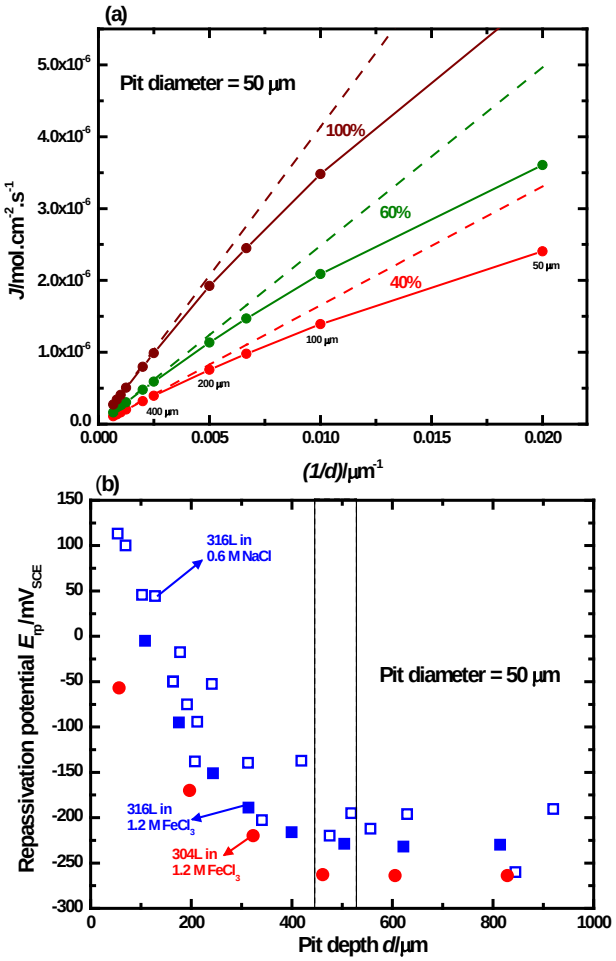

Figure 2.15. Implications of pit depth on measured repassivation parameters and critical conditions for pit stability. (a) Comparison of theoretical and simulated flux across pit depths with successive dilutions of cation concentration at the corroding surface. The dashed lines represent the theoretical flux and the connected symbols denote the simulations. (b) Observed behavior of repassivation potential with pit depth from artificial pit experiments on stainless steels in chloride media. The shaded region signifies the depths at which the E_{rp} 'saturates' or approaches a plateau – at around 400 to 500 µm, these depths are approximately 8 to 10 times the pit diameter. Data for $FeCl_3$ are reproduced from Woldemedhin *et al.*[27]

2.7. Conclusion

This study employed artificial pit experiments as well as finite element modeling to elucidate the effects of pit depth on the flux emanating from 1–D pits, providing commentary on proper collection, analysis, and interpretation of pit stability data from artificial experiments. For shallow pits, the hemispherical boundary layer at the pit mouth significantly affected the flux characteristics. It was only once pits had attained depths of around eight times the diameter that the overall diffusion length could be approximated well by the pit depth alone. The examination of results from artificial pit experiments reinforced the importance of obtaining data from deep pits so that pit stability parameters extracted not only reflected true 1–D mass transport based on the pit depth, but also were not affected by the bulk electrolyte. Artificial pit experiments performed in several configurations ruled out the influence of convective transport and the precipitation of corrosion products on the mass transport in pits of small diameter. The trends observed in published experimental data were also explained by the inferences bulk electrolyte effects obtained from this work. Finally, the results of this investigation were also used to rationalize the observed dependence of repassivation potential on pit depth, thereby providing a quantitative connection between pit stability and repassivation studies.

2.8. References

1. J. Mankowski and Z. Szklarska-Smialowska, *Corrosion Science*, **15**, 493–501 (1975).

2. H.-H. Strehblow and M. B. Ives, *Corrosion Science*, **16**, 317–321 (1976).

3. J. R. Galvele, *Journal of The Electrochemical Society*, **123**, 464–474 (1976).

4. I. Epelboin, C. Gabrielli, M. Keddam, and H. Takenouti, *Zeitschrift für physikalische Chemie (Neue Folge)*, **98**, 215–232 (1975).

5. I. Epelboin, C. Gabrielli, and M. Keddam, *Corrosion Science*, **15**, 155–171 (1975).

6. P. C. Pistorius and G. T. Burstein, *Philosophical Transactions: Physical Sciences and Engineering*, **341**, 531–559 (1992).

7. G. T. Burstein, P. C. Pistorius, and S. P. Mattin, *Corrosion Science*, **35**, 57–62 (1993).

8. Z. Y. Chen, F. Cui, and R. G. Kelly, *Journal of The Electrochemical Society*, **155**, C360–C368 (2008).

9. Z. Y. Chen and R. G. Kelly, *Journal of The Electrochemical Society*, **157**, C69–C78 (2010).

10. M. T. Woldemedhin, M. E. Shedd, and R. G. Kelly, *Journal of the Electrochemical Society*, **161**, E3216–E3224 (2014).

11. J. Srinivasan and R. G. Kelly, in *Paper no. 5531, CORROSION 2015,*, NACE International, Dallas, TX (2015).

12. T. R. Beck, *Journal of The Electrochemical Society*, **120**, 1317–1324 (1973).

13. R. C. Newman and H. S. Isaacs, *Journal of The Electrochemical Society*, **130**, 1621–1624 (1983).

14. G. T. Gaudet et al., *AIChE J.*, **32**, 949–958 (1986).

15. R. C. Newman, *Corrosion Science*, **25**, 341–350 (1985).

16. R. C. Newman, M. A. A. Ajjawi, H. Ezuber, and S. Turgoose, *Corrosion Science*, **28**, 471–477 (1988).

17. K. P. Wong and R. C. Alkire, *J. Electrochem. Soc.*, **137**, 3010–3015 (1990).

18. H. S. Isaacs, *J. Electrochem. Soc.*, **120**, 1456–1462 (1973).

19. J. W. Tester and H. S. Isaacs, *Journal of The Electrochemical Society*, **122**, 1438–1445 (1975).

20. I. L. Rosenfeld, I. S. Danilov, and R. N. Oranskaya, *Journal of The Electrochemical Society*, **125**, 1729–1735 (1978).

21. T. R. Beck, *Journal of The Electrochemical Society*, **126**, 1662 (1979).

22. N. Sato, *Journal of The Electrochemical Society*, **129**, 260–264 (1982).

23. T. R. Beck, *Electrochimica Acta*, **29**, 485–491 (1984).

24. R. C. Alkire and K. P. Wong, *Corrosion Science*, **28**, 411–421 (1988).

25. N. J. Laycock and R. C. Newman, *Corrosion Science*, **39**, 1771–1790 (1997).

26. M. H. Moayed and R. C. Newman, *Journal of The Electrochemical Society*, **153**, B330–B335 (2006).

27. M. T. Woldemedhin, J. Srinivasan, and R. G. Kelly, *Journal of Solid State Electrochemistry*, **19**, 3449–3461 (2015).

28. J. Srinivasan, M. J. McGrath, and R. G. Kelly, *J. Electrochem. Soc.*, **162**, C725–C731 (2015).

29. P. Ernst and R. C. Newman, *Corrosion Science*, **49**, 3705–3715 (2007).

30. J. Srinivasan, M. J. McGrath, and R. G. Kelly, *ECS Transactions*, **58**, 1–11 (2014).

31. J. N. Harb and R. C. Alkire, *J. Electrochem. Soc.*, **138**, 2594–2600 (1991).

32. N. Sridhar and G. A. Cragnolino, *Corrosion*, **49**, 885–894 (1993).

33. A. Anderko, N. Sridhar, and D. S. Dunn, *Corrosion Science*, **46**, 1583–1612 (2004).

34. J. Srinivasan and R. G. Kelly, *Corrosion*, **70**, 1172–1174 (2014).

35. H. S. Isaacs, J.-H. Cho, M. L. Rivers, and S. R. Sutton, *Journal of The Electrochemical Society*, **142**, 1111–1118 (1995).

36. J. Jun, G. S. Frankel, and N. Sridhar, *J Solid State Electrochem*, **19**, 3439–3447 (2015).

37. J. N. Harb and R. C. Alkire, *Corrosion Science*, **29**, 31–43 (1989).

38. J. N. Harb and R. C. Alkire, *J. Electrochem. Soc.*, **138**, 3568–3575 (1991).

39. R. C. Alkire, D. B. Reiser, and R. L. Sani, *J. Electrochem. Soc.*, **131**, 2795–2800 (1984).

40. J. S. Lee, M. L. Reed, and R. G. Kelly, *J. Electrochem. Soc.*, **151**, B423–B433 (2004).

41. R. C. Alkire, H. Deligianni, and J.-B. Ju, *J. Electrochem. Soc.*, **137**, 818–824 (1990).

42. N. J. Laycock et al., *ECS Transactions*, **41**, 3–16 (2012).

43. H. C. Kuo and D. Landolt, *Electrochimica Acta*, **20**, 393–399 (1975).

44. R. C. Newman and H. S. Isaacs, *Passivity of Metals and Semiconductors* M. Froment, Editor, Elsevier B.V, Bombannes, France, (1983).

45. T. Suzuki and Y. Kitamura, *Corrosion*, **28**, 1–6 (1972).

Chapter 3

3.1. Overview

This chapter illustrates the development of the quantitative framework relating experimental measurements of pit stability and repassivation – expressed in terms of the Galvele pit stability product and the repassivation potential – to the concentration of metal cations at the corroding surface. Utilizing the insights provided in Chapter 2 regarding the pit depth dependence of mass transport, artificial pit experiments as well as analytical and computational 1-D diffusion modeling are employed to examine the surface conditions as the pit approaches repassivation. This combined approach provides an estimate of the critical surface concentration when the pit transitions from an actively dissolving to a repassivated state. The critical value so obtained is also utilized to rationalize pit stability phenomenology relevant to atmospheric corrosion conditions.

An original research article based on this chapter has been published in the Journal of The Electrochemical Society, and can be accessed by the following description:

J. Srinivasan and R. G. Kelly: *One-Dimensional Pit Experiments and Modeling to Determine Critical Factors for Pitting Stability and Repassivation*. ***Journal of The Electrochemical Society*** 163, 13 (2016): pp. C759-767.

3.2. Abstract

Experiments on stainless steel artificial pit electrodes in sodium chloride were used to inform a diffusion model developed based on the mass transport behavior within a one-dimensional corroding pit. Measurable estimates of the dissolution flux as well as the potential describing the conditions of interest were obtained from experiment as the one-dimensional pit stability product under a salt film $(i \cdot x)_{saltfilm}$ and the repassivation potential E_{rp}, respectively. These parameter estimates were acquired as a function of pit depth and were related to the concentration of the metal cation at the corroding surface at each depth via a one-dimensional mass transport model. These results allowed for the construction of a quantitative framework relating the various electrochemical parameters describing the transition from pit stability to repassivation. Such an analysis permitted the straightforward evaluation of the critical surface concentration associated with this transition, which resulted in a single conservative lower bound of 50% of the saturation concentration for the minimum aggressive chemistry to sustain stable pitting and prevent repassivation. Along with published data, these results were utilized to advance the idea that the critical pit solution chemistry is independent of bulk chloride concentration up to 4 M, a range frequently encountered in atmospheric conditions.

3.3. Introduction

Many authors have separately reported the critical electrochemical conditions necessary for stable pitting and repassivation, focusing on dissolution flux[1–8], pit solution chemistry,[9–16] or potential.[17–31] The existence of these critical parameters is predicated upon the steady state relationship that emerges between two competing processes: metal dissolution and hydrolysis that results in a local aggressive chemistry inside the pit which supports active corrosion, and the dilution of this chemistry by diffusion out of the pit which contributes to repassivation[32–34]. The mathematical description of this relationship for a one-dimensional pit was framed by Galvele[1] in terms of the product of the current density and the pit depth, ($i \cdot x$), which was termed the pit stability product in later studies.[35–38] Once this product decreased below a critical value, $(i \cdot x)_{crit}$, the conditions in the pit would no longer be able to sustain the local aggressive chemistry necessary for active dissolution. Galvele's formulation, originally intended to describe the conditions leading to pit initiation, has also been successfully extended to pit propagation.[4,7,35–37] Experimental assessment of the Galvele pit model is typically performed using the artificial pit or lead-in-pencil electrode,[4,7,39–42] which consists of a metal wire embedded in epoxy. The lead-in-pencil electrode is particularly useful because it closely represents the configuration of the Galvele 1–D pit model, *i.e.* a single activated surface and inert walls[7,8]. Additionally, the precipitation of a salt film[40,43–48] at high anodic potentials in corrosive solution leads to diffusion-limited dissolution – a quasi-steady state condition that permits the study of one-dimensional mass transport. Consequently, the presence of a salt film at the corroding surface was considered necessary as a critical condition for stable pitting.[13,36,37,49] However, studies have shown that pits continued to corrode at applied anodic potentials lower than those at which salt films were stable, [5,50] thus indicating the possible existence of intermediate steady states corresponding to lower

degrees of saturation. This reasoning motivated attempts by Isaacs and coworkers to identify such film-free steady-states.[4,7,42] The results of these studies indicated the presence of such states associated with several surface concentrations, thereby demonstrating that single, unambiguous critical values for the surface concentration and the associated potential at which stable pitting was sustained could not be extracted. Nonetheless, these data provided the commonly accepted range of 60-80% of saturation as the critical surface concentration which has informed the view of many authors investigating pitting stability as a function of chloride concentration.[8,51–55]

In a similar vein, there has been considerable debate over the identification and measurement of a critical potential which could be used to characterize stable pitting. Initial perspectives on a critical potential below which pitting would not be stable suggested either the open circuit potential in the pit solution or the pitting potential as possible candidates.[1,17,18,20,23,56–58] The selection of the open circuit potential in the pit solution as a critical potential was based on the understanding that a net cathodic reaction would be expected to ensue should the pit electrochemistry cause the potential to decrease below this value.[20] This choice for the critical potential was hamstrung by the fact that equal rates of the anodic and the cathodic reactions in the pit would not result in the aggressive local chemistry[9,12,59,60] required to sustain pitting. Laycock and Newman[8] presented the argument that the critical potential was one below which the salt film would not be stable, calling this parameter the transition potential E_T. Their work showed that E_T was equivalent to the pitting potential but in a pit solution chemistry corresponding to a salt film on the surface. This interpretation for a critical potential however, relies on the salt film representing the critical solution chemistry, which is not necessary for stable pitting as has been stated previously. The value of utilizing the pitting potential as a critical parameter was also called into question when it was observed that it was dependent on

the scan rate employed in the cyclic potentiodynamic polarization scans typically used for its measurement.[22,61,62] These tests also showed that the repassivation potential – recorded as the potential at which the reverse scan attained the passive current during the measurement – was also affected by the scan rate. The repassivation potential value appeared to be dependent on the charge density passed,[22] as it decreased with decreasing scan rate. These insights on the influence of prior pit growth on repassivation were used by Thompson and Syrett[28] to advance the idea that the critical potential describing both pitting initiation and repassivation was a single unique potential. The authors posited that this potential was artificially separated into the pitting potential and the protection potential by the cyclic experimental technique that tended to minimize incubation time and maximize pit growth following initiation. This concept was similar to the one proposed by Smialowska and Mankowski[24], which examined the development of a critical potential based on the comparison of pitting and crevice corrosion of stainless steel in chloride media.

On the other hand, Pickering and coworkers[21,27,63] argued for pit loss of pit stability on the basis of an ohmic (IR) drop mechanism that would result in lower potentials and current densities as the pit grew deeper. However, when the Galvele criterion is applied to this interpretation, extremely deep pits would be expected to remain stable as long as they were sustained by a correspondingly low current density. This inference is challenged by the observation that pits cannot grow indefinitely and necessarily do repassivate, thereby implying the necessary existence of critical lower bounding conditions. Also, provided that the critical potential is one at which the pit still remains active, this value cannot be lower than the potential where the net anodic current density vanishes, *i.e.*, the open circuit potential in the pit solution noted previously.

Sridhar and coworkers[29,64–66] attempted to address the diverse viewpoints on the critical potential by defining a parameter that could serve as conservative lower bound, which would be useful in engineering practice. Their methodology involved measuring repassivation potential using a variant of the THE method,[25,26,67] which essentially consisted of potentiostatic pit initiation and galvanostatic propagation, followed by the application of stepped potential holds until a finite low anodic current density was attained. Potential steps below this value would lead to a rapid decrease in current density, indicating repassivation. Results from these tests showed that the repassivation potential decreased with increasing charge density before approaching a plateau value at sufficiently large charge densities. Very long-term (> 5 years) testing indicated that samples held above this plateau value underwent pitting. On the other hand, samples held below this value did not initiate new pits and neither did existing pits continue to grow. This measure of the critical potential was therefore adopted as the repassivation potential (E_{rp}) because it provided a measurable, consistent, conservative lower bounding estimate. Rebak and coworkers[31,68,69] have extended these results to crevice corrosion in nickel alloys, attesting to this measure of the critical potential as a consistent evaluation. A qualitative discussion on how this potential was related to surface concentration at repassivation based on arguments using ohmic drop[21,27,27] as well as mass transport restriction due to pit geometry was proposed in these studies. However, the authors only provided a limited quantitative assessment of the critical solution chemistry associated with this potential – a treatment with respect to behavior in simulated pit solutions of different pH, which showed an active-to-passive transition when the pH was increased. Furthermore, despite the indubitable lower bound obtained in potential, the use of large-area samples meant that the occurrence of multiple pits resulted in some ambiguity about the charge density calculation. Recent work based on this study has focused on developing

a general repassivation potential model[66,70,71] based on oxide nucleation[72] in competition with the presence of a hydrous metal halide, which has been useful in calculating the E_{rp} in various field environments. The objective of these studies, however, was not to quantitatively associate E_{rp} with the other critical factors describing the transition from pit stability to repassivation. The authors considered that a surface concentration close to, but not at saturation, represented the critical value, but this value was not quantified. These latter studies also adopted the repassivation potential obtained from creviced samples as the conservative lower bound for E_{rp}. This consideration is consistent with the reasoning presented by Srinivasan *et al*.[73], who showed that crevice formation in large-area samples resulted in attaining the E_{rp} lower bound at lower measured charge densities than with artificial pits.

It must therefore be recognized, as noted by Newman[74], that whether expressed as solution chemistry, dissolution flux, or potential, these critical factors describe the same phenomenon, which is the transition between stable pitting and repassivation. As has been stated, studies that have discussed a single critical parameter have not quantitatively related it to the other associated factors. Therefore, a mathematical framework is required to establish a scientifically defendable, quantitative connection among the critical electrochemical parameters that characterize the conditions in the pit that mark the boundary between active dissolution and repassivation. Determining these critical factors accurately and in quantitative relation to each other is necessitated by their substantial effect on *a priori* damage size bounding estimates when used as input data in predictive models[75–78] useful for structural integrity analyses. Maximum pit size estimates using these models have been shown to vary by up to a factor of 3 depending on the critical value of surface concentration[78]; this variation can have a significant impact on fracture mechanics-based design for metallic components employed in corrosive

atmospheres.[79,80] In this study, the one-dimensional architecture of the artificial pit technique is leveraged to both obtain experimental measures of steady state dissolution flux and repassivation potential. These experiments are combined with mass transport modeling that utilizes these parameters to determine the concentration at the corroding surface, which is difficult to access directly due to the restrictive geometry and aggressive chemistry of the pit. Previous work on artificial pits that has considered pit stability in the context of repassivation[73,81] is also visited in order to rationalize the results obtained so that the quantitative strength of the framework is reinforced. This study therefore provides a single experimental and modeling paradigm to evaluate the critical surface concentration and potential characterizing the transition from pit stability to repassivation.

3.4. Experimental

Artificial pit experiments

One-dimensional artificial pit electrodes were constructed using 316L stainless steel wires (California Fine Wire Company, Grover Beach, CA) of diameter 50.8 μm embedded in epoxy. The composition of the wires is shown in Table 3.1. The electrode surface was polished to 320 grit with SiC abrasive paper and then placed upright in a test cell containing 0.6 M NaCl solution. The exposed area of the electrode was 2.03×10^{-5} cm^2. A saturated calomel reference electrode (SCE) and a platinum mesh counter electrode were utilized for all tests.

Alloy	C	Mn	P	S	Si	Cr	Ni	Mo	N	Cu	Fe
316L	0.019	1.356	0.030	0.0287	0.406	**17.07**	**10.66**	**2.16**	0.0499	0.232	**67.98**

Table 3.1. Composition of 316L (Fe, Ni, Mo, and Cr contents marked in bold) wire employed in study. All values in weight per cent. Composition provided by vendor was confirmed by quantitative speciation using inductively coupled plasma optical emission spectroscopy (ICP-OES).

Pitting was initiated by applying a potential of +750 mV_{SCE} for a short duration (2 to 5 minutes) and then propagated to various depths by applying a lower potential of +450 mV_{SCE}. This sequence was followed by a rapid cathodic polarization scan at 5 mV/s to a final potential of –900 mV_{SCE} in order to obtain measurable estimates of $(i \cdot x)_{saltfilm}$ and E_{rp}. Variants of this procedure have been employed in other recent pitting studies that have focused on pit stability

and repassivation[73,81,82]. All electrochemical testing was carried out at an average ambient temperature of 22 °C using either a Gamry Reference 600™ (Gamry Instruments, Inc., Warminster, PA) potentiostat or a Bio-Logic SP-150 (Bio-Logic SAS, Claix, France) potentiostat.

Mass transport modeling

In order to relate the experimentally measured electrochemical parameters of dissolution flux and potential to pit solution chemistry, the one-dimensional diffusion kinetics of the artificial pit electrode were modeled. The model geometry was set up as shown in Figure 3.1 with the following constraints:

- The system is considered to be axisymmetrical with respect to the x-axis as shown.
- Initial concentration at the bottom of the pit $C\,(x = 0, t = 0) = C_{sat}$.
- Concentration at the pit mouth set to zero for all time.
- A linear concentration gradient was set up within the pit at t = 0, i.e, $C\,(x, t = 0) = C_{sat}\frac{x}{d}$.
- The walls of the pit were considered to be inert, i.e., flux across these boundaries was set to zero for all time.
- A constant diffusion coefficient D of 8.24×10^{-6} cm^2/s as employed by Gaudet *et al.*[7] based on $FeCl_2$ diffusion in 1 M HCl.[*]

The time-evolution of the mass transport of this system was analyzed for three different flux boundary conditions at the bottom of the pit: zero flux, constant flux, and a transient flux.

[*] This value falls within the range of the values of 7×10^{-6} cm^2/s to 1×10^{-5} cm^2/s reported for D in the literature. [54,82–84] Also, using a constant diffusivity has been shown to approximate to a good degree the combined effects of variable diffusivity and electromigration on the flux of the system[4,7].

Analytical solutions were obtained for the system under the boundary conditions of zero flux and constant flux at the corroding surface. For the transient flux however, numerical methods involving finite element analysis had to be employed. The COMSOL Multiphysics® v5.2 (COMSOL, Inc., Burlington, MA) software was used to model the geometry in Figure 3.1 (b) under the specified boundary conditions. Simulations were run until differences in calculations from successive iterations as determined by the error estimation capability of the software decreased to lower than the threshold tolerance of 0.1%.

The values for the constant flux and transient flux were estimated from the experimental data from each pit depth in two ways:

i) Constant flux: An average current density was calculated by integrating the area under the current density versus time curve between the limits of recording the potentials corresponding to the two surface conditions of interest, i.e., the transition potential E_T where the salt film disappears[8] and the repassivation potential E_{rp} (Figure 3.2 (a)). The time variable t_{act} was defined as the experimental time taken for the instrument to scan from a surface condition described by 100% saturation to the surface condition at which the E_{rp} measurement is made. The expression for t_{act} can be written in terms of the potentials that describe the respective surface conditions of interest and the scan rate ((dE/dt)):

$$t_{act} = \frac{\left(E_T - E_{rp}\right)}{\left(dE/dt\right)} \quad \text{..... (3.1)}$$

The average current density i_{avg} can then be expressed as:

$$i_{avg} = \frac{\int_{time(E_T)}^{time(E_{rp})} i(t)dt}{t_{act}} \quad \text{..... (3.2)}$$

This average value was expressed as a fraction φ of the measured diffusion-limited dissolution current density i_L which is obtained from experiment (Figure 3.2):

$$i_{avg} = \varphi \cdot i_L \quad \text{..... (3.3)}$$

ii) Transient flux: The transient current density response $i(t)$ obtained from experimental data was input as the flux boundary condition $J(t) = \frac{i(t)}{zF}$, where z is the average number of electrons transferred during every instance of the congruent dissolution of 316L = 2.2, and F is Faraday's constant = 96485 C/mol-equivalent; these values are consistent with those used in the literature[5,7,8,54].

The resulting time-dependent concentration at the corroding surface was then directly obtained from the simulations for different pit depths, expressed as a fraction f of the saturation concentration C_{sat}.

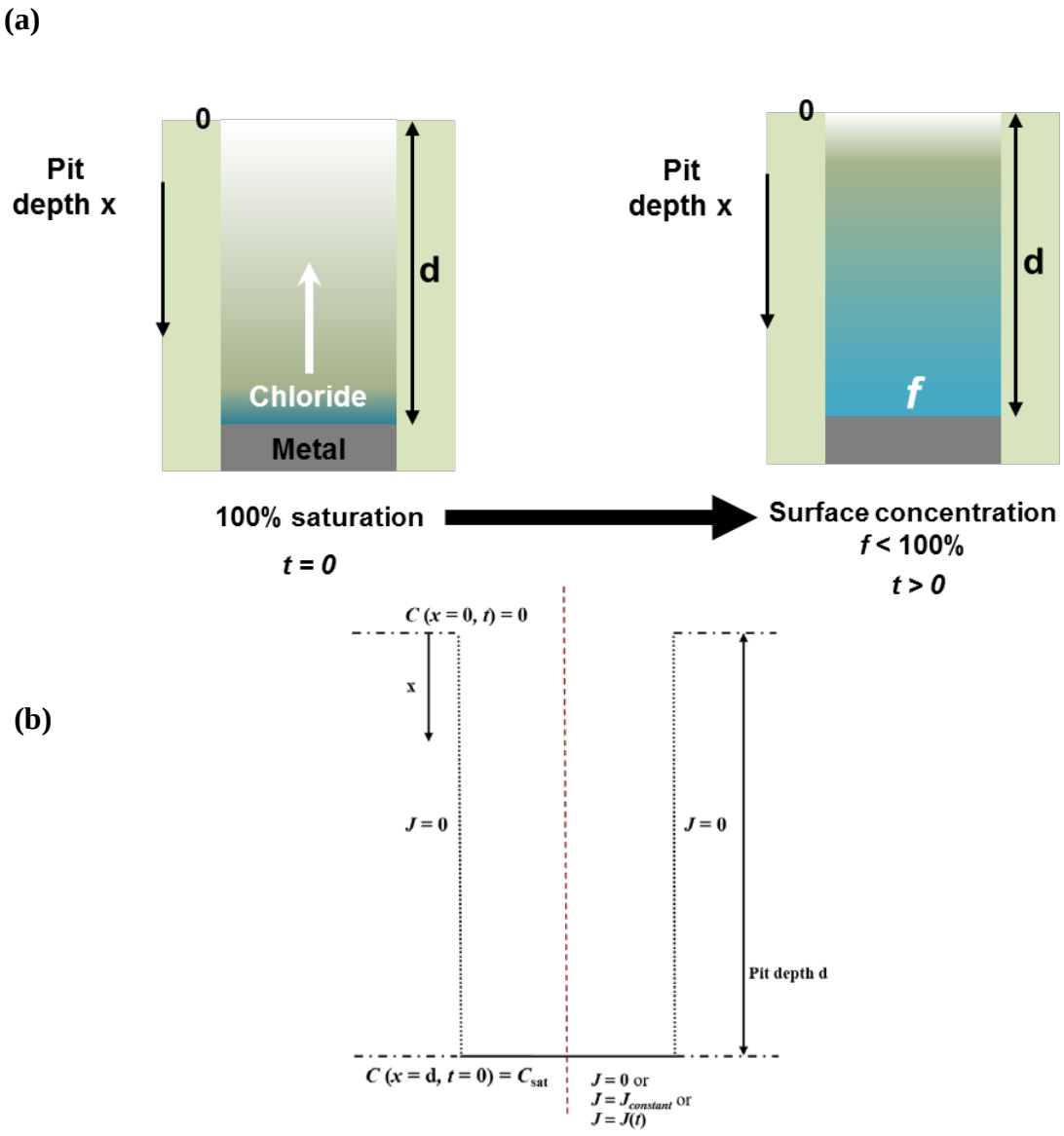

Figure 3.1. One-dimensional pit system considered in model (diagrams not to scale). (a) Schematic depiction of process modeled. (b) Geometry of system utilized in model. The one-dimensional diffusional characteristics are considered along the x-axis. Time-evolution of the system was modeled for three flux cases at the pit bottom. The origin was considered to be at the center of the pit mouth. Inert boundaries are indicated by the dotted lines.

3.5. Results

Artificial pit experiments

The main advantage of the one-dimensional artificial pit configuration is the ability to obtain a straightforward, unambiguous geometry in which the pit depth serves as a single externally controlled variable against which electrochemical parameters associated with pitting and repassivation can be mapped. The pit depth was calculated directly from the charge density passed during the two potential holds. The rapid scan rate employed during the potentiodynamic polarization sequence meant that very little additional dissolution occurred[73] during this step. Furthermore, as attested to by other studies in the literature[73,82,85], the rapid scan rate permitted analysis of the kinetics of the system without substantial dilution of the aggressive chemistry at the pit base. Extraction of the kinetic parameters from the experimental data (Figure 3.2 (a)) followed the method described by Srinivasan *et al.*[73] Linear regression was performed on the data obtained by plotting the value of the diffusion-limited dissolution current density against the reciprocal of the pit depth. The slope of this linear fit provided an estimate of the pit stability product under a salt film $(i \cdot x)_{saltfilm}$, as shown in Figure 3.2 (b). It is also important to ensure that the value of $(i \cdot x)_{saltfilm}$ implemented be isolated from the effect of bulk $[Cl^-]$. This requirement can be accomplished by either collecting pit stability data exclusively from depths deeper than approximately eight to ten times the pit diameter[81] or by using the relationship developed by Woldemedhin *et al.*[82] which maps the linear dependence of $(i \cdot x)_{saltfilm}$ on bulk $[Cl^-]$, which for 18-8 stainless steels in chloride has been calculated to be 0.9 A/m. From Figure 3.2 (b), the value of $(i \cdot x)_{saltfilm}$ in 0.6 M NaCl is determined to be 0.8 A/m. This estimate agrees well with the reported $(i \cdot x)_{saltfilm}$ value of 0.83 A/m for a bulk $[Cl^-]$ of 0.6 M from the Woldemedhin *et al.*[82] study.

At each pit depth attained following growth under potentiostatic control, the potential at which the subsequent polarization scan attained an anodic current density value of 30 $\mu A/cm^2$ was recorded as an estimate of the repassivation potential E_{rp}. As shown in Figure 3.3, the measured E_{rp} decreased initially as the pit depth increased, but became relatively independent of depth once sufficient charge density had been passed (or equivalently, a sufficiently large pit depth had been attained). This depth at which the E_{rp} saturates can be determined from statistical analysis as well as phenomenological evidence. For a given dataset collected at a particular scan rate[73], the value of the depth beyond which the E_{rp} does not change over a large range was calculated via a Student's t-test (at the 95% confidence level). This depth is then compared to the value at which the steady state flux emanating from the pit can be definitively approximated by one-dimensional mass transport based on the pit depth as a measure of the diffusion length, as reported by Srinivasan *et al*.[81] This latter value therefore serves as an internal consistency check on the scan rate employed. The recorded E_{rp} values at depths greater than this value are then averaged to obtain the mean E_{rp}, which is recorded as the repassivation potential of the alloy in the conditions of interest, as denoted on the plot in Figure 3.3. These results, both in trend and in value, were consistent with other studies on E_{rp} in the literature[29,64–66,70,71,73,82].

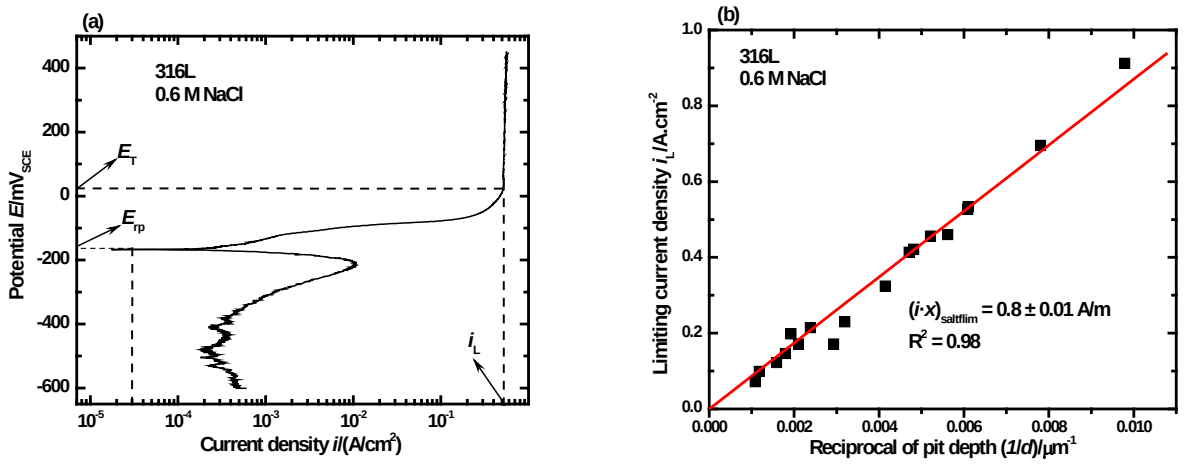

Figure 3.2. Extraction of kinetic parameters from experiment. (a) Polarization kinetics data indicating measurements of the diffusion-limited dissolution current density i_L, the repassivation potential E_{rp} and the transition potential E_T. (b) Extraction of pit stability product under a salt film across various pit depths. All data refer to 316L in bulk 0.6 M NaCl.

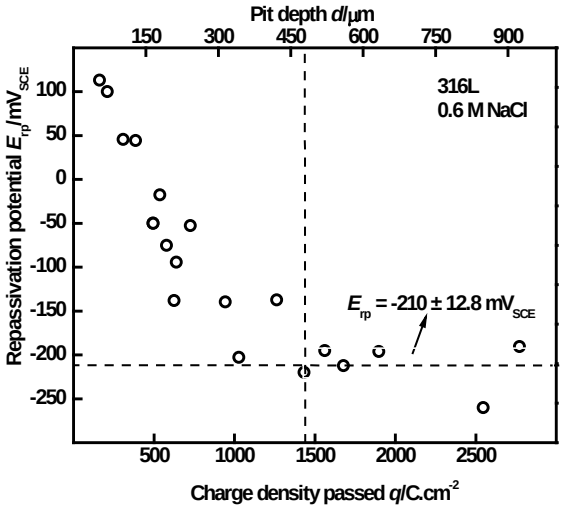

Figure 3.3. Extraction of the measured repassivation potential E_{rp} from anodic kinetics data at various pit depths. The E_{rp} value denoted is the plateau which the recorded values approach at deep pit depths/high charge density. Data refer to 316L in bulk 0.6 M NaCl.

3.6. Discussion

The results obtained from experiments and modeling were synthesized to determine the concentration of the corroding surface of the pit as it is about to repassivate. This analysis involved analyzing the steady state flux of the system as the measurement of repassivation potential was made. The effects of varying boundary conditions on the critical surface concentration as well as the impact of scan rate on repassivation were investigated. The possibility of a single critical pit solution chemistry governing anodic stability criteria across bulk environments encountered during atmospheric corrosion were also examined.

Steady state flux is modeled by mass transport analysis as E_{rp} is measured

The mass transport model provided an estimate of the time taken for the corroding surface to dilute from a chemistry described by 100% saturation of the cation chlorides (salt film) to lower concentrations, described by the parameter *f*. The evolution of surface concentration as the pit dilutes was derived in terms of the pit depth *d* and time *t*, for a constant diffusion coefficient *D*:

$$f = \frac{C_S}{C_{sat}} = \frac{8}{\pi^2}\sum_{n=1}^{\infty}\frac{1}{(2n-1)^2}\exp\left[\frac{(2n-1)\pi^2}{2d}Dt\right] \quad \text{..... (3.4)}$$

This expression is similar in form to that obtained by Newman and Isaacs[4]. The value of *D* is taken to be 8.24×10^{-5} cm^2/s, a value close to that of Fe^{+2} in 1 M HCl[86], that has been shown to be a valid approximation of the effective diffusion coefficient of the 'stainless steel cation' in multiple studies[7,42,54,73,82].

Approximating the series to the first term and solving for the time to dilution (denoted as t_f) yields the following expression:

$$t_f = \frac{4d^2}{\pi^2 D} \ln \frac{8}{\pi^2 f} \text{ ..... (3.5)}$$

As Figure 4 shows, the truncated series expression (Equation 3.5) closely approximates the time to dilution calculated from the complete solution obtained by finite element analysis using COMSOL Multiphysics®, particularly for values of f less than 70%. In order to calculate the concentration of the corroding surface at the point where the pit begins to repassivate, it is instructive to observe how the surface concentration at the moment of experimental measurement of E_{rp} varies at different pit depths. Comparing t_f with t_{act} (defined in the previous section) for various pit depths would permit the estimation of the surface concentration when the experimental measurement of E_{rp} is recorded. In this case, t_{act} effectively serves as a measure of the time available for the corroding surface to dilute from 100% saturation.

The experimental time t_{act} is compared to the calculated time to dilution t_f, to obtain the difference Δt:

$$\Delta t = t_{act} - t_f \text{ ..... (3.6)}$$

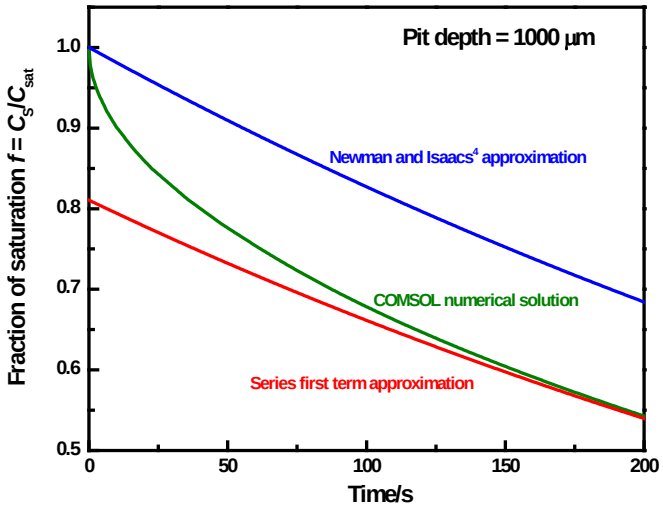

Figure 3.4. Time-evolution of the surface concentration in the system considered in model as estimated by three different methods. (a) Base-10 logarithmic approximation reported by Newman and Isaacs.[4] (b) Complete solution obtained using finite-element analysis. (c) Expression obtained in Eq. 5 following truncating the series in Eq. 4 to the first term.

The variation of Δt with pit depth at different levels of dilution can be examined, as shown in Figure 3.5 for a surface concentration corresponding to 60% of saturation. This plot can be analyzed to evalute how concentration of the cation chloride at the corroding surface changes as E_{rp} measurements are made at different pit depths, permitting an interpretation of the effect of diffusive transport on repassivation. From the data in Figure 3.5, it can be seen that at shallow pit depths, $\Delta t > 0$ because given the short diffusion length, the time *provided* (because of the experimental scan rate) for the pit to dilute to 60% of saturation is greater than the time *required* for the pit to dilute to this value. Therefore, by the time the E_{rp} is measured, the actual surface concentration is less than the value represented by the curve. Conversely for deep pits, $\Delta t < 0$ because mass transport out of the pit is more restricted due to the longer diffusion path. Therefore, the time *permitted* for the pit to dilute to 60% of saturation is less than the time

required for the pit to dilute to this value. It follows then that, by the time the E_{rp} is measured for deep pits, the actual surface concentration is higher than the value represented by the curve. These observations imply that, for some intermediate pit depth, t_{act} will be equal to t_f and thus $\Delta t = 0$. At this pit depth, the surface concentration when the E_{rp} measurement is made would be equal to the value described by the curve.

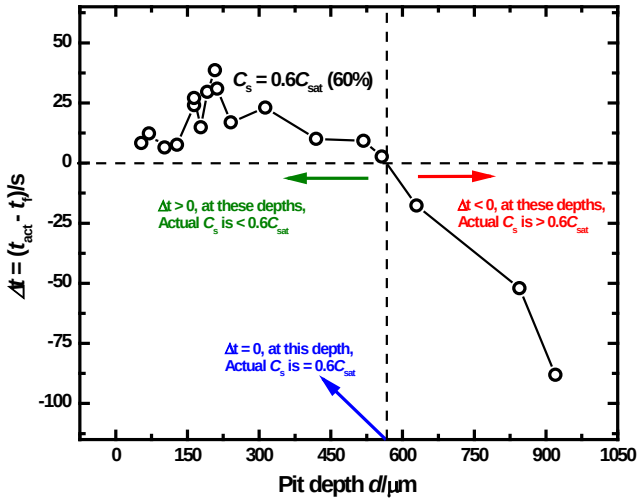

Figure 3.5. Estimation of concentration of '316L cation' at the corroding surface of the one-dimensional pit at various pit depths as the E_{rp} is measured. This plot compares how the time to dilute to 60% of saturation is affected by the imposed constraints of an experimental scan rate.

Following the logic thus outlined, a series of curves mapping Δt as a function of pit depth can be obtained for various values of f. These curves are shown in Figure 3.6, from which the corresponding depths at which $\Delta t = 0$ can be estimated for each surface concentration. In order to determine which of these values of surface concentration truly represents repassivation of the surface, the plot of repassivation potential versus pit depth as obtained from the artificial pit

experiments is examined. As shown in Figure 3.3, the E_{rp} is seen to decrease with increasing pit depth before settling to a plateau for sufficiently deep pits. The depth at which this transition to the plateau occurs indicates that the mass transport is sufficiently restricted such that the aggressive solution chemistry is not lost by diffusion before the experimental measurement of E_{rp} is recorded.[29,64–66,81]

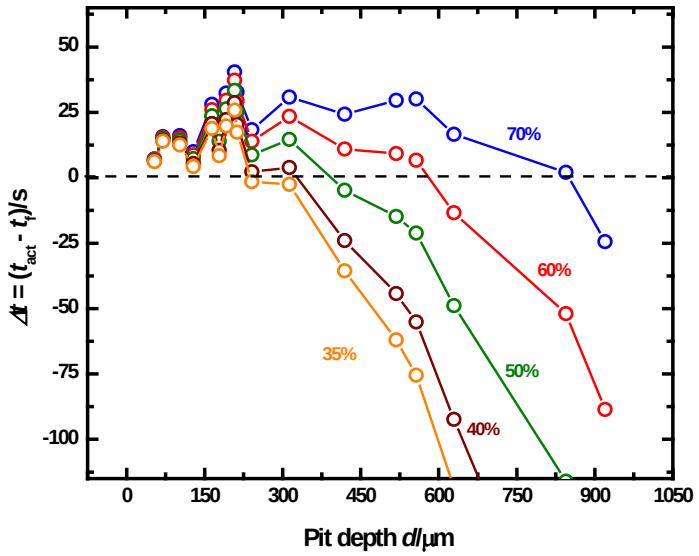

Figure 3.6. Δt mapped as a function of pit depth for different values of surface concentration of cations at the corroding surface. Note that as pit chemistry becomes more aggressive, a deeper pit is required to provide sufficient mass transport restriction to achieve stability (as indicated by the depth where Δt = 0).

Figure 3.7 shows a composite of the two pit-depth dependent plots of Δt and E_{rp}. By comparing the depths at which $\Delta t = 0$ for various levels of dilution to the depth at which the transition to the E_{rp} plateau occurs, the value of f describing the surface condition as repassivation is about to set in can be estimated. In this manner, a pit depth value serves as a

surrogate indicator of critical pit solution chemistry. Using the data in Figure 3.7, an estimate of this critical surface concentration is seen to be between 50% and 60% of saturation, with the lower value chosen as a conservative estimate. This approach shows that the critical solution chemistry is in fact lower than the estimates of 60-80% obtained by Gaudet *et al.*[7] based on the multiple intermediate steady states that follow salt film-free dissolution of stainless steel artificial pits. The ambiguity in identifying a critical surface concentration because of intermediate steady states[7,42] is avoided in this study which provides a *single* value of the critical solution chemistry and relates it to a critical potential E_{rp} defined with respect to a critical steady state flux. In this manner, the method described herein illustrates a comprehensive, quantitative framework that identifies and measures a set of electrochemical parameters critical to both pit stability and repassivation.

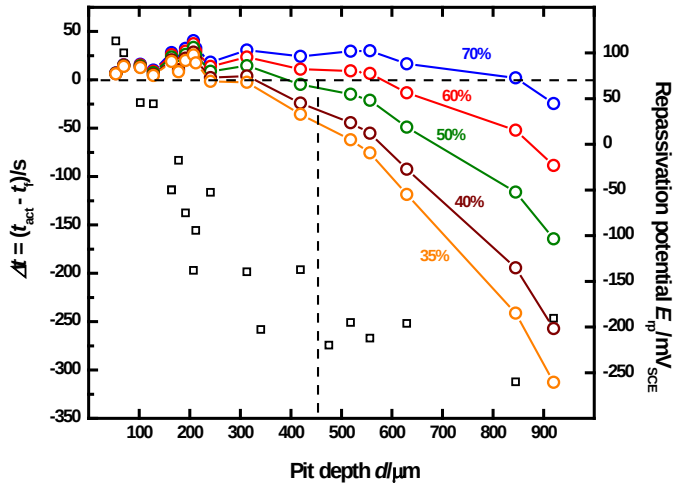

Figure 3.7. Estimation of the concentration of metal cations at the corroding surface as the pit transitions from stability to repassivation, under zero flux boundary conditions.

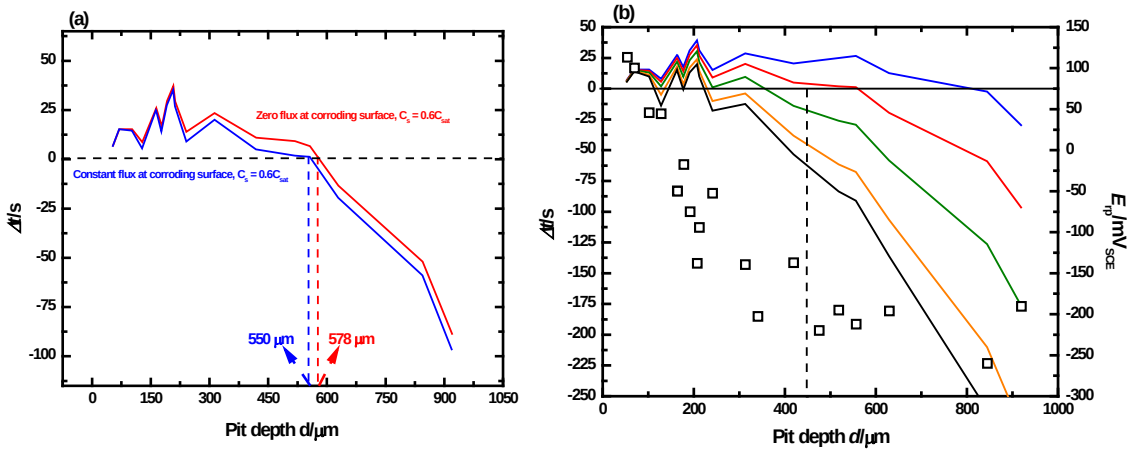

Figure 3.8. Estimation of the concentration of metal cations at the corroding surface as the pit transitions from stability to repassivation, under constant flux boundary conditions. (a) Δt obtained under both zero flux and constant flux boundary conditions considered, mapped as a function of pit depth for a surface concentration at 60% of saturation. Note that the pit depth where Δt = 0 is practically identical for both cases. (b) Estimation of the concentration of metal cations at the corroding surface as the pit transitions from stability to repassivation, under constant flux boundary conditions.

Conservative estimate of surface concentration consistent with altered boundary conditions

The quantitative framework proposed in this study showed similar results upon extension to experiments that considered a non-zero flux at the corroding boundary. Figure 3.8 (a) shows how the results obtained using a constant flux boundary condition are practically identical to those obtained with the simpler zero flux consideration. Figure 3.8 (b) shows the series of curves drawn in the manner of those shown in Figure 3.6, but with t_f determined using the constant flux boundary condition. The resulting estimate of the critical surface concentration is slightly less than 60%, which agrees well with the solution obtained using a zero flux boundary condition

(between 50% and 60%). The constant flux boundary conditions applied served as an upper bound for this approach and therefore the use of 50% of saturation as the critical surface concentration as a conservative estimate is justified.

The framework considered in this work can also accommodate time-dependent flux boundary conditions, where the transient flux is associated with the moment the E_{rp} is measured in the experiment. As a result of the manner in which the E_{rp} is measured (as described in the experimental section), the calculations based on this flux consideration directly provide the surface concentration where $\Delta t = 0$ as a function of pit depth, thereby precluding the intermediate step of comparing t_{act} and t_f. These values of surface concentration where $\Delta t = 0$ are then compared with the depth beyond which E_{rp} reaches a plateau value to extract the critical surface concentration, similar to the non-transient flux cases considered previously. Figure 3.9 depicts these results, and the critical surface concentration is estimated to be slightly lower than 60% of the concentration at saturation. There is experimental scatter associated with this estimate because there is no inherent smoothing of the input data. The calculations based on the zero flux and constant non-zero flux boundary conditions do not encounter this problem because both utilize constant input; the former uses zero whereas the latter uses a value obtained from data averaging. However, despite this limitation, the critical value of surface concentration determined using the transient flux boundary conditions is in good agreement with - and bounded by - the conservative estimate of 50% of saturation from the zero flux consideration.

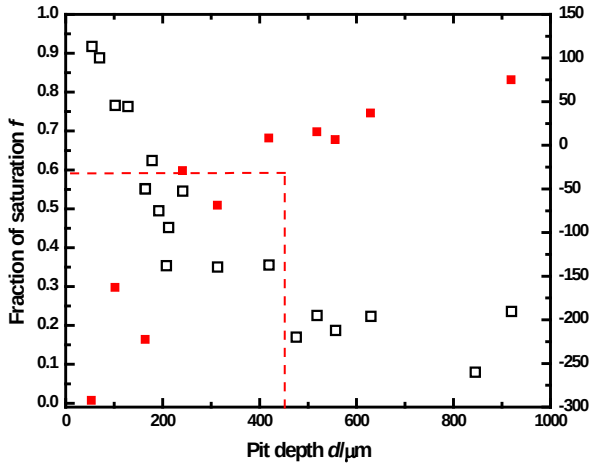

Figure 3.9. Estimation of the concentration of metal cations at the corroding surface as the pit transitions from stability to repassivation, when the transient current density in the polarization scan sequence is considered as the time-dependent flux.

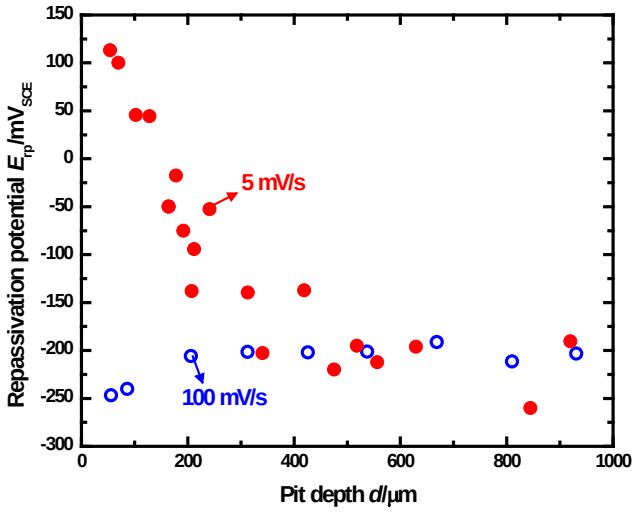

Figure 3.10. Effect of scan rate on E_{rp} behavior with increasing pit depth.

Scan rate does not affect repassivation potential once steady state conditions are attained

Figure 3.10 compares the E_{rp} behavior with pit depth obtained at a higher scan rate of 100 mV/s, to the data obtained at 5 mV/s. Although the nature of the approach to the E_{rp} plateau is reversed from that observed for the data obtained at 5 mV/s, with more negative potential values measured at shallow pit depths, the value to which the repassivation potential saturates is essentially identical. It is important to note that at depths greater than 400 μm (which correspond to a truly one-dimensional steady state mass transport response based on the pit depth[81]), the measured repassivation potential is stable around −200 mV_{SCE}, which is the plateau value obtained at 5 mV/s as well. The active potentials recorded at pits shallower than 200 μm may be attributed to the fact that true 1–D mass transport is not reached until about 400 μm.[81] An experimental caveat regarding the choice of the scan rate in order to obtain the E_{rp} trend with pit depth (decreasing at *d* increases, until a plateau is reached) has been reported in published high-throughput artificial pit studies.[73] The results of this study indicate that this choice can be quantified based on the attainment of true 1–D mass transport conditions.

Criterion of single critical surface concentration valid across most atmospheric conditions

Previous artificial pit studies have shown that $(i \cdot x)_{saltfilm}$ ought to be corrected for the effect of bulk $[Cl^-]$,[81,82] so that the experimental data may accurately reflect the theoretical 1–D Galvele mass transport formulation based on the cation concentration gradient in the pit.[1] The results of this study, interpreted in this context, would therefore indicate that the critical surface concentration for pit stability is independent of the bulk electrolyte. Woldemedhin *et al.*[82] assumed a constant value for *D* to rationalize the linear relationship observed between $(i \cdot x)_{saltfilm}$ and bulk $[Cl^-]$. Although this assumption simplifies the behavior of the system at high bulk $[Cl^-]$,

these data may be revisited to investigate the notion that a single critical pit solution chemistry describes pit stability across various bulk chloride compositions. Figure 3.11 depicts the variation of the pit stability product (in terms of both ($i \cdot x$) as well as $D \cdot C$) across a range of bulk [Cl^-] up to 4 M. Included in this figure, apart from the replotted $(i \cdot x)_{saltfilm}$ data from Woldemedhin *et al.*,[82] are pit stability product calculations for the following cases:

- Constant $D = 8.24 \times 10^{-6}$ cm^2/s, C_{sat} varies with bulk [Cl^-] corrected for the common ion effect via numerical calculations based on the solubility product $K_{sp} = [Me^{+z}]\,[Cl^-]^z$, as shown by Ernst and Newman for $FeCl_2$.[54] The value of C_{sat} at zero bulk [Cl^-] is assumed to be 5.02 M, as reported by Isaacs *et al*. from *in situ* X-ray studies.[87] This value is in close agreement with $(i \cdot x)_{saltfilm}$ values extrapolated to zero bulk [Cl^-] reported by Srinivasan *et al.*[81]
- Both D and C_{sat} vary with bulk [Cl^-]. Calculation of the variation in C_{sat} follows the procedure outlined previously. D is varied based on the change in dynamic viscosity (η) with [Cl^-] within the pit following the method of Jun *et al.*[84] OLI Analyzer Studio 9.2 is used to calculate the behavior of η in different concentrations of the solutions of interest (NaCl, LiCl, and $FeCl_3$) at 25 °C. η varies in the pit as a function of distance from the pit base. The concentrations of the 316L cation and Cl^- were fixed at the pit base ($C_{316L} = C_{sat}$, [Cl^-] = $z \cdot C_{sat}$) and pit mouth ($C_{316L} = 0$, [Cl^-] = bulk [Cl^-]). The concentration of the bulk cation was allowed to then vary within the pit under the constraints of electroneutrality. A total pit depth of 500 μm was considered so that the system was definitively under 1–D mass transport in accordance with the work of Srinivasan *et al.*[81]

The Stokes-Einstein equation is then used to calculate D as a function of varying η:

$$D = \frac{kT}{6\pi\eta r} \quad \text{..... (3.7)}$$

where k is the Boltzmann constant (= 1.38×10^{-23} J. mol^{-1}. K^{-1}), T is the temperature in kelvin (= 298 K), and r is radius of the species whose transport is being considered. Values for the radii of the hydrated cations of iron(II), chromium(III), and nickel(II) were taken from Kielland.[88] The radius for a hydrated 316L cation is calculated by weighting the radii of these individual cations in stoichiometric proportion of dissolution, which resulted in a value of 3.32 Å. Although not all cations in solution need exist in the hydrated state, this assumption serves as a reasonable lower bound on the diffusion coefficient obtained via these calculations.

Figure 3.11 (a) shows that the pit stability data (represented in terms of $D \cdot C$) at low bulk [Cl^-] is well approximated by the assumption of constant D. The experimental data at high bulk [Cl^-] is observed to be described well by the diffusion behavior of hydrated cations in concentrated solution. Figure 3.11 (b) shows the same pit stability data as Figure 11 (a), but instead plotted in terms of ($i \cdot x$). The value of $(i \cdot x)_{crit}$ obtained from this study (corresponding to 50% of saturation of cation) is observed to be a valid lower bound on the pit stability data. These results therefore suggest that anodic stability criteria across a range of bulk chloride concentrations can be described by a single critical value. Depending on the influence of the common ion effect arising from the contribution of the bulk electrolyte to the solubility of the cationic chlorides, the critical value of 50% may lead to the precipitation of a salt film, particularly at high bulk [Cl^-]. These results are in good agreement with the trends reported by Laycock *et al.*,[55] which state that E_T (the lowest potential at which the salt film is stable) decreases with increasing bulk [Cl^-]. It would seem therefore, that for sufficiently high bulk [Cl^-], the surface condition corresponding to the transition between active dissolution and repassivation may correspond to a salt film but with the cation concentration lower than 100% saturation.

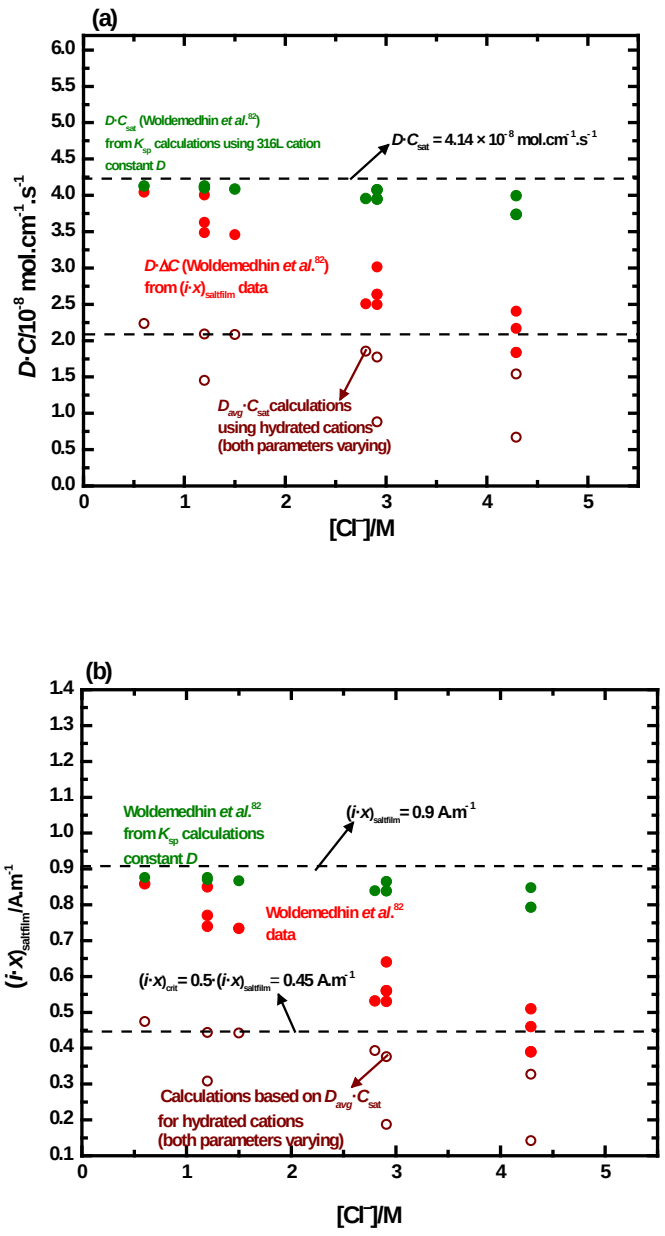

Figure 3.11. Bulk electrolyte effects on pit stability. Data plotted in terms of (a) $D{\cdot}C$ and (b) $(i{\cdot}x)_{\text{saltfilm}}$. Note that the critical surface concentration obtained by this study results in a lower bound for the experimental data across various bulk [Cl^-].

3.7. Conclusion

A comprehensive quantitative framework to assess the electrochemical factors critical to both pit stability and repassivation was developed using artificial pit experiments and mass transport modeling. The artificial pit experiments informed a one-dimensional diffusion model by providing electrochemical parameters describing the dissolution flux and the repassivation potential in terms of the pit depth. Results from the model ascertained 50% of the cation concentration at saturation as the critical value of the chemistry of the actively corroding surface for the onset of repassivation. This critical value was determined to be a conservative lower bound for different boundary conditions. In this manner, the study quantitatively established that that the same critical factors described both pit stability and repassivation by evaluating them via a unified methodology. Analysis of published pit stability data was extended to investigate the idea emerging from this work that a single critical surface concentration, independent of bulk environment, governed anodic dissolution during pitting. The rationale provided by this interpretation was demonstrated to account for the apparent dependence of the measured pit stability product on bulk [Cl^-]. These results also indicate that the critical pit solution chemistry, calculated based on the cation concentration gradient, was constant for a range of bulk chloride concentration up to 4 M.

3.8. References

1. J. R. Galvele, *J. Electrochem. Soc.*, **123**, 464–474 (1976).

2. J. R. Galvele, *Corros. Sci.*, **21**, 551–579 (1981).

3. S. M. Gravano and J. R. Galvele, *Corros. Sci.*, **24**, 517–534 (1984).

4. R. C. Newman and H. S. Isaacs, *J. Electrochem. Soc.*, **130**, 1621–1624 (1983).

5. R. C. Newman and H. S. Isaacs, *Passivity of Metals and Semiconductors* M. Froment, Editor, Elsevier B.V, Bombannes, France, (1983).

6. R. C. Newman and E. M. Franz, *Corrosion*, **40**, 325–330 (1984).

7. G. T. Gaudet et al., *AIChE J.*, **32**, 949–958 (1986).

8. N. J. Laycock and R. C. Newman, *Corros. Sci.*, **39**, 1771–1790 (1997).

9. G. Butler, H. C. K. Ison, and A. D. Mercer, *Br. Corros. J.*, **6**, 31–38 (1971).

10. Z. Szklarska-Smialowska and J. Mankowski, *Corros. Sci.*, **12**, 925–934 (1972).

11. T. Suzuki, M. Yamabe, and Y. Kitamura, *Corrosion*, **29**, 18–22 (1973).

12. J. Mankowski and Z. Szklarska-Smialowska, *Corros. Sci.*, **15**, 493–501 (1975).

13. H.-H. Strehblow and M. B. Ives, *Corros. Sci.*, **16**, 317–321 (1976).

14. A. Turnbull, *Corros. Sci.*, **23**, 833–870 (1983).

15. T. Hakkarainen, in *Corrosion Chemistry within Pits, Crevices and Cracks*, A. Turnbull, Editor, p. 17–26, Her Majesty's Stationery Office, London, United Kingdom (1987).

16. G. S. Frankel, *J. Electrochem. Soc.*, **145**, 2186–2198 (1998).

17. M. Pourbaix, *Corrosion*, **26**, 431–438 (1970).

18. Z. Szklarska-Smialowska and M. Janik-Czachor, *Corros. Sci.*, **11**, 901–914 (1971).

19. N. Pessall and C. Liu, *Electrochimica Acta*, **16**, 1987–2003 (1971).

20. T. Suzuki and Y. Kitamura, *Corrosion*, **28**, 1–6 (1972).

21. H. W. Pickering and R. P. Frankenthal, *J. Electrochem. Soc.*, **119**, 1297–1304 (1972).

22. B. E. Wilde and E. Williams, *Electrochimica Acta*, **16**, 1971–1985 (1971).

23. K. K. Starr, E. D. Verink, and M. Pourbaix, *Corrosion*, **32**, 47–51 (1976).

24. Z. Szklarska-Smialowska and J. Mankowski, *Corros. Sci.*, **18**, 953–960 (1978).

25. S. Tsujikawa and Y. Hisamatsu, *Boshoku Gijutsu - Corros. Eng.*, **29**, 37–40 (1980).

26. S. Tsujikawa and Y. Hisamatsu, in *Improvement of Corrosion Resistance of Structural Materials in Aggressive Media*, J. M. Kolotyrkin, Editor, Nauka Publishers, Moscow, Russia (1984).

27. H. W. Pickering, *Corros. Sci.*, **29**, 325–341 (1989).

28. N. G. Thompson and B. C. Syrett, *Corrosion*, **48**, 649–659 (1992).

29. N. Sridhar and G. A. Cragnolino, *Corrosion*, **49**, 885–894 (1993).

30. F. Bocher, R. Huang, and J. R. Scully, *Corrosion*, **66**, 55002-55002–15 (2010).

31. M. R. Ortíz, M. A. Rodríguez, R. M. Carranza, and R. B. Rebak, *Corrosion*, **66**, 105002-105002–12 (2010).

32. I. Epelboin, C. Gabrielli, M. Keddam, and H. Takenouti, *Z. Für Phys. Chem. N. F.*, **98**, 215–232 (1975).

33. I. Epelboin, C. Gabrielli, and M. Keddam, *Corros. Sci.*, **15**, 155–171 (1975).

34. H.-H. Strehblow, *Mater. Corros.*, **27**, 792–799 (1976).

35. G. S. Frankel, L. Stockert, F. Hunkeler, and H. Boehni, *Corrosion*, **43**, 429–436 (1987).

36. G. T. Burstein, P. C. Pistorius, and S. P. Mattin, *Corros. Sci.*, **35**, 57–62 (1993).

37. P. C. Pistorius and G. T. Burstein, *Philos. Trans. Phys. Sci. Eng.*, **341**, 531–559 (1992).

38. S. T. Pride, J. R. Scully, and J. L. Hudson, *J. Electrochem. Soc.*, **141**, 3028–3040 (1994).

39. T. R. Beck, *J. Electrochem. Soc.*, **120**, 1317–1324 (1973).

40. R. C. Alkire and K. P. Wong, *Corros. Sci.*, **28**, 411–421 (1988).

41. R. C. Newman, M. A. A. Ajjawi, H. Ezuber, and S. Turgoose, *Corros. Sci.*, **28**, 471–477 (1988).

42. U. Steinsmo and H. S. Isaacs, *Corros. Sci.*, **35**, 83–88 (1993).

43. H. S. Isaacs, *J. Electrochem. Soc.*, **120**, 1456–1462 (1973).

44. J. W. Tester and H. S. Isaacs, *J. Electrochem. Soc.*, **122**, 1438–1445 (1975).

45. I. L. Rosenfeld, I. S. Danilov, and R. N. Oranskaya, *J. Electrochem. Soc.*, **125**, 1729–1735 (1978).

46. T. R. Beck, *J. Electrochem. Soc.*, **126**, 1662 (1979).

47. N. Sato, *J. Electrochem. Soc.*, **129**, 260–264 (1982).

48. T. R. Beck, *Electrochimica Acta*, **29**, 485–491 (1984).

49. K. J. Vetter and H. H. Strehblow, in *Localized Corrosion*, R. W. Staehle, B. F. Brown, J. Kruger, and A. Agrawal, Editors, p. 240, NACE, Houston (1974).

50. G. S. Frankel, J. R. Scully, and C. V. Jahnes, *J. Electrochem. Soc.*, **143**, 1834–1840 (1996).

51. P. Ernst, N. J. Laycock, M. H. Moayed, and R. C. Newman, *Corros. Sci.*, **39**, 1133–1136 (1997).

52. P. Ernst and R. C. Newman, *Corros. Sci.*, **44**, 927–941 (2002).

53. P. Ernst and R. C. Newman, *Corros. Sci.*, **44**, 943–954 (2002).

54. P. Ernst and R. C. Newman, *Corros. Sci.*, **49**, 3705–3715 (2007).

55. N. J. Laycock et al., *ECS Trans.*, **41**, 3–16 (2012).

56. M. Pourbaix et al., *Corros. Sci.*, **3**, 239–259 (1963).

57. J. M. Kolotyrkin, *Corrosion*, **19**, 261t–268t (1963).

58. J. Horvath and H. H. Uhlig, *J. Electrochem. Soc.*, **115**, 791 (1968).

59. J. L. Crolet and J. M. Defranoux, *Corros. Sci.*, **13**, 575–585 (1973).

60. S. Okayama, S. Tsujikawa, and K. Kikuchi, *Boshoku Gijutsu - Corros. Eng.*, **36**, 631–638 (1987).

61. B. E. Wilde, in *Localized Corrosion*, R. W. Staehle, B. F. Brown, J. Kruger, and A. Agarwal, Editors, p. 342–352, NACE, Houston, TX (1974).

62. *ASTM G61-86 Standard Test Method for Conducting Cyclic Potentiodynamic Polarization Measurements for Localized Corrosion Susceptibility of Iron-, Nickel-, or Cobalt-Based Alloys*, ASTM International, West Conshohocken, PA, (2009).

63. H. W. Pickering, *J. Electrochem. Soc.*, **150**, K1 (2003).

64. D. S. Dunn, N. Sridhar, and G. A. Cragnolino, *Corrosion*, **52**, 115–124 (1996).

65. D. S. Dunn, G. A. Cragnolino, and N. Sridhar, *Corrosion*, **56**, 90–104 (2000).

66. A. Anderko, N. Sridhar, and D. S. Dunn, *Corros. Sci.*, **46**, 1583–1612 (2004).

67. *ASTM G192-08 Standard Test Method for Determining the Crevice Repassivation Potential of Corrosion-Resistant Alloys Using a Potentiodynamic-Galvanostatic-Potentiostatic Technique*, ASTM International, West Conshohocken, PA, (2008).

68. K. J. Evans et al., *JOM*, **57**, 56–61 (2005).

69. N. S. Zadorozne, C. M. Giordano, M. A. Rodríguez, R. M. Carranza, and R. B. Rebak, *Electrochimica Acta*, **76**, 94–101 (2012).

70. A. Anderko, F. Gui, L. Cao, N. Sridhar, and G. R. Engelhardt, *Corrosion*, **71**, 1197–1212 (2015).

71. L. Cao, A. Anderko, F. Gui, and N. Sridhar, *Corrosion*, 636–654 (2016).

72. T. Okada, *J. Electrochem. Soc.*, **131**, 1026–1032 (1984).

73. J. Srinivasan, M. J. McGrath, and R. G. Kelly, *J. Electrochem. Soc.*, **162**, C725–C731 (2015).

74. R. C. Newman, *Corros. Sci.*, **23**, 1045–1046 (1983).

75. Z. Y. Chen, F. Cui, and R. G. Kelly, *J. Electrochem. Soc.*, **155**, C360–C368 (2008).

76. Z. Y. Chen and R. G. Kelly, *J. Electrochem. Soc.*, **157**, C69–C78 (2010).

77. M. T. Woldemedhin, M. E. Shedd, and R. G. Kelly, *J. Electrochem. Soc.*, **161**, E3216–E3224 (2014).

78. J. Srinivasan, M. J. McGrath, and R. G. Kelly, *ECS Trans.*, **58**, 1–11 (2014).

79. Y. Kondo, *Corrosion*, **45**, 7–11 (1989).

80. T. Mills, S. Prost-Domasky, K. Honeycutt, and C. Brooks, in *Corrosion Control in the Aerospace Industry*, S. Benavides, Editor, CRC Press LLC, Boca Raton, FL (2009).

81. J. Srinivasan, C. Liu, and R. G. Kelly, *J. Electrochem. Soc.* (submitted).

82. M. T. Woldemedhin, J. Srinivasan, and R. G. Kelly, *J. Solid State Electrochem.*, **19**, 3449–3461 (2015).

83. M. H. Moayed and R. C. Newman, *J. Electrochem. Soc.*, **153**, B330–B335 (2006).

84. J. Jun, G. S. Frankel, and N. Sridhar, *J. Solid State Electrochem.*, **19**, 3439–3447 (2015).

85. A. M. Lucente and J. R. Scully, *J. Electrochem. Soc.*, **155**, C234–C243 (2008).

86. H. C. Kuo and D. Landolt, *Electrochimica Acta*, **20**, 393–399 (1975).

87. H. S. Isaacs, J.-H. Cho, M. L. Rivers, and S. R. Sutton, *J. Electrochem. Soc.*, **142**, 1111–1118 (1995).

88. J. Kielland, *J. Am. Chem. Soc.*, **59**, 1675–1678 (1937).

Chapter 4

4.1. Overview

This chapter builds upon the work presented in Chapter 3 by integrating the chemistry at the corroding surface into the quantitative framework for pitting stability. The diffusional model described in the framework is leveraged to design artificial pit experiments to examine anodic kinetics at different surface concentrations for changes in corrosion behavior as the surface transitions from active dissolution to repassivation. The influence of the local cathodic reaction (hydrogen evolution reaction, or HER) on the pH of the corroding surface is studied using cation hydrolysis. These studies permit the extraction of a critical pH condition based on repassivation proceeding as a result of oxide nucleation. This criterion is then utilized to investigate the self-consistency of the quantitative framework as a descriptor of conditions for repassivation. Mixed potential analysis contributes to this validation by providing a mechanistic rationale for the repassivation process.

An original research article based on this chapter has been published in the Journal of The Electrochemical Society, and can be accessed by the following description:

J. Srinivasan and R. G. Kelly: *Evaluating the Critical Chemistry for Repassivation at the Corroding Surface Using Mass Transport Model-Based Artificial Pit Experiments.* ***Journal of The Electrochemical Society*** 163, 13 (2016): pp. C768-C777.

4.2. Abstract

One-dimensional mass transport model calculations were utilized to design experiments with stainless steel artificial pit electrodes to determine the critical concentration of cations at the corroding surface representing the transition between stable pitting and repassivation. Rapid polarization scans following salt film precipitation and consequent open circuit dilution to different surface concentrations permitted the evaluation of kinetics at various degrees of saturation. These experiments showed a distinct change in kinetics as the surface concentration decreased, thus identifying the critical pit chemistry for the onset of repassivation. Chemical modeling of oxide precipitation from solution as a function of pH across varying surface concentration permitted the investigation of oxide nucleation as the cause of repassivation. This analysis enabled the estimation of the pH at which the first oxide would precipitate in the critical pit solution chemistry, which when combined with cation hydrolysis calculations resulted in the evaluation of the critical pH at the transition between pit stability and repassivation. A mixed potential theory-based analysis of these results was utilized to provide mechanistic strength to the quantitative framework describing critical factors for pitting stability and repassivation.

4.3. Introduction

The chemistry of the corroding surface of an active pit is typically characterized in terms of the concentration of the cations produced by dissolution and the acidic pH that results from their subsequent hydrolysis.[1–7] Efforts to determine the critical concentration of metal cations required to sustain pitting have included direct *in situ* methods,[4,8–10] electrochemical measurements in simulated pit solutions[4–6,11,12], as well as artificial pits.[13–17] Invasive interrogation techniques result in the perturbation of the corroding solution which introduces additional mass transport, thereby complicating the interpretation of the resulting information.[7,18] Kinetics measurements in simulated solutions approximate the pit chemistry in terms of the species involved and their concentration.[12,19,20] Experiments based on the artificial pit technique possess an advantage over other methods because of the simplicity of their construction and access of the chemistry at the actual corroding surface via the associated potential and current density. Use of the lead-in-pencil artificial pit geometry in particular has been successful in estimating surface concentration from the dissolution flux via one-dimensional mass transport analysis.[16,21–29] The critical value of this concentration – below which the pit is no longer stable and begins to repassivate – remains a topic of debate. Opinion is divided[16,22–26,26,30–37] over whether or not a salt film (and as a result, a solution at 100% saturation) is a necessary requisite for pitting to stably proceed.

In any case, the loss of the critical solution chemistry is expected to be accompanied by a rise in local pH due to the decrease in metal dissolution rate and subsequently diminished cation hydrolysis.[5,38] Several authors have reported that high concentrations of Fe, Ni, and Cr result in an increase in H^+ activity.[5,6,39–43] Oldfield and Sutton[6] formulated an empirical relationship between the measured pH in stainless steel pit solutions and the concentration of cationic

chlorides, which was primarily based on the hydrolysis of $CrCl_3$. Experimental measurements have resulted in a range of pH values from −0.13 to 2.3 being reported.[4,7,9,11,41,44,45] It must be noted however, that these studies investigated dissolution in highly concentrated pit solutions (close to saturation). This chemistry was obtained either by the application of high potential or experimentally simulated as an aqueous mixture of dissolved cationic chlorides. Long-term testing of stainless steel crevices has recorded pH values between 2 and 3.[46] However, these estimates have not been quantitatively examined in the context of critical conditions associated with the transition from pit stability to repassivation. Attempts to investigate these conditions in concert have been impeded by the aforementioned difficulty in accessing occlusions without solution perturbation[7,18].

Suzuki and Kitamura[38] acknowledged that for repassivation to occur, the local cathodic reaction inside the pit must play a role in increasing the pH beyond a critical value, concomitant with a decrease in the surface concentration. The influence of the local cathodic reaction on the chemistry of the corroding surface has been outlined in a number of studies relating to stainless steel crevice corrosion and crack tip electrochemistry.[7,47–50] The basis for this argument emerges from charge conservation: the anodic dissolution current must be balanced by cathodic currents from *both* the external cathodic reaction on the surface exposed to the bulk solution *and* the internal cathodic reaction at the pit base. Owing to the anoxic conditions within the pit, the local cathodic reaction is typically the hydrogen evolution reaction (HER) via the reduction of water, which contributes hydroxyl ions that cause the pH at the corroding surface to rise. It stands to reason therefore, that any consideration of the chemistry at repassivation has to include the effect of the local HER.

On the basis of thermodynamic calculations, Okada[51] posited that repassivation occurred as a result of the nucleation of a protective oxide in competition with the stability of a hydrous salt film. The general repassivation model developed by Anderko and coworkers[52–56] was founded upon this view. However, the authors assumed the surface condition at repassivation to be at or near saturation. The relationship between the critical potential that described the corroding surface at repassivation (E_{rp}, the repassivation potential) and the actual local chemistry was not quantitatively examined with respect to whether such conditions would in fact result in oxide nucleation. Furthermore, although the E_{rp} has been defined as the potential below which no further pitting takes place, its measurement in experiment has been based on a user-selected current density being approached. Multiple values for this current density have been utilized in the literature,[19,20,52,57–60] from 1 μA/cm^2 to 100 μA/cm^2; however, a quantitative argument justifying this choice with respect to the chemistry at the repassivating surface has not been presented.

Recently, Srinivasan *et al.*[26–29,37] have discussed the utility of using the artificial pit technique to probe critical conditions that govern the transition from stable pitting (active dissolution) to repassivation. These studies described a framework that utilized mass transport modeling to quantitatively connect measured estimates of both the Galvele[14] pit stability product ($i \cdot x$) and long-term E_{rp},[19] which resulted in a methodology to evaluate the degree of saturation at the corroding surface as the pit approaches repassivation. These results were also applied in combination with pit stability data in concentrated chlorides[25,35,36,61] towards understanding the anodic stability criteria for stainless steel pitting in atmospheric conditions.

The work presented in this paper focuses on incorporating the local chemistry of the corroding surface into this comprehensive paradigm for critical pitting factors. Artificial pit data

at successively dilute surface concentrations are examined for a transition in surface kinetics from dissolution to repassivation. Chemical modeling using solution thermodynamics is utilized to simulate both electrochemical processes occurring at the corroding surface – anodic dissolution as well as the local HER. This procedure permits the systematic study of the tendency of oxides to spontaneously precipitate from solutions corresponding to varying local chemistry, thereby enabling the evaluation of a critical pH that results in repassivation via oxide nucleation. These efforts are directed towards employing the critical pH as a physical basis for repassivation and developing a mechanistic foundation for the reported quantitative framework describing pit stability and repassivation.

4.4. Experimental

Mass Transport Modeling

The diffusion equation was solved for a one-dimensional pit configuration, applying the boundary condition of zero flux at the corroding surface. The schematic of this mass transport model is shown in Figure 4.1; the model itself has been discussed in detail by Srinivasan and Kelly.[37] This solution yields an expression for surface concentration as a function of time and pit depth (d) for a given value of the diffusion coefficient (D). The dilution time (t_f) for a metal cation at the corroding surface from a saturated condition was then calculated for different values of the surface concentration (indicated by f, the fraction of concentration at saturation) using the following expression:

$$t_f = \frac{4d^2}{\pi^2 D} \ln \frac{8}{\pi^2 f} \quad \text{..... (4.1)}$$

This expression for t_f was derived by truncating the first term of the series obtained as the solution for f. The value used for D (= 8.24×10^{-6} cm^2/s) was taken from studies on one-dimensional pitting in the literature.[16,20,22,25] The time to dilute the surface concentration from 100% saturation to lower fractions (t_f) was calculated for various pit depths. These values were then utilized in the setup of the artificial pit electrochemical technique as will be described.

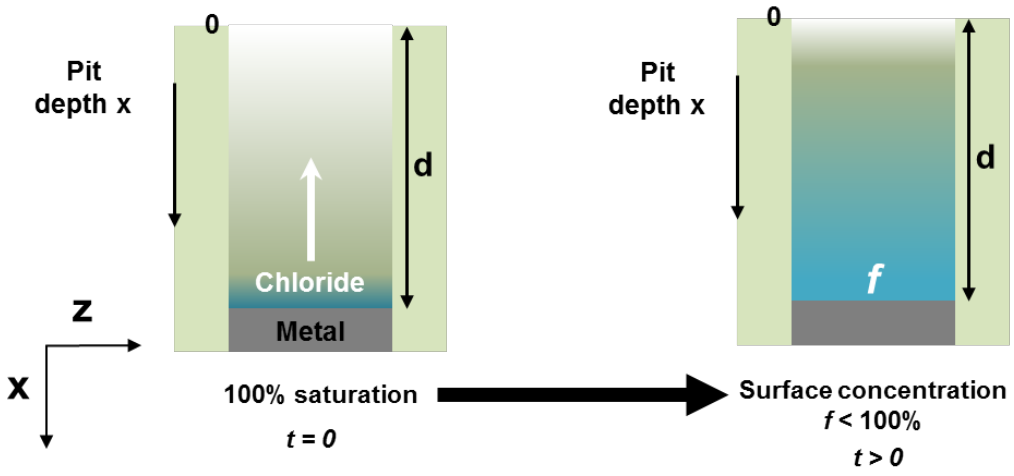

Figure 4.1. Schematic depiction of one-dimensional pit modeled. The one-dimensional diffusional characteristics of the system were considered along the x-axis as indicated.

Artificial pit experiments

One-dimensional artificial pit (lead-in-pencil) electrodes were constructed from 316L stainless steel wires (California Fine Wire Company, Grover Beach, CA) of diameter 50.8 μm embedded in epoxy. The composition of the wires used is shown in Table 4.1. Once prepared, the electrode surface was polished to a finish of 320 grit with SiC abrasive paper. The electrode, with an exposed area of 2.03×10^{-5} cm^2, was then placed upright in a test cell containing 0.6 M NaCl solution. A saturated calomel electrode (SCE) and a platinum mesh were employed as the reference electrode and counter electrode, respectively. All tests were performed at an average ambient temperature of 22 °C using a Bio-Logic SP-200 (Bio-Logic SAS, Claix, France) potentiostat.

Alloy	C	Mn	P	S	Si	Cr	Ni	Mo	N	Cu	Fe
316L	0.019	1.356	0.030	0.0287	0.406	17.07	10.66	2.16	0.0499	0.232	67.98

Table 4.1. Composition of 316L stainless steel wire used (all values in weight percent).

Pitting was initiated following a potentiostatic hold at +750 mV_{SCE} for a short duration (2 to 5 minutes) and propagated to a depth of 1000 μm under a salt film via a second potentiostatic hold at +450 mV_{SCE}. This depth was chosen to ensure definitive one-dimensional mass transport, as demonstrated by Srinivasan *et al.*[29]. Following the second potentiostatic hold, the pit was allowed to dilute from 100% saturation to different fractions under open-circuit conditions based on the time to dilution (t_f) calculated using Equation 4.1. A rapid anodic polarization scan at 100 mV/s from open circuit to a final potential of +450 mV_{SCE} was performed once each surface concentration was attained. A potentiostatic hold at +450 mV_{SCE} ensured that salt film was re-precipitated prior to each successive dilution so that the surface condition would be reinitialized to 100% saturation. The duration of each of these potential holds was very brief (≈ 2 to 5 minutes), and therefore did not result in any substantial additional pit growth. In this manner, anodic kinetics data were extracted at each surface concentration, thereby permitting the systematic examination of the local conditions in the pit as they varied from active dissolution to repassivation.

Chemical solution modeling

The local chemistry of the corroding pit surface was modeled using the solution thermodynamics database of the OLI Analyzer Studio 9.2 (OLI Systems, Inc., Cedar Knolls, NJ) software. The saturated solution of $FeCl_2$, $CrCl_3$, $NiCl_2$, and $MoCl_3$ was simulated as a mixture of the four salts in stoichiometric proportion assuming congruent dissolution of Fe, Cr, Ni, and Mo for 316L corroding in sodium chloride at a temperature of 25 °C and a pressure of 1 atm. The chemistry resulting from anodic kinetics with increasing dilution was simulated by successively decreasing the concentration from saturation while maintaining the stoichiometric proportion of the salts. The equilibrium pH of the modeled solution at each surface concentration was then calculated. The range of surface concentration chosen spanned from 5% to 75%. Concentrations outside this range were excluded because they caused the spontaneous precipitation of either CrO(OH) (at $f < 5\%$) or $FeCl_2$ (at $f > 75\%$), which disturbed the stoichiometric proportion.

The local cathodic reaction (HER) was modeled via what amounts to an artificial titration at each successive dilution of the metal ion concentration at saturation (as described previously) from pH 0 to pH 7. As the rate of HER at the corroding surface increases, a simultaneous increase in pH at the surface would occur. To simulate this effect in the concentrated solution modeling, acid (introduced as $HClO_4$) or alkali (introduced as LiOH) was added to the solution of interest. These species were chosen based on the fact that they would not interfere with the results by way of a common ion effect on the cationic chlorides generated from the stainless steel. Different oxide species were estimated to spontaneously precipitate depending upon the pH modeled in this manner. These oxides were mapped versus pH across a range of surface concentration from $f = 5\%$ to $f = 75\%$. Concentrations greater than $f = 75\%$ were excluded because these values resulted in $FeCl_2$ precipitating prior to any oxides.

4.5. Results

The anodic kinetics for 316L obtained at increasingly dilute surface concentrations are shown in Figure 4.2. A distinct transition in kinetics is observed as the pit dilutes to successively lower concentrations. At an intermediate surface concentration corresponding to 55% of saturation, an active-passive nose is seen, marking the onset of repassivation. These results agree with the estimate of critical surface concentration obtained in previous work by Srinivasan and Kelly[37], which is reproduced in Figure 4.3. The open circuit potential (E_{OCP}) of the pit solution as the pit dilutes to each surface concentration is plotted in terms of time and corresponding calculated value of f in Figures 4.4 (a) and 4.4 (b) respectively. These data support the estimate of 50-55% of saturation as the critical value of surface concentration obtained by Srinivasan and Kelly[37] because the E_{OCP} rises slowly with time (as shown in Figure 4.4 (a)) once the pit has diluted to at least this level.

Figure 4.5 shows the pH values calculated using the chemical solution model considering only anodic dissolution. This plot is also representative of simulated pit solutions prepared by mixing the respective cationic chloride salts in stoichiometric proportion in water which represent the condition with no cathodic reaction within the pit – as would be expected at high anodic dissolution rates. The solution pH increases gradually from values close to −0.25 for the most concentrated solutions considered (f = 75%) to 2.8 for the highest level of dilution considered (f = 5%), a change of nearly three orders of magnitude in H_3O^+ activity. These results are consistent with those obtained via the empirical relationship between cationic chloride concentration and pH reported by Oldfield and Sutton.[6]

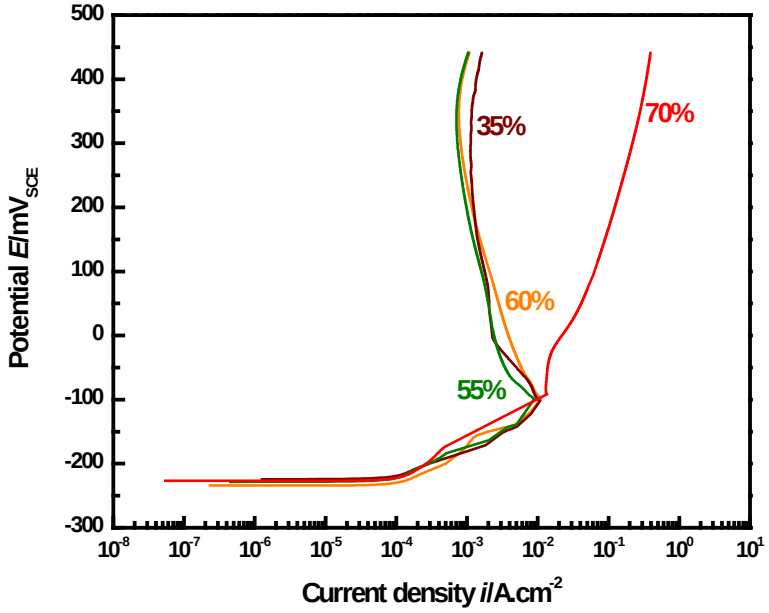

Figure 4.2. Results from anodic scans at successive dilution. Note the active-passive nose that emerges for 316L at concentrations lower than 60%, marking the change from active dissolution to repassivation.

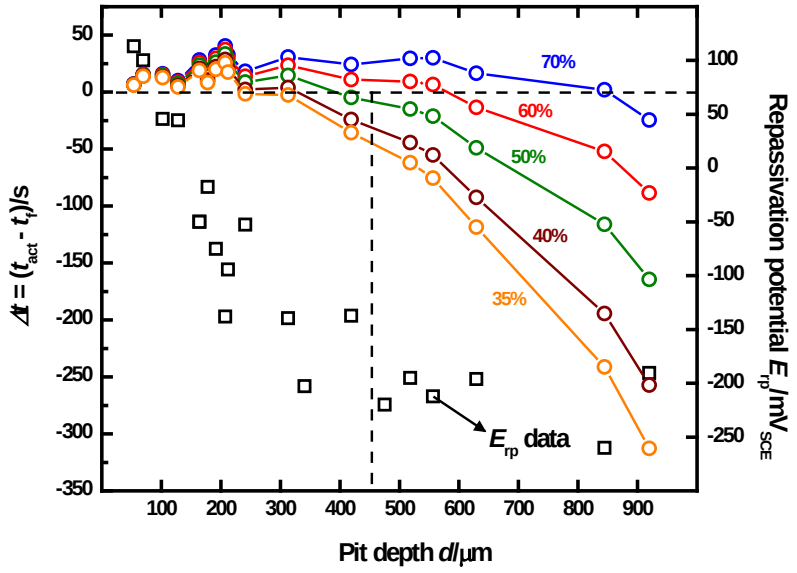

Figure 4.3. Estimation of concentration of metal cations at the corroding surface as the 316L pit transitions from stability to repassivation (replotted from Srinivasan and Kelly[37]). The data points represented as squares are the measured E_{rp} values at each pit depth. The curves indicated by the connected circles denote at each pit depth Δt, the difference between the time provided for the instrument to scan between surface conditions where the salt film is present to that represented by the E_{rp} (t_{act}), and the time to dilution (t_f). Note that the estimate of 50% of saturation serves as a conservative bound for the surface concentration at which the transition in kinetics is observed in the data in Figure 4.2.

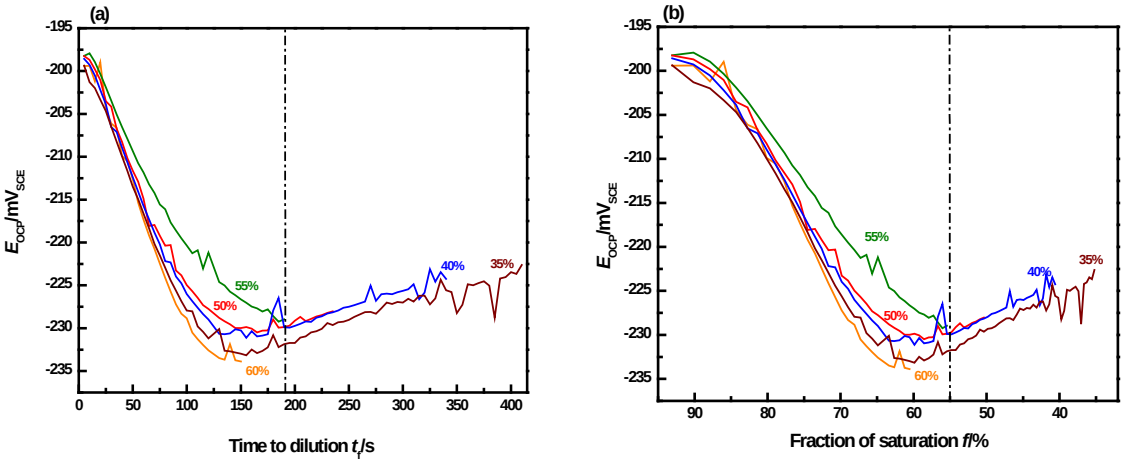

Figure 4.4. Open-circuit potential (E_{OCP}) measurements prior to polarization scans at successive dilutions following re-precipitation of salt film. The percentages denoted indicate the fraction of saturation to which the corroding surface dilutes to at the end of the measurement. (a) E_{OCP} variation with time. (b) E_{OCP} variation with time re-plotted in terms of instantaneous fraction of saturation. The broken line in both plots indicates 55% of saturation – the E_{OCP} decreases until at least this value is reached before gradually rising, suggesting the onset of repassivation.

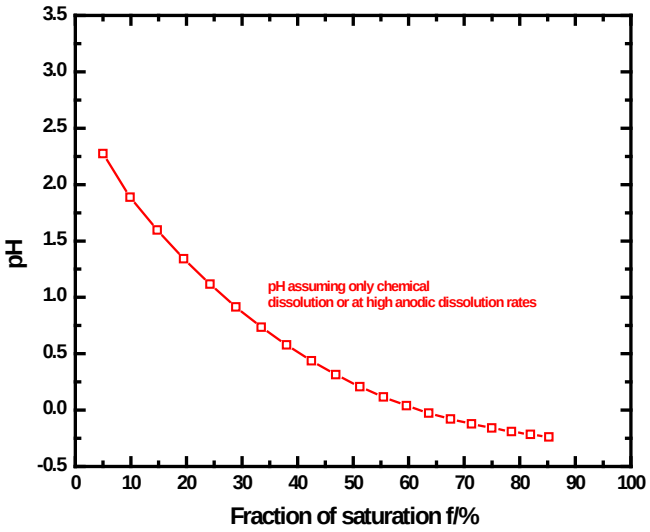

Figure 4.5. Calculated equilibrium pH resulting from chemical dissolution of cationic chlorides in stoichiometric proportion.

4.6. Discussion

The results from experiments and modeling in this study were amalgamated to investigate the influence of the local cathodic reaction on repassivation. The availability of the hydroxyl ion was utilized as a proxy variable to survey the effect of the local cathodic reaction on the pH of the corroding surface at successive dilution, permitting the estimation of the pH at which the first oxide nucleated at each surface concentration. Anodic kinetics provided the estimate of critical surface concentration, and in this chemistry, the critical pH was that value at which oxide precipitation occurred. Finally, employing the critical pH as a criterion for repassivation, the validity of the quantitative framework connecting critical factors for pitting stability was examined using mechanistic arguments based on mixed potential analysis of dissolution and HER kinetics.

Local cathodic reaction can result in pH rise which initiates repassivation

As outlined in the introduction, anoxic conditions result in the HER as the primary cathodic reaction inside the pit. The HER acts as a source of OH^- which affects the pH at the corroding surface. The influence of this introduction of OH^- on the transition from active dissolution to repassivation can be investigated in terms of the reaction equilibrium of cation hydrolysis. This approach is analogous to the rationale of Galvele *et* al.[62,63] in considering the effect of OH^- from the bulk solution on passivity breakdown. The following reactions summarize the processes occurring at the corroding surface:

- Anodic dissolution: $Me \rightarrow Me^{+z} + ze^-$

where Me^{+z} represents the '316L cation', a stoichiometric proportion of Fe^{+2}, Cr^{+3}, Ni^{+2}, and Mo^{+3}; z = 2.2 as has been utilized in several studies.[16,23,28,36,59]

- Cation hydrolysis: $Me^{+z} + H_2O \leftrightarrow Me(OH)^{+(z-1)} + H^+$

  The above expression denotes a series of hydrolysis reactions dependent on the value of *z*, the valence of the 316L cation. As pH increases, a greater availability of OH^- leads to the cation being hydrolyzed closer to the limit of its valence.

- External cathodic reaction (assuming oxygen reduction): $O_2 + 2H_2O + 4e^- \rightarrow 4OH^-$

- Internal (local) cathodic reaction (assuming HER): $2H_2O + 2e^- \rightarrow 2OH^- + H_2$

When anodic dissolution occurs at high rates, the local HER rate and its consequent effect on pH are low. However, once potentials close to repassivation are approached, anodic dissolution rates would decrease, and accordingly, the local cathodic reaction would have a greater effect on pH in the pit. This relationship is schematically shown in Figure 4.6.

The influence of the local cathodic reaction on pH can be examined in the context of the extent of cation hydrolysis, which is quantitatively expressed as the number of hydroxyl ions consumed per cation produced from dissolution. Complete hydrolysis occurs when the number of hydroxyl ions consumed per cation is equal to its valence. The consumption of hydroxyl ions is dependent on their availability which is determined by the rate of the local HER. A quantitative descriptor of the availability of hydroxyl ions is provided by the pH. In this manner, the pH can be related to the local HER rate.

Applying this rationale to the electrochemical processes at the corroding surface, complete hydrolysis necessitates that the anodic dissolution current demand is satisfied entirely by the local cathodic reaction. Once the anodic current is completely balanced by the local cathodic

current, the driving force for corrosion provided by the external cathodic reaction (galvanic separation) disappears. The extent of cation hydrolysis therefore provides an estimate of the contribution of the local cathodic reaction towards the pit chemistry. Assuming congruent dissolution for the stainless steel, the Fe^{+2}, Cr^{+3}, Ni^{+2}, and Mo^{+3} ions would be present in the solution according to the stoichiometric ratios as their respective elements in the alloy. Similarly, the hydrolysis of the 316L cation can be considered to be based on the three respective metal cations Fe^{+2}, Cr^{+3}, Ni^{+2}, and Mo^{+3} following the same stoichiometry. Therefore, the extent of the hydrolysis for the stainless steel can be modeled as a linear combination of the hydrolysis of each cation weighted according to the proportions determined by stoichiometry. The resulting pH from such a combined hydrolysis can then be calculated.

Figure 4.7 illustrates these calculations for Fe^{+2}, Cr^{+3}, Ni^{+2}, and Mo^{+3} as well as for 316L. Values for the hydrolysis equilibrium constants for Fe^{+2}, Cr^{+3}, and Ni^{+} were taken from Baes and Mesmer.[64] Hydrolysis data for Mo^{+3} were provided by the work of Anderko *et al*.[65] At acidic pH, the low availability of hydroxyl ions results in very few of these ions being consumed per cation produced. Conversely, when alkaline pH values are approached, the higher availability of OH^{-} accelerates their consumption in order to maintain equilibrium. The pH that results when a cation is hydrolyzed to the full extent of its valence can also be estimated from the plot. For example, this value is about 7 for Mo^{+3}. These results can also be interpreted in terms of the contribution of the local cathodic reaction in satisfying the anodic current density. Figure 4.8 illustrates the relationship between the extent of cation hydrolysis as the fraction of anodic current balanced by the local cathodic current and pH. As is evident from the plot, only a minor fraction of the anodic current is met by the local cathodic reaction at acidic pH. The remainder is balanced by the external cathodic reaction, which due to its physical separation from the anode, has no effect on

the chemistry of the corroding surface. As pH increases, a greater fraction of the anodic current is met locally. From the figures, it is evident that the hydrolysis behavior of the stainless steels is greatly influenced by Cr and Mo at acidic pH and by Fe and Ni at alkaline pH.

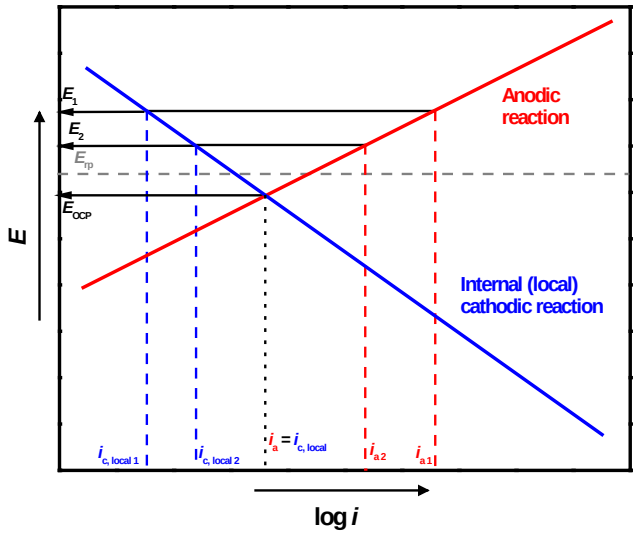

Figure 4.6. Schematic representation of the increasing influence of the local cathodic reaction towards balancing the current from anodic dissolution, as potentials close to repassivation are reached.

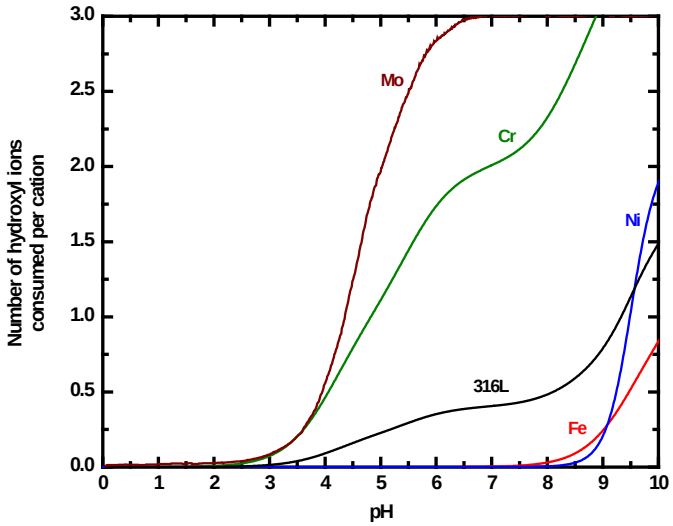

Figure 4.7. Relationship between increasing availability of hydroxyl ions and the pH, represented by the calculations of the extent of cation hydrolysis. The extent of hydrolysis progresses towards completion (number of OH^- per 316L cation = cation valence) as more hydroxyl ions are available, which is equivalent to a higher pH. Note how the presence of Cr and Mo in the alloys biases the extent of hydrolysis towards lower pH values.

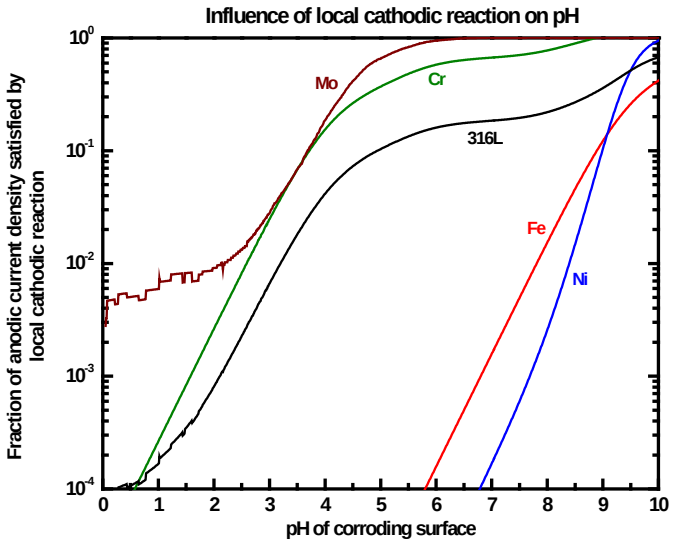

Figure 4.8. Influence of local cathodic reaction on the pH. The ratio $i_{c,local}/i_a$ is calculated by considering the fraction of cations hydrolyzed to cations produced. This fraction increases as the local HER accelerates, resulting in greater OH^- availability, more complete hydrolysis, and a rise in pH. Note how that, at acidic pH, local cathodic reaction rates do not have to be very high to effect changes in H^+ across orders of magnitude.

Oxide nucleation at critical pH leads to repassivation

Chemical modeling by artificial titration at successive dilution permitted the simulation of the local surface conditions as the pit approaches repassivation. The pH dependence of oxide speciation at different surface concentrations was thus evaluated. Such a calculation for a corroding 316L pit is depicted in Figure 4.9. The chromium(III) oxide species CrO(OH) was the first oxide to appear at a pH of 2.65, followed by the spinel $FeCr_2O_4$, and the hydroxides $Ni(OH)_2$ and $Fe(OH)_2$. Figure 10 indicates the pH values at which the first oxide precipitate is observed for various degrees of saturation at the corroding surface. CrO(OH) was estimated to be

first oxide to appear at all levels of dilution, precipitating at a pH of 2.65. The appearance of CrO(OH) as the stable oxide is consistent with the surface analysis studies of passive films on stainless steels in chloride solutions reported in the literature.[66–69] Figure 4.10 also displays the pH values that result from modeling the surface chemistry when the local cathodic reaction is not considered. This latter plot is equivalent to Figure 4.5; it indicates the pH that would result from solely considering chemical dissolution, as would be expected when the respective cation chloride salts are dissolved in stoichiometric proportion or when anodic dissolution rates are very high. The absence of a local hydroxyl source implies that the pH of the solution considering only chemical dissolution is lower than the value obtained with the local cathodic reaction taken in to account. These results support the assertion that the local cathodic reaction causes repassivation to set in at higher surface concentrations than would be predicted from anodic dissolution alone. Additionally, these data also indicate that oxide nucleation and subsequent repassivation is unlikely to occur if the pH at the corroding surface is not close to 2.5, which reinforces the argument against an extremely low value for the critical pH as has been measured in simulated pit solutions. The results from this study therefore indicate that the pH values around 0 to 1 reported in the literature modeled conditions of very high anodic dissolution, and therefore were not representative of the repassivating pit.

This work suggests that the pH of the corroding surface is a key critical parameter in determining the tendency towards repassivation by creating local conditions favorable for oxide nucleation. The pH necessary to nucleate an oxide can be attained either by sufficient dilution of the metal cation or the presence of local HER. However, the fact that corrosion is an electrochemical process necessitates the role of the local HER for repassivation because of the requirement for charge conservation. The results from this study reinforce this assertion due to

the fact that the anodic kinetics display evidence of repassivation at higher surface concentrations than would be expected from only surface dilution.

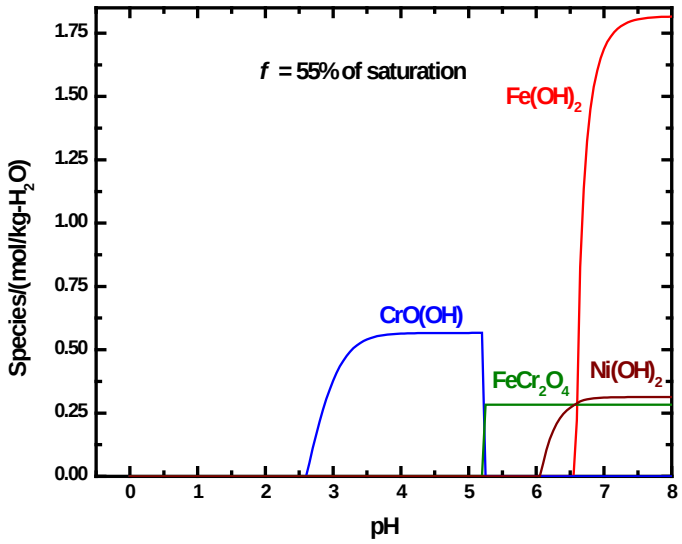

Figure 4.9. Calculation of oxide speciation as a function of pH for 316L. The surface concentration considered in this representative calculation is 55% of saturation.

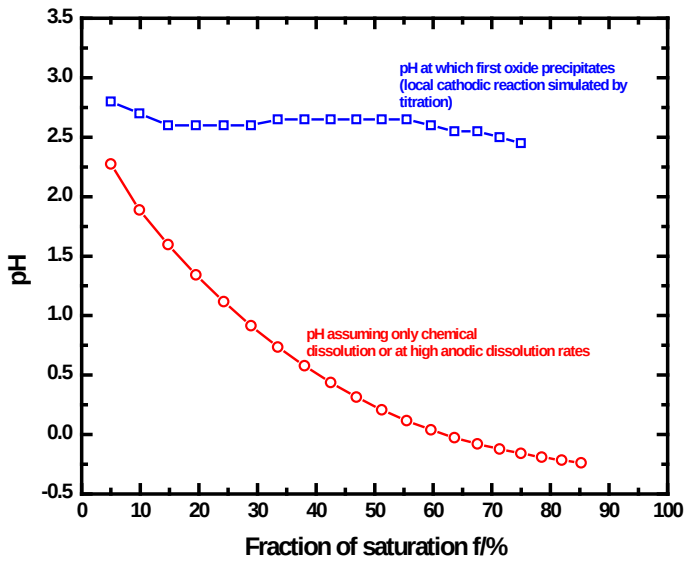

Figure 4.10. Effect of surface concentration on the pH at which the first oxide precipitates in the pit solution when the local HER is modeled via chemical simulation of titration. For each surface concentration, the pH values at which the first oxide precipitates are discernibly higher than those obtained if only anodic dissolution were considered.

Cathodic kinetics required for repassivation can be estimated from conditions for oxide nucleation

Having established the pH required for repassivation via oxide nucleation at the critical surface concentration, the local cathodic kinetics necessary to facilitate these conditions can be evaluated via mixed potential analysis. Anodic kinetics data were extracted via Tafel extrapolation of the polarization scans corresponding to the lowest surface concentration where active dissolution was observed to occur. The repassivation potential E_{rp}, as measured in previous work,[26,27,36,37] is used in combination with these data to estimate the anodic Tafel slope

at the critical surface concentration. From Figure 4.10, the pH at which the oxide nucleates in a pit solution at the critical surface concentration of f = 55% of saturation is calculated to be 2.65. Figure 4.8 indicates that this equilibrium pH for 316L is attained when the local cathodic reaction rate is 0.3% of the anodic dissolution rate. Figure 4.11 depicts the Tafel extrapolation of the experimental 316L anodic kinetics data from which the theoretical local HER line to satisfy these repassivation conditions is then generated.

The Tafel slope for the anodic dissolution kinetics from the experimental data at 55% of saturation is estimated to be 62 mV/decade. This value is in good agreement with Tafel slopes of about 60-70 mV/decade reported in the literature for the dissolution of 302 and 304 stainless steel[16,22,70] and Fe-Cr-Mo model alloys[71] in chloride media. From these results, the anodic current density at the E_{rp} (= −210 mV_{SCE})[26–28,37] is calculated to be i_a = 201 μA/cm^2. The E_{OCP} measured at 55% of saturation is −228 mV_{SCE} (from Figure 4). Using these values, the Tafel slope for the local HER under these conditions is calculated to be 8 mV/decade. These calculations are depicted in Figure 4.12. The net current density when E_{rp} is measured is denoted as i_{rp} and is nearly equal to i_a at E_{rp} due to the critical condition that $i_{c,local}/i_a$ = 0.3%.

The value of i_{rp} calculated by this analysis is observed to be nearly an order of magnitude greater than the current density at which the E_{rp} measurement was recorded (i_{rp} = 30 μA/cm^2) in the experiments reported in the literature[26–28,37]. Another observation is that the cathodic slope calculated in this manner does not correspond to reported values for established HER mechanisms. There are two primary pathways typically considered to govern the kinetics of the HER: the Volmer-Tafel (b_c = 30 mV/decade) or the Volmer-Heyrovsky (b_c = 118 mV/decade)

mechanisms.[72,73†] The apparent discrepancy observed between the experiments and calculations is likely due to the user-specified choice of the experimental i_{rp} value at which the E_{rp} measurement was made. As mentioned in the introduction, although long-term defined the E_{rp} as the potential below which no pitting proceeded, the actual measurement of the value depends on a user-specified current density – a value that has ranged from 1 μA/cm^2 to 100 μA/cm^2.[19,57,59,60,74–76] The value used in studies by Srinivasan *et al.*[26–28,37] was 30 μA/cm^2, based on current densities similar to those employed by Tsujikawa *et al.*[57,74,75] and Sridhar and coworkers,[19,77] as well as the ASTM G-192 standard.[78] The validity of this specification and its sensitivity to the individual anodic and cathodic kinetics can be examined using mixed potential theory under the constraints of the critical pH condition.

† These reaction mechanisms are based on the relative velocities of the two steps in the series for the HER to occur: a) electron discharge and b) surface desorption. The Volmer-Tafel mechanism describes a fast discharge-slow desorption process whereas the Volmer-Heyrovsky reaction path characterizes a slow discharge-fast desorption course.

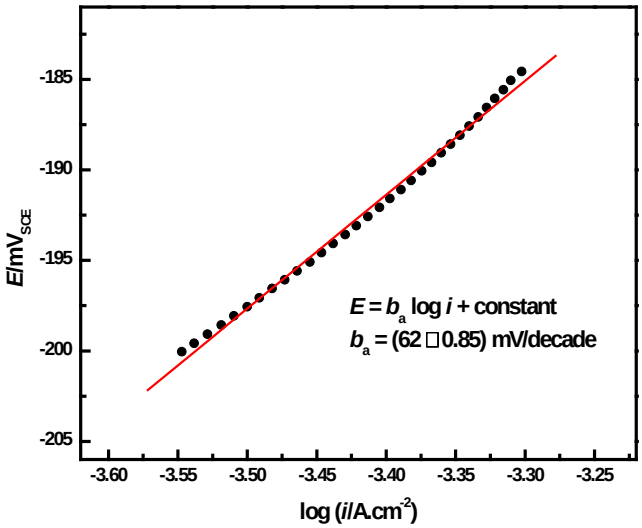

Figure 4.11. Tafel extrapolation of anodic scan at the critical surface concentration (55%) to determine b_a.

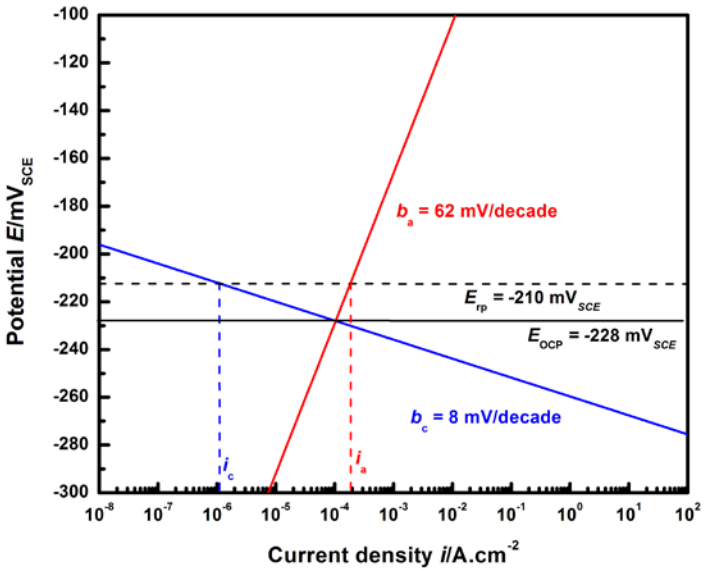

Figure 4.12. Calculation of the cathodic Tafel slope from the estimated anodic kinetics at 55% of saturation.

Critical pH provides physical basis for measurement of E_{rp} based on HER kinetics

The establishment of the minimum pH for oxide nucleation in this study as a critical factor for repassivation permitted its utilization to assess the selection of an appropriate current density at which the measurement of E_{rp} is recorded. Mixed potential theory was employed to examine the anodic kinetics data with respect to specific HER mechanisms. This treatment permitted the formulation of a physical basis for the selection of experimental parameters in determining critical factors and allowed for the examination of the self-consistency of the quantitative framework for pit stability and repassivation proposed by Srinivasan *et al.*[26–28,37]

As denoted in Figure 4.8, the ratio $i_{c,local}/i_a$ corresponding to the critical pH for repassivation is 0.3%. Based on this critical condition, mixed potential analysis is performed in

order to estimate the E_{rp} required to attain this ratio, under the conditions of the individual anodic and cathodic kinetics relevant to the reactions at the corroding surface. This estimate is then compared to the experimentally observed E_{rp} and the current density at which it was measured. Agreement of the calculated estimates with the experimental values would indicate whether the quantitative framework proposed is self-consistent with the critical surface condition for repassivation.

Calculations were performed considering the cathodic Tafel slopes corresponding to the Volmer-Tafel and the Volmer-Heyrovsky mechanisms as bounding values, *i.e.* 30 mV/decade and 118 mV/decade respectively, and the E_{OCP} from the experimental data in Figure 4.4 for 55% of saturation, −228 mV_{SCE}. The corrosion current density assumed in these calculations is the one obtained from Figure 4.12, *i.e.* 104 μA/cm^2. The anodic Tafel slope used is 62 mV/decade, as obtained from the experimental data in this study. Figure 4.13 illustrates these calculations. The E_{rp} values obtained were −175 mV_{SCE} (Volmer-Tafel) and −122 mV_{SCE} (Volmer-Heyrovsky). The value of ($i_a - i_{c,local}$) at these values provides the appropriate net current density (i_{rp}) at which the E_{rp} may be experimentally recorded, which correspond to nearly 0.75 mA/cm^2 for the Volmer-Tafel case and 5 mA/cm^2 for the Volmer-Heyrovsky case. The E_{rp} value measured by Srinivasan and Kelly[37] (−210 mV_{SCE} ±12.8 mV) has an upper bound of −197 mV_{SCE}, which is about 20 mV lower than the calculations for the Volmer-Tafel case, suggesting that these HER kinetics likely approximate actual conditions. The E_{rp} estimate obtained assuming the Volmer-Tafel HER mechanism is also close to the upper bound of the experimental scatter of the E_{rp} data measured from high-throughput artificial pit studies by Srinivasan *et al.*[28] The i_{rp} values obtained for both cathodic slopes are one to two orders of magnitude greater than the value employed in the experimental method used in the quantitative framework. These results suggest that a similar

sensitivity analysis of the repassivation conditions in terms of the anodic Tafel slope bounds needs to be performed in order to fully rationalize the observed data.

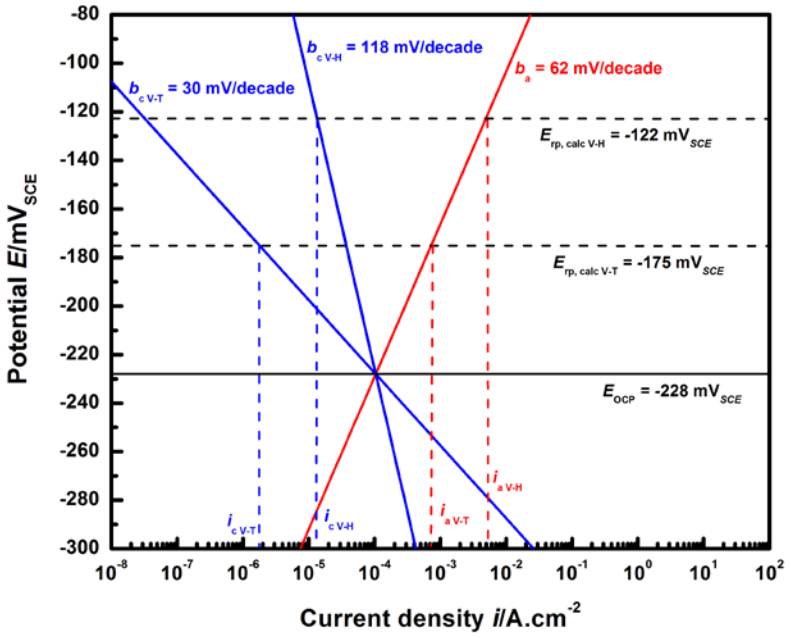

Figure 4.13. Sensitivity analysis of cathodic kinetics. Calculations were performed using the anodic Tafel slope from this study (b_a = 62 mV/decade) and cathodic HER Tafel kinetics corresponding to the Volmer-Tafel (b_c = 30 mV/decade) and Volmer-Heyrovsky (b_c = 118 mV/decade) mechanisms.

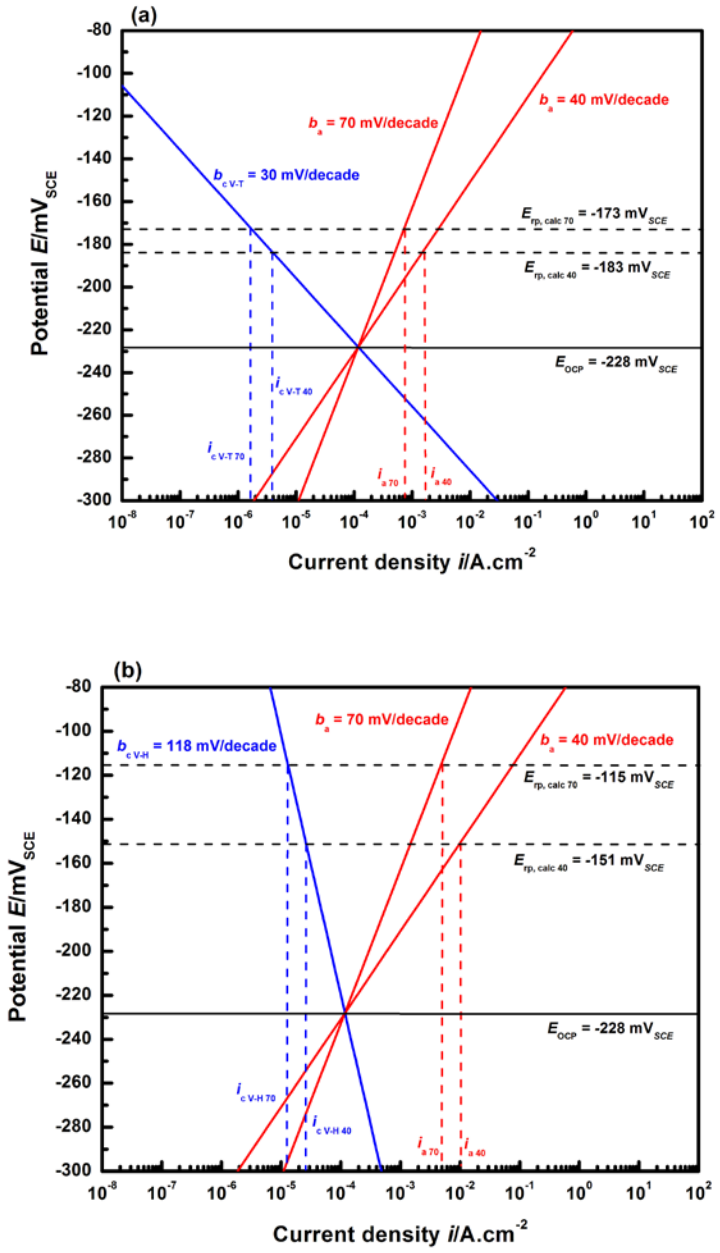

Figure 4.14. Sensitivity analysis of anodic kinetics with the Tafel slope lower bound at b_a = 40 mV/decade and the upper bound at b_a = 70 mV/decade. Calculations were performed using (a) b_c = 40 mV/decade (Volmer-Tafel HER kinetics) and (b) b_c = 118 mV/decade (Volmer-Heyrovsky HER kinetics).

Figure 4.14 displays the results for an anodic sensitivity analysis. In addition to the reported value of 70 mV/decade for stainless steels in chloride media[70,71] which serves as an upper bound, a Tafel slope of 40 mV/decade is introduced as the lower bound. This value has been reported for iron dissolution kinetics in acidic chloride and sulfate media.[79,80] Figure 4.14 (a) depicts the results utilizing cathodic kinetics corresponding to the Volmer-Tafel mechanism. The calculated E_{rp} values differ from each other by only 10 mV, at −183 mV_{SCE} (b_a = 40 mV/decade) and −173 mV_{SCE} (b_a = 70 mV/decade). The corresponding values of calculated i_{rp} are 0.72 mA/cm^2 and 1.4 mA/cm^2, which are approximately an order of magnitude larger than the values specified for E_{rp} measurement in experiments. A similar set of calculations is performed using these anodic bounds and HER kinetics corresponding to the Volmer-Heyrovsky mechanism, as shown in Figure 4.14 (b). The E_{rp} values obtained are −151 mV_{SCE} and −115 mV_{SCE} for the lower and upper anodic bounds, respectively. The i_{rp} values this analysis yields are 5 mA/cm^2 and 10 mA/cm^2, which exceed the experimentally selected current density by two orders of magnitude.

Calculations based on the lower bound of the anodic Tafel slope are thus seen to be in better agreement with repassivation behavior observed. These results also appears to suggest that the appropriate current density to be selected for E_{rp} ought to be an order of magnitude greater than presently in practice, so as to correspond to the critical condition for repassivation based on the pH for oxide nucleation. However, it must be noted here that the critical pH condition obtained in this study is based on thermodynamic modeling. Fluctuations in pit solution during the experiment may result in a higher *steady state* concentration of available OH^- only at lower current densities, creating kinetically favorable conditions for repassivation. In any case, the E_{rp} value measured at the current density selected in the experimental methodology of the proposed

framework serves as a conservative lower bound. The fact that the E_{rp} estimates using the Volmer-Tafel HER kinetics from this study are approached by the upper bound of experimental scatter from high-throughput data[28] also allays the concern raised by Anderko *et al.*[52,55] that the E_{rp} measured in this manner at high scan rates may be an overly conservative estimate.

The kinetics at repassivation are observed to be much more sensitive to variations in cathodic behavior than anodic dissolution, underscoring the importance of the local HER. The HER kinetics themselves appear to follow the Volmer-Tafel mechanism more closely than the Volmer-Heyrovsky mechanism. The rationale that the local HER follows the Volmer-Tafel pathway finds thermodynamic support in the literature. Trasatti[81] has analyzed the HER on various metal surfaces in acidic media based on their values of the standard free energy of hydrogen adsorption, which indicates that the metal-hydrogen bonds formed by Fe, Cr, Ni, and Mo are highly stable (large negative ΔG). These metals are the primary constituents of 316L as indicated in Table 4.1. The removal of the H-atom to form molecular H_2 would consequently be encumbered by a large energy barrier when it is bonded to these metal ions. Surface desorption can be considered to be the rate-determining step for hydrogen evolution under these circumstances, implying that the reaction proceeds via the Volmer-Tafel mechanism.

These results therefore demonstrate a methodology to evaluate the self-consistency of the quantitative framework employed to understand pit stability and repassivation by utilizing the pH for oxide nucleation in the pit solution as a critical condition. Analysis of the experimental kinetic data at repassivation indicated that the E_{rp} as measured by the framework serves as a conservative bound for the critical chemical conditions at the corroding surface, based on mixed potential calculations using established anodic and cathodic kinetics. Mechanistic support for the

framework was also provided by this treatment, which rationalized the observed transition from stability to repassivation to be primarily controlled by the local cathodic reaction.

4.7. Conclusion

This work employed calculations obtained from mass transport modeling to design artificial pit experiments for probing the critical pit chemistry at the transition from active dissolution to repassivation. Rapid polarization scans at various levels of dilution from saturation indicated the appearance of a well-defined change in anodic behavior, as the chemistry inside the pit grew less aggressive. The critical value of surface concentration obtained in this manner was observed to agree well with independently determined estimates from studies on pit stability at the onset of repassivation. In addition, the pH associated with the onset of repassivation was investigated using Tafel extrapolation of the polarization scans in combination with cation hydrolysis calculations. Examination of oxide speciation with respect to increasing pH at varying surface concentrations confirmed that this critical pH marked the chemistry at which oxide nucleation commenced, indicating the physical cause for the pit repassivation. This criterion was then utilized in designing arguments based on mixed potential theory that supplied a mechanistic foundation describing the critical chemistry for a pit to remain stable, which underscored the importance of the local cathodic reaction to the onset of repassivation.

4.8. References

1. N. D. Greene and M. G. Fontana, *Corrosion*, **15**, 48–54 (1959).

2. N. D. Greene and M. G. Fontana, *Corrosion*, **15**, 55–60 (1959).

3. N. D. Greene and G. Judd, *Corrosion*, **21**, 15–18 (1965).

4. T. Suzuki, M. Yamabe, and Y. Kitamura, *Corrosion*, **29**, 18–22 (1973).

5. J. Mankowski and Z. Szklarska-Smialowska, *Corros. Sci.*, **15**, 493–501 (1975).

6. J. W. Oldfield and W. H. Sutton, *Br. Corros. J.*, **13**, 104–111 (1978).

7. A. Turnbull, *Corros. Sci.*, **23**, 833–870 (1983).

8. G. Butler, H. C. K. Ison, and A. D. Mercer, *Br. Corros. J.*, **6**, 31–38 (1971).

9. M. Marek and R. F. Hochman, *Corrosion*, **30**, 208–210 (1974).

10. H. S. Isaacs, J.-H. Cho, M. L. Rivers, and S. R. Sutton, *J. Electrochem. Soc.*, **142**, 1111–1118 (1995).

11. S. Brennert and G. Eklund, *Scand. J. Metall.*, **2**, 269–272 (1973).

12. T. Hakkarainen, in *Corrosion Chemistry within Pits, Crevices and Cracks*, A. Turnbull, Editor, p. 17–26, Her Majesty's Stationery Office, London, United Kingdom (1987).

13. T. R. Beck, *J. Electrochem. Soc.*, **120**, 1317–1324 (1973).

14. J. R. Galvele, *J. Electrochem. Soc.*, **123**, 464–474 (1976).

15. H. S. Isaacs and R. C. Newman, *Corrosion Chemistry within Pits, Crevices and Cracks* A. Turnbull, Editor, Her Majesty's Stationery Office, London, (1984).

16. G. T. Gaudet et al., *AIChE J.*, **32**, 949–958 (1986).

17. R. C. Alkire and K. P. Wong, *Corros. Sci.*, **28**, 411–421 (1988).

18. G. Sandoz, C. T. Fujii, and B. F. Brown, *Corros. Sci.*, **10**, 839 (1970).

19. N. Sridhar and G. A. Cragnolino, *Corrosion*, **49**, 885–894 (1993).

20. F. Bocher and J. R. Scully, *Corrosion*, **71**, 1049–1063 (2015).

21. J. W. Tester and H. S. Isaacs, *J. Electrochem. Soc.*, **122**, 1438–1445 (1975).

22. R. C. Newman and H. S. Isaacs, *J. Electrochem. Soc.*, **130**, 1621–1624 (1983).

23. U. Steinsmo and H. S. Isaacs, *Corros. Sci.*, **35**, 83–88 (1993).

24. N. J. Laycock and R. C. Newman, *Corros. Sci.*, **39**, 1771–1790 (1997).

25. P. Ernst and R. C. Newman, *Corros. Sci.*, **49**, 3705–3715 (2007).

26. J. Srinivasan, M. J. McGrath, and R. G. Kelly, *ECS Trans.*, **58**, 1–11 (2014).

27. J. Srinivasan and R. G. Kelly, *Corrosion*, **70**, 1172–1174 (2014).

28. J. Srinivasan, M. J. McGrath, and R. G. Kelly, *J. Electrochem. Soc.*, **162**, C725–C731 (2015).

29. J. Srinivasan, C. Liu, and R. G. Kelly, *J. Electrochem. Soc.*, **163**, C694–C703 (2016).

30. T. R. Beck, *J. Electrochem. Soc.*, **126**, 1662 (1979).

31. N. Sato, *J. Electrochem. Soc.*, **129**, 260–264 (1982).

32. P. C. Pistorius and G. T. Burstein, *Philos. Trans. Phys. Sci. Eng.*, **341**, 531–559 (1992).

33. G. T. Burstein, P. C. Pistorius, and S. P. Mattin, *Corros. Sci.*, **35**, 57–62 (1993).

34. M. H. Moayed and R. C. Newman, *J. Electrochem. Soc.*, **153**, B330–B335 (2006).

35. N. J. Laycock et al., *ECS Trans.*, **41**, 3–16 (2012).

36. M. T. Woldemedhin, J. Srinivasan, and R. G. Kelly, *J. Solid State Electrochem.*, **19**, 3449–3461 (2015).

37. J. Srinivasan and R. G. Kelly, *J. Electrochem. Soc.*, **163**, C759–C767 (2016).

38. T. Suzuki and Y. Kitamura, *Corrosion*, **28**, 1–6 (1972).

39. P. R. Rhodes, *Corrosion*, **25**, 462–472 (1969).

40. Y. Hisamatsu, *Pitting Corrosion of Stainless Steels in Chloride Solution* R. W. Staehle and H. Okada, Editors, p. 99, NACE, Houston, TX, (1976).

41. D. A. Jones and B. E. Wilde, *Corros. Sci.*, **18**, 631–643 (1978).

42. R. S. Lillard, M. P. Jurinski, and J. R. Scully, *Corrosion*, **50**, 251–265 (1994).

43. H. W. Pickering, M. Wang, and Y. Xu, in *Proceedings of the Symposium on Critical Factors in Localized Corrosion II*,, vol. 95–15, p. 151–158, The Electrochemical Society, Inc., Chicago, IL (1996).

44. H. Peterson, T. J. Lennox, Jr., and R. E. Groover, *Mater. Prot.*, **9**, 23–26 (1970).

45. N. Lukomski and K. Bohnenkamp, *Mater. Corros.*, **30**, 482–486 (1979).

46. J. L. Crolet and J. M. Defranoux, *Corros. Sci.*, **13**, 575–585 (1973).

47. A. Turnbull and J. G. N. Thomas, *J. Electrochem. Soc.*, **129**, 1412–1422 (1982).

48. A. Turnbull, *Br. Corros. J.*, **32**, 283–290 (1997).

49. A. Turnbull, *Corros. Sci.*, **40**, 843–845 (1998).

50. K. C. Stewart, thesis, University of Virginia, Charlottesville, VA (1999).

51. T. Okada, *J. Electrochem. Soc.*, **131**, 1026–1032 (1984).

52. A. Anderko, N. Sridhar, and D. S. Dunn, *Corros. Sci.*, **46**, 1583–1612 (2004).

53. G. Tormoen, N. Sridhar, and A. Anderko, *Corros. Eng. Sci. Technol.*, **45**, 155–162 (2010).

54. A. Anderko, N. Sridhar, and G. Tormoen, *Corros. Eng. Sci. Technol.*, **45**, 204–223 (2010).

55. A. Anderko, F. Gui, L. Cao, N. Sridhar, and G. R. Engelhardt, *Corrosion*, **71**, 1197–1212 (2015).

56. L. Cao, A. Anderko, F. Gui, and N. Sridhar, *Corrosion*, 636–654 (2016).

57. S. Tsujikawa and Y. Hisamatsu, *Boshoku Gijutsu - Corros. Eng.*, **29**, 37–40 (1980).

58. K. J. Evans et al., *JOM*, **57**, 56–61 (2005).

59. J. H. Macha and J. R. Scully, *Corrosion*, **65**, 472–490 (2009).

60. M. R. Ortíz, M. A. Rodríguez, R. M. Carranza, and R. B. Rebak, *Corrosion*, **66**, 105002-105002–12 (2010).

61. J. Jun, G. S. Frankel, and N. Sridhar, *J. Solid State Electrochem.*, **19**, 3439–3447 (2015).

62. J. R. Galvele, *Corros. Sci.*, **21**, 551–579 (1981).

63. S. M. Gravano and J. R. Galvele, *Corros. Sci.*, **24**, 517–534 (1984).

64. C. F. Baes Jr. and R. E. Mesmer, *The Hydrolysis of Cations*, John Wiley & Sons, Inc., New York, NY, (1976).

65. A. Anderko, P. Wang, and R. D. Springer, *Modeling Chemical Environments Within Corroding Crevices in Alloy 22 - Final Technical Report*, OLI Systems Inc., Morris Plains, NJ, (2008).

66. W. P. Yang, D. Costa, and P. Marcus, *J. Electrochem. Soc.*, **141**, 2669–2676 (1994).

67. V. Maurice, W. P. Yang, and P. Marcus, *J. Electrochem. Soc.*, **145**, 909–920 (1998).

68. B. MacDougall and M. J. Graham, in *Corrosion Mechanisms in Theory and Practice*, P. Marcus, Editor, p. 209, Marcel Dekker, Inc., New York, NY (2002).

69. C. R. Clayton and I. Olefjord, in *Corrosion Mechanisms in Theory and Practice*, P. Marcus, Editor, p. 217–219, Marcel Dekker, Inc., New York, NY (2002).

70. K. Ogle and S. Weber, *J. Electrochem. Soc.*, **147**, 1770–1780 (2000).

71. R. C. Newman, *Corros. Sci.*, **25**, 341–350 (1985).

72. N. Kobosew and N. I. Nekrassow, *Z. Für Elektrochem. Angew. Phys. Chem.*, **36**, 529–544 (1930).

73. J. O. Bockris and H. Mauser, *Can. J. Chem.*, **37**, 475–488 (1959).

74. S. Tsujikawa and Y. Hisamatsu, in *Improvement of Corrosion Resistance of Structural Materials in Aggressive Media*, J. M. Kolotyrkin, Editor, Nauka Publishers, Moscow, Russia (1984).

75. S. Tsujikawa and S. Okayama, *Corros. Sci.*, **31**, 441–446 (1990).

76. N. S. Zadorozne, C. M. Giordano, M. A. Rodríguez, R. M. Carranza, and R. B. Rebak, *Electrochimica Acta*, **76**, 94–101 (2012).

77. D. S. Dunn, G. A. Cragnolino, and N. Sridhar, *Corrosion*, **56**, 90–104 (2000).

78. *ASTM G192-08 Standard Test Method for Determining the Crevice Repassivation Potential of Corrosion-Resistant Alloys Using a Potentiodynamic-Galvanostatic-Potentiostatic Technique*, ASTM International, West Conshohocken, PA, (2008).

79. J. O. Bockris, D. Drazic, and A. R. Despic, *Electrochimica Acta*, **4**, 325–361 (1961).

80. E. J. Kelly, *J. Electrochem. Soc.*, **112**, 124–131 (1965).

81. S. Trasatti, *J. Electroanal. Chem. Interfacial Electrochem.*, **39**, 163–184 (1972).

Chapter 5

5.1. Overview

This chapter, in concluding the dissertation, extends the key inference obtained at the end of Chapter 4 – the mechanistic interpretation of conditions for stability based on the critical pH to precipitate a passive oxide – by examining its utility in defining a scientifically defendable basis for repassivation. First, a summary of the major conclusions of this work is presented followed by an assessment of their contribution to the current understanding of pit stability and repassivation. Secondly, the impact of the framework on the application of critical factors towards localized corrosion measurement in engineering circumstances is also explored. Finally, the limitations of the framework that emerge from the assumptions employed are considered at some length, suggesting prospective avenues for further research.

A manuscript entitled *Overview of a Recent Quantitative Framework Utilizing the Galvele Stability Product to Examine the Critical Electrochemical Factors for Localized Corrosion* authored by **J. Srinivasan** and R. G. Kelly, based on parts of this chapter has been submitted to Corrosion as an Invited Review for a Special Issue in memoriam of Prof. José R. Galvele to be published in March 2017.

5.2. Summary and Conclusions

1. An artificial pit technique to obtain measurable estimates relevant to both pit stability and repassivation was developed. Results from a high-throughput version of this technique indicated that sufficiently deep pits had to be accessed in order to obtain pit stability data that corresponds to truly 1-D mass transport. Both modeling and experiments were utilized to systematically investigate the effect of geometry on the dimensionality of flux from a 1-D pit. This combined approach demonstrated that the minimum depth to be attained for 1-D flux was nearly eight times the pit diameter. This minimum characteristic depth was also shown to have implications on the pit stability data representative of the cation concentration gradient that exists in the pit, isolated from effects of chloride from the bulk electrolyte. Finally, results from this study indicated that the relative independence of the measured E_{rp} with pit depth occurred once this characteristic value was attained, thus providing a quantitative connection between diffusive transport and repassivation.

2. Cathodic polarization of artificial pit electrodes following pit growth enabled the recording of the time taken to scan from the potential at which the salt film disappeared to the potential at which repassivation was recorded. These potentials were representative of the surface conditions under a salt film and at repassivation, respectively, and varied with pit depth. Mass transport modeling based on the one-dimensional pit provided information on the time required for the corroding surface to dilute to different concentrations from saturation, also as a function of pit depth. A comparison of these two time variables enabled the extraction of the pit depth at which the surface concentration

estimated from the experimental measurement of repassivation was equal to that obtained by dilution from saturation. When combined with the minimum pit depth beyond which E_{rp} remained independent, these calculations provided an estimate of the surface concentration as the pit was about to repassivate. This critical surface concentration was conservatively estimated to be 50%, providing a quantitative framework to extract a single value for the solution chemistry describing the transition from active dissolution to repassivation. This value of the surface concentration was also observed to bound pit stability criteria for a range of bulk chloride concentrations encountered in atmospheric conditions.

3. Calculations of the time to dilution to various surface concentrations from saturation for a one-dimensional pit were utilized to design anodic kinetics experiments. These tests investigated the electrochemical kinetics of the corroding surface at different degrees of saturation. A distinct transition from active dissolution to passivating behavior was observed when the surface condition was at 55% of saturation, indicating the onset of repassivation. In this manner, an estimate for the critical surface concentration was obtained. This value agreed well with the conservative bound obtained from the previous treatment described. The extent of cation hydrolysis and its relationship with pH were employed as a means to simulate the influence of the local cathodic reaction at the corroding surface. The resulting pH was compared to the minimum pH required to nucleate an oxide precipitate at the critical surface concentration obtained from anodic kinetics. This analysis provided an estimate of the critical fraction of the anodic current that was required to be satisfied by the local cathodic reaction in order to induce

repassivation by oxide nucleation. The pH value corresponding to this fraction at the critical surface concentration from anodic kinetics was determined to be the critical pH. This value was then used to evaluate the self-consistency of the quantitative framework that related pit stability and repassivation. Tafel extrapolation of the anodic kinetics at the critical surface concentration in combination with established kinetics of the hydrogen evolution reaction was utilized in a mixed potential analysis of the repassivation process. This approach validated the experimental selection of parameters in the quantitative framework, verifying its self-consistency, and provided a mechanistic basis for the transition from pit stability to repassivation.

5.3. Impact of the framework on present understanding of the critical factors

The repassivation condition defined by this framework is a mechanistic criterion based on the critical pH for oxide nucleation at the critical surface concentration. Galvele considered the minimum potential for pitting to occur to be dependent upon the corrosion potential, the overpotential and ohmic drop in the pit to maintain the critical value of ($i \cdot x$), and any ennoblement due to inhibitor action. Expressed equivalently for a repassivation potential, the relationship among these terms is:

$$E_{rp} = E_{corr} + \eta + \Delta\phi + E_{inh} \ldots\ldots. (5.1)$$

The individual terms E_{corr}, η, $\Delta\phi$, and E_{inh} denote the corrosion potential (open circuit potential) in the critical pit solution, overpotential for repassivation, ohmic drop in the pit, and the effect of inhibitors on raising the E_{rp}, respectively. Based on the arguments presented in this study, two major points of critique can be leveled at other studies in past literature that have considered repassivation in the context of the terms of the Galvele acidification model.[1–8] Firstly, the choice of the critical pit solution chemistry in which to determine E_{corr} and η measurement has considered only anodic dissolution (either by using simulated crevice/pit solutions prepared from the cationic chlorides or by pH control of metal dissolved at high potentials), typically at or close to 100% saturation.[4,7,9–14] Secondly, the value of η has been defined based on an arbitrary critical pit stability product[6,7,14] – therefore, for each pit depth considered, the current density would consequently change so as to satisfy the chosen value of $(i \cdot x)_{\text{crit}}$. The associated value of the repassivation potential would therefore change with pit depth. Galvele's original argument that the corrosion potential would serve as a logical lower bound would not be tenable because the net current density at that potential would *ipso facto* vanish, resulting in an ($i \cdot x$) value of zero. The framework described in this dissertation resolves these issues by expressing conditions for

stability in terms of a single critical pit solution chemistry at repassivation. An unambiguous measure of the critical surface concentration of cations at which to determine E_{corr} was obtained from the artificial pit studies. Secondly, the overpotential was evaluated based on the critical pH emerging from the tendency of oxide precipitation owing to the increasing influence of the local cathodic reaction at repassivation. The conditions for stability having been defined in this manner permitted the direct evaluation of the overpotential for repassivation once the Tafel slopes were obtained. The overpotential was ascertained by the ratio $i_{c,local}/i_a$ necessary to produce a local pH at which a protective oxide would precipitate. The current density at repassivation (i_{rp}) was then consequently calculatedas $i_{rp} = i_a - i_{c,local}$. The framework therefore removed the necessity to define an arbitrary repassivation current density by basing i_{rp} on mechanistic criteria.

The ohmic drop has not been considered to have a substantial effect on the E_{rp} in this framework because of the low current density at repassivation. A representative calculation justifies this assumption: for a 1 mm deep 1–D pit, allowing for a current density range at repassivation from 100 μA/cm^2 to 1 mA/cm^2 in a pit solution with an average resistivity of 6.9 Ω.cm,[‡] the average ohmic drop is calculated to be between 0.1 mV and 0.7 mV. Following the preceding arguments, the critical acidification model can therefore be reformulated as:

$$E_{rp} = E_{corr,f_{crit}} + \eta_{pHcrit} \ldots\ldots. (5.2)$$

$E_{corr,fcrit}$ denotes the corrosion potential in the critical pit solution chemistry ($C_{s,crit} = f_{crit} \cdot C_{sat}$). The term η_{pHcrit} denotes the overpotential determined from the critical ratio of the local cathodic reaction to the anodic reaction ($i_{c,local}/i_a$) required to attain the critical pH (pH_{crit}) in the critical

[‡] The OLI Analyzer Studio 9.3 software (OLI Systems, Inc., Cedar Knolls, NJ) was used to calculate the average resistivity, with its true value in solution approximated by the arithmetic mean of two simulated solutions: the mixture of cationic chlorides at 55% saturation and the bulk solution 0.6 M NaCl. The mixed chloride solution was simulated to consist of $FeCl_2$, $CrCl_3$, $NiCl_2$, and $MoCl_3$ in the same stoichiometric proportion as the metals appear in the alloy 316L.

solution chemistry $C_{s,crit}$. With this reformulation, both the Galvele local acidification model and the stability criterion as applied towards repassivation can be examined quantitatively, as shown in the next section.

5.4. The pit stability product and the choice of current density at repassivation

As discussed previously, this work provided a quantitative mechanistic basis for determining the current density at repassivation (i_{rp}). This choice of i_{rp} is related mechanistically to the critical pH for oxide nucleation at the critical surface concentration; therefore, it describes the actual surface conditions that cause repassivation. A quantitative defense for the assignment of i_{rp} on this basis in preference to the arbitrary selection utilized in prior studies is presented in this section, to support the qualitative argument provided previously. Figure 5.1 (a) depicts Evans lines for the anodic and cathodic reactions of interest within the pit, which utilize values for b_a, b_c and $E_{corr,\ fcrit}$ determined as described in Chapter 4. The ratio $i_{c,local}/i_a$ resulting from an i_{rp} choice close to 100% saturation[4,15] (= $i_{lim} \approx 100$ mA/cm^2) would be approximately 1×10^{-6} %, which would produce a very low pH according to Figure 1 (b), which as argued in Chapter 4, is not sufficient to precipitate an oxide. Similarly, assuming 150 μA/cm^2 for i_{rp}[6–8,16] would result in an $i_{c,local}/i_a$ ratio of 20% and a pH of 7.5. This value would be too alkaline to represent a critical condition because repassivation would be expected to have already set in due to oxide nucleation at much lower pH values (starting at 2.65, as shown in Chapter 4). The framework developed in this study provides an alternative by basing the i_{rp} upon oxide nucleation in a single critical pit chemistry.

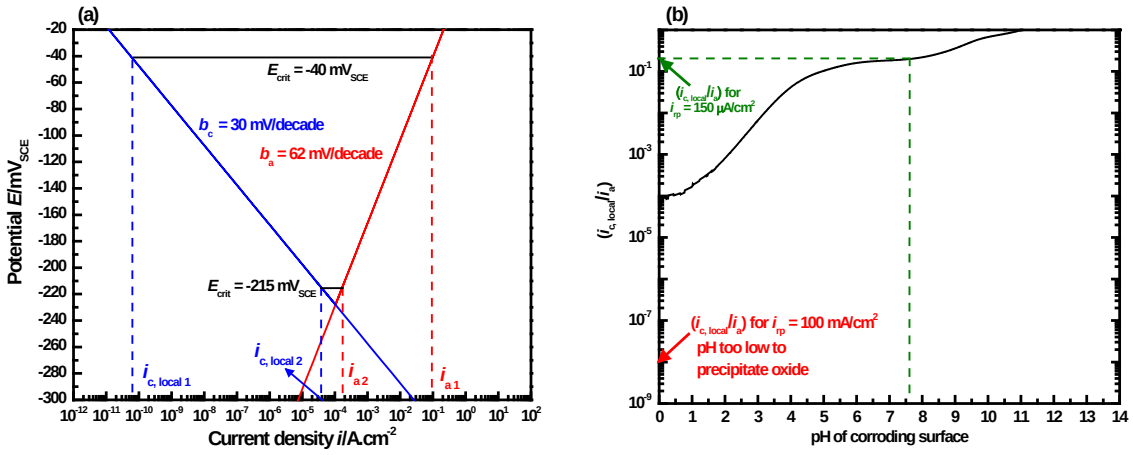

Figure 5.1. A Mixed Potential Theory-based analysis that considers the ramifications of the choice of an arbitrary current density at repassivation i_{rp}, for 316L. (a) The choice of i_{rp} fixes the ratio $i_{c,local}/i_a$ and the associated E_{crit}. This results in the estimation of very high values for E_{rp} (denoted as E_{crit} to underscore its property as a *critical potential*) if i_{rp} is considered near 100% saturation. (b) A high value for i_{rp} results in pH values too low to precipitate oxides. Conversely, adopting too low an i_{rp} is also problematic – although the estimated E_{crit} (from (a)) is close to the measured mean E_{rp} from the framework, the pH to which this potential corresponds is an overestimate of the alkalinity at repassivation; oxide nucleation would have already started and repassivation set in at much lower pH values.

The problem of a non-conservative critical potential that would result from a constantly decreasing i_{rp} with increasing pit depth were the Galvele pit stability product used as the sole criterion was introduced in the previous section. The framework presented in this dissertation circumvents this issue by decoupling repassivation from the geometric aspect of the pit stability product. Quantitatively considered, Figure 5.2 contrasts the critical potential obtained based solely on the critical pit stability product with the conservative, geometry-independent E_{rp}

determined using the critical pH criterion. There is no expectation for the former to assume a lower bounding value as it is not mechanistically related to repassivation. This higher measure of E_{rp} based solely on the $(i \cdot x)_{crit}$ value may be useful for some engineering cases in which the localized corrosion geometry allows for rapid diffusion out of pits. The associated current density and the dissolution rate were this E_{rp} value chosen as the critical potential, can still be calculated. However, in cases where the localized corrosion geometry is restricted or difficult to determine (due to the tortuosity of the transport path, for instance), a mechanistically-based E_{rp} which is also conservative serves as a more useful E_{rp}, particularly with respect to predictive modeling. When considered as a lower bound, an E_{rp} value of this nature therefore assures repassivation regardless of system geometry. The framework developed in this work therefore provides this important insight: Although diffusion path that restricts mass transport would facilitate the maintenance of the minimum critical chemistry for pit stability, geometry by itself not a fundamental critical factor in describing localized corrosion.

As mentioned, this result has particular utility in damage size estimation models which consider the growth of pits based on the supporting cathodic current available.[17–19] Typically, these studies have assumed that the the dissolving pit is hemispherical, with the associated hemispherical pit stability product related to the 1–D parameter as: $(I/r)_{crit} = 3 \cdot (i \cdot x)_{crit}$.[19] The deconvolution of critical factors from geometry therefore permits the anticipation of pit evolution in non-hemispherical shapes, as has been observed in some atmospheric pitting studies.[20–22] In other words, if there is not sufficient cathodic current to support hemispherical pit growth, localized corrosion could still propagate by adopting a non-hemispherical geometry with the only requirement that the minimum critical chemistry be maintained at the corroding surface. The lower bound on the anodic stability criterion in such circumstances would be the

1–D parameter $(i \cdot x)_{crit}$. Therefore, clarifying the minimum critical chemistry and the repassivation potential as fundamental critical factors independent of pit geometry thus not only justifies using 1–D artificial pits as an appropriate experimental technique to study general pitting characteristics but also warrants the use of the mechanistic, conservative value of E_{rp} in order to model such possible non-hemispherical outcomes. Finally, this analysis also implies that critical potential and critical dissolution flux alone do not completely describe conditions for pit stability, but that these factors vitally depend on the knowledge of a mechanistically defined critical pH.

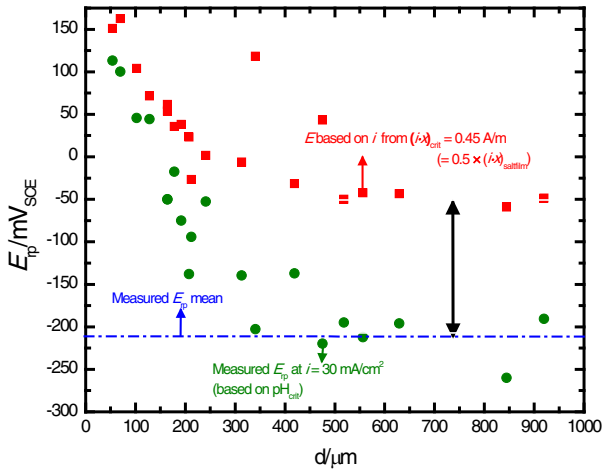

Figure 5.2. E_{rp} defined based on solely the Galvele pit stability product results in a non-mechanistic, non-conservative value which is nobler than the E_{rp} defined in this framework in terms of the critical pH for oxide nucleation. Data shown represent 316L pits of 50 μm diameter in 0.6 M bulk NaCl. Basing the repassivation criterion solely on $(i{\cdot}x)_{crit}$ results in a decreasing value of current density as pit depth increases, and consequently a progressively lower, non-conservative E_{rp} (which populates the shaded region shown). On the other hand, the E_{rp} value defined based on the critical pH provides an estimate that is both geometry-independent and conservative.

Limitations and Future Work

The present framework has been built upon experiments performed on 316L stainless steel in chloride solution, but it is reasonable to extend the general paradigm presented to other systems that undergo pitting or crevice corrosion as the primary mode of localized corrosion. However, the limitations involved in the development of the framework must be noted for its prudent use for other systems. Awareness of these limitations also provides opportunities for future refinement of the framework.

Although efforts have been attempted to characterize critical factors similarly for intergranular corrosion observed in non-heat-treatable Al-Mg alloys, challenges persist in these cases owing to the microstructural heterogeneity of corrosion front.[23] Also, Al^{+3} ions tend to form polynuclear hydrolysis products,[24,25] complicating the calculation of pH based on cation hydrolysis as was applied in stainless steels in this work.

One important assumption employed throughout this work was that mass transport was primarily diffusion-based for the system under study. The predominance of highly conductive electrolytic environments in localized corrosion justifies this assumption;[26–28] however, the ion migration may play a large role in transport in highly dilute solutions or at high temperatures.[29] Furthermore, if the current densities at repassivation following an analysis similar to that presented in this framework are calculated to be high, the resulting ohmic drop would also be considerable. Future model refinements could also incorporate the effects of porosity to account for amorphous and voluminous corrosion products which would act as additional diffusion barriers.[30]

In Chapter 3, the relevance of experimental selection of scan rate with respect to its effects on the time to dilution of the corroding surface was elaborated quantitatively, which has also been attested to in other studies.[5,16,31,32] Scan rate may also affect the nature of the dissolution products in the pit, which sometimes result in unexpectedly noble E_{rp} values, as has been observed for 17-4 PH stainless steel.[33] It has been suggested that these higher E_{rp} values may result from the participation of copper which may redeposit from solution or be involved in redox reactions, obfuscating the measurement of the local HER.[34–39] In fact, the presence of electroactive copper may accelerate repassivation as some of these studies have suggested.[36,38,40]

The simulation of oxide nucleation in the critical pit solution in Chapter 4 was simulated using thermodynamic data for the speciation of bulk oxides. A better approximation for the repassivation process in this context would be provided by surface oxide data. While studies abound on passive oxides grown on stainless steel surfaces in bulk solutions,[41–45] the literature on oxide growth in critical pit chemistry – which would provide experimental support to models such those discussed in this work – is sparse. Improved data on molybdenum speciation in the critical chemistry would refine the evaluation of the critical pH for oxide nucleation on 316L as well parse the inhibitory action of Mo in terms of its oxidation states.[12,46–50]

Several topics were mentioned in the introductory chapter of this dissertation as being outside the scope of this investigation. These areas are also certainly potential avenues of future research. Of particular importance would be the study of the effects of temperature simultaneously on the critical factors for pit stability and repassivation, which would find utility in addressing a wider range of applications, specifically in the nuclear industry.[51,52]

Finally, the critical pH criterion could be leveraged to develop a design paradigm for inhibitor efficacy, which would bring the complete representation of the Galvele pit acidification model within the ambit of the framework. The experimental methodology utilized in this work could be extended to study the effects of inhibitory oxyanions [53–55] on the critical factors, particularly in the context of a mixed potential theory-based analysis similar to the one developed in Chapter 4. The analysis providing the mechanistic rationale for the framework employed an experimental estimate of the anodic Tafel slope and cathodic slopes based on well-known HER pathways. As has been mentioned previously, high-resolution data collection at the low currents encountered near repassivation would permit improved experimental estimates of both values. The specific effects of alloying constituents and inhibitors on the anodic kinetics and/or the cathodic kinetics can then be assessed with data from a range of alloy-electrolyte systems. Such evaluation of the response of the local cathodic reaction to inhibitor chemistry and concentration would enable devising localized corrosion inhibition strategies from a quantitative mechanistic perspective. In a similar vein, localized corrosion mitigation strategies can also be designed based on enhancing the local cathodic reaction to attain the critical pH for repassivation, an idea which has found support in the literature.[56]

5.5. References

1. J. R. Galvele, *Journal of The Electrochemical Society*, **123**, 464–474 (1976).

2. J. R. Galvele, *Corrosion Science*, **21**, 551–579 (1981).

3. S. M. Gravano and J. R. Galvele, *Corrosion Science*, **24**, 517–534 (1984).

4. T. Hakkarainen, in *Corrosion Chemistry within Pits, Crevices and Cracks,* A. Turnbull, Editor, p. 17–26, Her Majesty's Stationery Office, London, United Kingdom (1987).

5. N. Sridhar and G. A. Cragnolino, *Corrosion*, **49**, 885–894 (1993).

6. J. R. Galvele, *Corrosion Science*, **47**, 3053–3067 (2005).

7. F. Bocher and J. R. Scully, *Corrosion*, **71**, 1049–1063 (2015).

8. E. Hornus, M. Rodríguez, R. Carranza, and R. Rebak, *CORROSION* (2016) http://www.corrosionjournal.org/doi/abs/10.5006/2179.

9. J. A. Smith, M. H. Peterson, and B. F. Brown, *Corrosion*, **26**, 539–542 (1970).

10. S. Brennert and G. Eklund, *Scandinavian Journal of Metallurgy*, **2**, 269–272 (1973).

11. A. Stenta et al., *CORROSION*, **72**, 1328–1341 (2016).

12. R. S. Lillard, M. P. Jurinski, and J. R. Scully, *Corrosion*, **50**, 251–265 (1994).

13. F. Bocher, R. Huang, and J. R. Scully, *Corrosion*, **66**, 55002-55002–15 (2010).

14. M. Kappes, M. Rincon Ortiz, M. Iannuzzi, and R. Carranza, *CORROSION* (2016) http://www.corrosionjournal.org/doi/abs/10.5006/2142.

15. N. J. Laycock and R. C. Newman, *Corrosion Science*, **39**, 1771–1790 (1997).

16. A. Anderko, N. Sridhar, and D. S. Dunn, *Corrosion Science*, **46**, 1583–1612 (2004).

17. Z. Y. Chen, F. Cui, and R. G. Kelly, *Journal of The Electrochemical Society*, **155**, C360–C368 (2008).

18. Z. Y. Chen and R. G. Kelly, *Journal of The Electrochemical Society*, **157**, C69–C78 (2010).

19. M. T. Woldemedhin, M. E. Shedd, and R. G. Kelly, *Journal of the Electrochemical Society*, **161**, E3216–E3224 (2014).

20. N. Mi, M. Ghahari, T. Rayment, and A. J. Davenport, *Corrosion Science*, **53**, 3114–3121 (2011).

21. D. Krouse, N. Laycock, and C. Padovani, *Corrosion Engineering, Science and Technology*, **49**, 521–528 (2014).

22. S. R. Street et al., *Faraday Discuss.*, **180**, 251–265 (2015).

23. M. L. C. Lim, thesis, University of Virginia, Charlottesville, VA (2016).

24. C. F. Baes Jr. and R. E. Mesmer, *The Hydrolysis of Cations*, John Wiley & Sons, Inc., New York, NY, (1976).

25. K. R. Cooper, thesis, University of Virginia, Charlottesville, VA (2001).

26. H. S. Isaacs, *J. Electrochem. Soc.*, **120**, 1456–1462 (1973).

27. J. C. Walton, G. Cragnolino, and S. K. Kalandros, *Corrosion Science*, **38**, 1–18 (1996).

28. M. T. Woldemedhin, J. Srinivasan, and R. G. Kelly, *Journal of Solid State Electrochemistry*, **19**, 3449–3461 (2015).

29. R. L. Cowan and A. I. Kaznoff, *CORROSION*, **29**, 123–132 (1973).

30. H. Ha, C. Taxen, K. Williams, and J. Scully, *Electrochimica Acta*, **56**, 6165–6183 (2011).

31. D. S. Dunn, N. Sridhar, and G. A. Cragnolino, *Corrosion*, **52**, 115–124 (1996).

32. B. A. Kehler, G. O. Ilevbare, and J. R. Scully, *Corrosion*, **57**, 1042–1065 (2001).

33. J. Srinivasan, M. J. McGrath, and R. G. Kelly, *ECS Transactions*, **58**, 1–11 (2014).

34. R. C. Newman and H. S. Isaacs, *Passivity of Metals and Semiconductors* M. Froment, Editor, Elsevier B.V, Bombannes, France, (1983).

35. W. R. Heineman and P. T. Kissinger, *Laboratory Techniques in Electroanalytical Chemistry* P. T. Kissinger and W. R. Heineman, Editors, Marcel Dekker, Inc., New York, NY, (1984).

36. T. Ujiro, S. Satoh, R. W. Staehle, and W. H. Smyrl, *Corrosion Science*, **43**, 2185–2200 (2001).

37. T. Sourisseau, E. Chauveau, and B. Baroux, *Corrosion Science*, **47**, 1097–1117 (2005).

38. A. Pardo, M. C. Merino, M. Carboneras, A. E. Coy, and R. Arrabal, *Corrosion Science*, **49**, 510–525 (2007).

39. K. Ogle and S. Weber, *J. Electrochem. Soc.*, **147**, 1770–1780 (2000).

40. K. Ogle, J. Baeyens, J. Swiatowska, and P. Volovitch, *Electrochimica Acta*, **54**, 5163–5170 (2009).

41. W. P. Yang, D. Costa, and P. Marcus, *J. Electrochem. Soc.*, **141**, 2669–2676 (1994).

42. A. Sadough Vanini, J.-P. Audouard, and P. Marcus, *Corrosion Science*, **36**, 1825–1834 (1994).

43. V. Maurice, W. P. Yang, and P. Marcus, *J. Electrochem. Soc.*, **145**, 909–920 (1998).

44. C. R. Clayton and I. Olefjord, in *Corrosion Mechanisms in Theory and Practice*, P. Marcus, Editor, p. 217–219, Marcel Dekker, Inc., New York, NY (2002).

45. B. MacDougall and M. J. Graham, in *Corrosion Mechanisms in Theory and Practice*, P. Marcus, Editor, p. 209, Marcel Dekker, Inc., New York, NY (2002).

46. J. N. Wanklyn, *Corrosion Science*, **21**, 211–225 (1981).

47. M. A. Cavanaugh, J. A. Kargol, J. Nickerson, and N. F. Fiore, *CORROSION*, **39**, 144–150 (1983).

48. R. C. Newman, *Corrosion Science*, **25**, 331–339 (1985).

49. R. C. Newman, *Corrosion Science*, **25**, 341–350 (1985).

50. P. Jakupi, F. Wang, J. J. Noël, and D. W. Shoesmith, *Corrosion Science*, **53**, 1670–1679 (2011).

51. D. H. Lister, R. D. Davidson, and E. McAlpine, *Corrosion Science*, **27**, 113–140 (1987).

52. J. Robertson, *Corrosion Science*, **32**, 443–465 (1991).

53. J. Horvath and H. H. Uhlig, *Journal of The Electrochemical Society*, **115**, 791 (1968).

54. H. P. Leckie and H. H. Uhlig, *Journal of The Electrochemical Society*, **113**, 1262–1267 (1966).

55. A. Turnbull, D. Coleman, A. J. Griffiths, P. E. Francis, and L. Orkney, *CORROSION*, **59**, 250–257 (2003).

56. A. Turnbull, *Corrosion Science*, **40**, 843–845 (1998).

Appendix

This section details the calculations on which some of the relationships referred to in the various chapters expand upon. The particular aspects discussed herein are:

1. **Pit stability phenomenology with bulk chloride concentration**: The observed linear dependence of the pit stability product on bulk chloride is introduced in Chapter 1. Chapter 2 discusses this relationship in the light of accessing sufficiently deep pits so that data properly representative of the cation concentration gradient *isolated from the effects of the bulk electrolyte* is collected. Chapter 3 utilizes these data to advance the case for a single critical surface concentration describing anodic stability across most conditions encountered in atmospheric corrosion.
2. **Mass transport model relating repassivation to diffusive transport**: The modeling aspect that supports the quantitative framework of this dissertation and forms a major portion of Chapters 3 and 4, is based upon an analytical solution to the one-dimensional diffusion equation. The mathematical formulation of this solution is laid out in this section and the different boundary conditions considered are discussed.
3. **Cation hydrolysis calculations to determine critical pH**: The development of the relationship between the influence of the local cathodic reaction and the pH at the corroding surface is predicated upon the extent of cation hydrolysis. The mathematical treatment of the calculations which the results discussed in Chapter 4 are based upon, form the focus of this section.

A.1. Diffusion-based rationale for effect of bulk electrolyte on pit stability

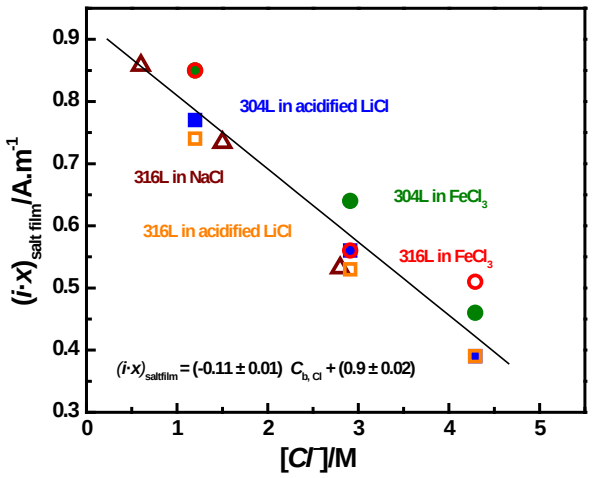

Figure A.1. Linear dependence of pit stability product on bulk [Cl^-]. Data replotted from Woldemedhin *et al.*[1]

Woldemedhin *et al.*[1] report the variation of $(i \cdot x)_{\text{saltfilm}}$ with bulk chloride concentration for 304L and 316L (Figure A.1). As shown in the figure, the pit stability product of both alloys decreased with increasing chloride concentration. The data were fit using linear regression (R^2 = 0.91) which resulted in the following relationship:

$$(i \cdot x)_{saltfilm} = -0.11[Cl^-] + 0.9$$

A diffusion transport-based rationale was proposed to explain this observed linear dependence. The following assumptions were made:

- The chloride ion Cl^- and the 'stainless steel cation' M^{n+} are the dominant ionic species in the pit.
- Ion migration effects are overwhelmed by diffusion.

Under these conditions, in order to preserve steady state diffusion, the following flux condition must be satisfied:

$$J_{Cl} = nJ_m$$

where J_{Cl} is the diffusion flux of chloride ions, J_{m} is the diffusion flux of 'stainless steel cation' (metal ion), and n is the valence of the 'stainless steel cation'.

Because both fluxes occur over the same diffusion length, Fick's 1st law can be rewritten as:

$$D_{Cl}\left(C_{s,Cl} - C_{b,Cl}\right) = nD_m\left(C_{sat,m} - C_\infty\right)$$

where $C_{\mathrm{s,Cl}}$ is the surface concentration of chloride, $C_{\mathrm{b,Cl}}$ is the bulk chloride concentration, $C_{sat,m}$ is the saturation concentration of metal chlorides, while D_{Cl} and D_{m} are diffusion coefficient of the chloride ion and the 'stainless steel cation, respectively.

The expression for the diffusion-limited current density for the metal ion with a minor rearrangement is:

$$\left(i \cdot x\right)_{saltfilm} = FnD_m\left(C_{sat,m} - C_\infty\right)$$

The term $nD_m(C_{sat,m} - C_\infty)$ can be inserted into the Fick's 1st law expression previously demonstrated to formulate the relationship:

$$\left(i \cdot x\right)_{saltfilm} = FD_{Cl}\left(C_{s,Cl} - C_{b,Cl}\right)$$

To satisfy electroneutrality within the pit, the concentrations of the metal cation and the chloride can be related as shown below:

$$C_{s,Cl} = nC_{sat,m}$$

Substituting for $C_{s,Cl}$ in the expression for the pit stability product with $nC_{sat,m}$ gives:

$$(i \cdot x)_{saltfilm} = FD_{Cl}\left(nC_{sat,m} - C_{b,Cl}\right)$$

The preceding equation can be expanded to:

$$(i \cdot x)_{saltfilm} = FD_{Cl}nC_{sat,m} - FD_{Cl}C_{b,Cl}$$

This provides an expression of the form that describes the linear relationship observed between the variables:

$$(i \cdot x)_{saltfilm} = A - BC_{b,Cl}$$

Therefore, the linear relationship of the pit stability product under a salt film with the bulk chloride concentration was rationalized as an alternative expression of the relationship between the diffusion fluxes of the metal cation and the chloride ion under steady-state conditions.

Stochiometric dissolution of the primary alloying components of 304L and 316L (Fe, Cr, Ni) was assumed yielding values of n = 2.2 and 2.245 which was then used to calculate the corresponding D. Based on equation 5 and 10, the value of D_{Cl} was calculated first from the slope value. Once D_{Cl} was determined, it was used to calculate $C_{sat,m}$ from the intercept. In all of the calculations, the diffusion coefficient was assumed to be independent of bulk chloride concentration. These calculations resulted in the following values for the diffusion coefficient of the 'stainless steel cation' and the concentration at saturation of the metal chlorides:

$$D_m = 9.2 \times 10^{-6}\ \text{cm}^2/\text{s}$$

$$C_{sat,m} = 3.72\ \text{M}$$

This value of D_m was seen to be comparable to values reported by Kuo and Landolt,[2] Gaudet *et al*., [3] and Ernst and Newman.[4] Isaacs et al.[5] reported the *in-situ* X-ray microprobe analysis of concentrations of Fe, Ni and Cr chlorides in the saturated solution produced by dissolution of 18-8 stainless steel. The saturation concentration, $C_{sat,m} = 3.72$ M, determined from this analysis is ≈ 74% of this reported value. In this manner, a simplified diffusion transport model was observed to explain the observed linear dependence of pit stability product on bulk chloride.

A.2. Analytical one-dimensional mass transport model

The mass transport model described in this dissertation resulted from the solution to the one-dimensional diffusion equation utilizing selected boundary conditions. Analytical solutions were obtained when the boundary conditions of zero flux and constant flux were employed at the corroding surface. When transient boundary conditions were considered, an FEM-based numerical solution had to be implemented as has been discussed in Chapter 3. The following equations describe the cases for which analytical solutions were obtained, *i. e.*, a) zero flux and b) constant flux at the corroding surface. The final solution in each case expresses the time taken for the corroding surface to dilute to a particular concentration from saturation. The geometry considered in both cases is shown in Figure A.2.

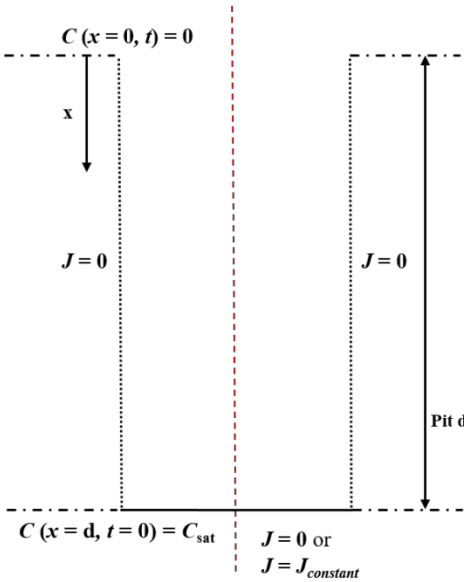

Figure A.2. Geometry of one-dimensional pit considered in the development of the mass transport model.

Case 1: Zero flux at the corroding surface (open-circuit dilution)

Boundary conditions:

$$C(0,t) = 0 \text{ (Bulk solution)}$$

$$\left(\frac{\partial C}{\partial x}\right)_{x=d} = 0 \text{ (No flux across pit base)}$$

Initial condition:

Linear concentration profile from presence of salt film prior to dilution implies:

$$C(x,0) = C_{sat}\frac{x}{d}$$

The general solution of the one-dimensional diffusion equation following separation of variables[6] yields the following expression:

$$C(x,t) = (C_1 \sin \lambda x + C_2 \cos \lambda x)\exp\left(-\lambda^2 Dt\right)$$

Applying the boundary conditions to Eq. 1:

1. $C(0,t) = 0$:

$$C(0,t) = (C_1 \cdot 0 + C_2)\exp\left(-\lambda^2 Dt\right)$$
$$\Rightarrow C_2 = 0$$

(because the exponential term is never zero or negative)

$$\Rightarrow C(x,t) = (C_1 \sin \lambda x)\exp\left(-\lambda^2 Dt\right)$$

2. $\left(\frac{\partial C}{\partial x}\right)_{x=d} = 0$:

$$C(x,t) = (C_1 \sin \lambda x) \exp\left(-\lambda^2 Dt\right)$$

$$\left(\frac{\partial C}{\partial x}\right) = (\lambda C_1 \cos \lambda x) \exp\left(-\lambda^2 Dt\right)$$

$$\left(\frac{\partial C}{\partial x}\right)_{x=d} = (\lambda C_1 \cos \lambda \cdot d) \exp\left(-\lambda^2 Dt\right) = 0$$

$$\Rightarrow \cos \lambda \cdot d = 0$$

$$\Rightarrow \lambda \cdot d = \frac{(2n+1)\pi}{2}$$

$$\Rightarrow \lambda = \frac{(2n+1)\pi}{2d}$$

$$\Rightarrow C(x,t) = (C_1 \sin \frac{(2n+1)\pi}{2d} x) \exp\left(-\frac{(2n+1)^2 \pi^2}{4d^2} Dt\right)$$

where *n* corresponds to integer values ≥ 0.

Applying the initial condition:

$$C(x,0) = C_{sat} \frac{x}{d}$$

$$C(x,t) = (C_1 \sin \frac{(2n+1)\pi}{2d} x) \exp\left(-\frac{(2n+1)^2 \pi^2}{4d^2} Dt\right)$$

$$C(x,0) = (C_1 \sin \frac{(2n+1)\pi}{2d} x) \exp\left(-\frac{(2n+1)^2 \pi^2}{4d^2} D \cdot 0\right) = (C_1 \sin \frac{(2n+1)\pi}{2d} x) = C_{sat} \frac{x}{d}$$

The orthogonality of sines can be applied to solve for C_1:

$$\int_0^d \sin\frac{(2n+1)\pi}{2d}x\cdot\sin\frac{(2p+1)\pi}{2d}xdx=\frac{d}{2}\delta_{np}$$

where n and p are integers ≥ 0 and δ_{np} is the Kronecker delta which is equal to 1 for n = p and zero elsewhere.

$$\Rightarrow C_1\int_0^d \sin\frac{(2n+1)\pi}{2d}x\cdot\sin\frac{(2p+1)\pi}{2d}xdx=C_1\frac{d}{2}\delta_{np}=C_{sat}\frac{x}{d}\int_0^d \sin\frac{(2p+1)\pi}{2d}x$$
$$\Rightarrow C_1\frac{d}{2}=\frac{C_{sat}}{d}\int_0^d x\sin\frac{(2p+1)\pi}{2d}xdx$$

$$\int x\sin axdx=\frac{\sin ax-ax\cos ax}{a^2}+c$$

$$\Rightarrow C_1\frac{d}{2}=\frac{C_{sat}}{d}\left|_0^d\frac{\left(\sin\frac{(2p+1)\pi}{2d}x\right)-\left(\frac{(2p+1)\pi}{2d}x\cos\frac{(2p+1)\pi}{2d}x\right)}{\frac{(2p+1)^2\pi^2}{4d^2}}\right.$$

Substituting for the limits of integration and solving for C_1:

$$\Rightarrow C_1\frac{d}{2}=\frac{C_{sat}}{d}\cdot\frac{4d^2}{(2p+1)^2\pi^2}\left((-1)^p-0-0+0\right)$$
$$\Rightarrow C_1=\frac{8C_{sat}}{(2p+1)^2\pi^2}(-1)^p$$

The general solution is a series expansion in terms of the eigenfunctions. The notation *p* for the integer values assumed by the terms in the series is replaced by the equivalent *n* to yield the expression:

$$C_{1n} = \frac{8C_{sat}}{\pi^2} \sum_{n=0}^{\infty} \frac{(-1)^n}{(2n+1)^2}$$

The solution to the diffusion equation for the system considered is therefore:

$$C(x,t) = \frac{8C_{sat}}{\pi^2} \sum_{n=0}^{\infty} \frac{(-1)^n}{(2n+1)^2} \sin\frac{(2n+1)\pi}{2d} x \exp\left(-\frac{(2n+1)^2\pi^2}{4d^2} Dt\right)$$

Solving for the concentration at the pit base by substituting *x* in the expression with the pit depth *d*:

$$C(d,t) = \frac{8C_{sat}}{\pi^2} \sum_{n=0}^{\infty} \frac{(-1)^n}{(2n+1)^2} \sin\frac{(2n+1)\pi}{2} \exp\left(-\frac{(2n+1)^2\pi^2}{4d^2} Dt\right)$$

$$\Rightarrow C(d,t) = \frac{8C_{sat}}{\pi^2} \sum_{n=0}^{\infty} \frac{(-1)^n}{(2n+1)^2} (-1)^n \exp\left(-\frac{(2n+1)^2\pi^2}{4d^2} Dt\right)$$

$$\Rightarrow C(d,t) = \frac{8C_{sat}}{\pi^2} \sum_{n=0}^{\infty} \frac{\exp\left(-\frac{(2n+1)^2\pi^2}{4d^2} Dt\right)}{(2n+1)^2}$$

The summation term converges rapidly to $\exp\left(\frac{-\pi^2 Dt}{4d^2}\right)$.

The expression for *C* (*d, t*) can be therefore approximated by:

$$C(d,t) = \frac{8C_{sat}}{\pi^2} \exp\left(\frac{-\pi^2 Dt}{4d^2}\right)$$

Expressing the concentration at the pit base as a fraction of saturation *f*:

$$f(d,t) = \frac{C(d,t)}{C_{sat}}$$
$$f(d,t) = \frac{8}{\pi^2}\exp\left(\frac{-\pi^2 Dt}{4d^2}\right)$$

The corresponding expression for the time required for the surface to dilute from saturation to a fraction *f*, t_f can be calculated by taking logarithms on both sides and solving for *t*:

$$t_f = \frac{4d^2}{\pi^2 D}\ln\frac{8}{\pi^2 f}$$

Case 2: Constant nonzero flux at the corroding surface

The diffusion equation solution for this case is set up with a modified concentration variable ρ which accounts for the fact that a constant flux exists at the corroding surface as it starts to dilute.

Under steady state conditions:

$$\frac{\partial C}{\partial t} = 0 \Rightarrow \frac{\partial^2 C}{\partial x^2} = 0$$

Given that $C(0) = 0$ (Bulk solution)

$$C_{steadystate}(x) = ax + b$$
$$C_{steadystate}(0) = 0 \Rightarrow C_{steadystate}(x) = ax$$
$$\Rightarrow \frac{\partial C}{\partial x} = a$$

The constant flux at the surface can be expressed in terms of the associated current density, which itself can be denoted as a fraction φ of the limiting current density that corresponds to the concentration at saturation, i_L. The constant a is related to this flux as follows:

$$J_{const} = \frac{i}{zF} = \frac{\varphi i_L}{zF}$$
$$a = \frac{\varphi i_L}{zFD}$$

The modified concentration variable ρ is defined as follows:

$$\rho(x,t) = C(x,t) - C_{steadystate}(x)$$

This definition results in the following modified boundary and initial conditions:

$$\rho(x,t) = C(x,t) - C_{steadystate}(x)$$
$$\Rightarrow \frac{\partial \rho}{\partial x}(d,t) = \frac{\partial C}{\partial x}(x,t) - \frac{\partial C_{steadystate}}{\partial x}(x) = 0 - 0 = 0$$
$$\therefore \left.\frac{\partial \rho}{\partial x}\right|_{x=d} = 0$$
$$\rho(0,t) = C(0,t) - C_{steadystate}(0) = 0 - 0 = 0$$
$$\rho(x,0) = \left(\frac{C_{sat}}{d} - \frac{\varphi i_L}{zFD}\right)x$$

The one-dimensional diffusion equation is now solved based on these modified conditions. Proceeding in a manner similar to that adopted for Case 1 (open-circuit dilution), separation of variables[6] results in the following expression:

$$\rho(x,t) = (\rho_1 \sin \lambda x + \rho_2 \cos \lambda x) \exp\left(-\lambda^2 Dt\right)$$

The application of the aforementioned modified boundary conditions and the initial condition, and solving via the orthogonality of sines as in Case 1 yields the solution to the diffusion equation as:

$$\rho(x,t)=\frac{8d}{\pi^2}\left(\frac{C_{sat}}{d}-\frac{\varphi i_L}{zFD}\right)\sum_{n=0}^{\infty}\frac{(-1)^n}{(2n+1)^2}\sin\frac{(2n+1)\pi}{2d}x\exp\left(-\frac{(2n+1)^2\pi^2}{4d^2}Dt\right)$$

Solving for ρ at the pit base by substituting x in the expression with the pit depth d:

$$\rho(d,t)=\frac{8d}{\pi^2}\left(\frac{C_{sat}}{d}-\frac{\varphi i_L}{zFD}\right)\sum_{n=0}^{\infty}\frac{\exp\left(-\frac{(2n+1)^2\pi^2}{4d^2}Dt\right)}{(2n+1)^2}$$

As in Case 1, the summation term converges rapidly to $\exp\left(\frac{-\pi^2 Dt}{4d^2}\right)$, resulting in the approximation:

$$\rho(d,t)=\frac{8d}{\pi^2}\left(\frac{C_{sat}}{d}-\frac{\varphi i_L}{zFD}\right)\exp\left(\frac{-\pi^2 Dt}{4d^2}\right)$$

The concentration at the pit base is now obtained by solving for C in the relationship between ρ and C denoted previously and rearranging:

$$C(d,t)=\left(\frac{8d}{\pi^2}\left(\frac{C_{sat}}{d}-\frac{\varphi i_L}{zFD}\right)\exp\left(\frac{-\pi^2 Dt}{4d^2}\right)\right)+\frac{\varphi i_L}{zFD}$$

From the diffusion-limited characteristics of dissolution under a salt film as introduced in Chapter 1:

$$i_L = \frac{zFDC_{sat}}{d}$$
$$\Rightarrow \frac{i_L d}{zFD} = C_{sat} \Rightarrow \frac{\varphi i_L}{zFD} = \varphi C_{sat}$$

The equation for $C(d, t)$ is therefore simplified:

$$C(d,t) = C_{sat}\left(\left(\frac{8}{\pi^2}\left(\frac{1-\varphi}{f-\varphi}\right)\exp\left(\frac{-\pi^2 Dt}{4d^2}\right)\right)+\varphi\right)$$

Expressing the concentration at the pit base as a fraction of saturation f:

$$f(d,t) = \left(\frac{8}{\pi^2}\left(\frac{1-\varphi}{f-\varphi}\right)\exp\left(\frac{-\pi^2 Dt}{4d^2}\right)\right)+\varphi$$

Following a procedure similar to Case 1, t_f for this case is calculated to be:

$$t_f = \frac{4d^2}{\pi^2 D}\ln\frac{8}{\pi^2}\left(\frac{1-\varphi}{f-\varphi}\right)$$

A.3. Cation hydrolysis equilibrium calculations

The procedure to estimate the critical pH for repassivation described in Chapter 4 was founded on the understanding that the local cathodic reaction provides a source of OH^-.[7–9] This availability of hydroxyl ions affects the pH of the corroding surface. Based on this rationale, the influence of the local cathodic reaction was monitored in terms of the extent of hydrolysis of the cations produced from dissolution. The following expressions detail the calculations that relate the extent of hydrolysis to pH.[10]

The mononuclear cation hydrolysis equilibrium is expressed as:

$$Me^{+z} + H_2O \leftrightarrow Me(OH)^{+(z-1)} + H^+$$

Assuming unity activity coefficients permits the expression of the hydrolysis equilibrium constant in terms of the concentrations of the species involved:

$$K_{11} = \frac{\left[Me(OH)^{+(z-1)}\right]\left[H^+\right]}{\left[Me^{+z}\right]}$$

where the brackets indicate concentrations of the respective species and K_{xy} refers to the hydrolysis equilibrium constant with the notation x indicating the number of nuclei that hydrolyze and y the ordinal number of the hydrolysis. The activity of water is assumed to be unity because of its large excess in the solution.

Subsequent hydrolysis products can be expressed similarly. The second hydrolysis equilibrium is shown below:

$$Me(OH)^{+(z-1)} + H_2O \leftrightarrow Me(OH)^{+(z-2)} + H^+$$

which can be also expressed in terms of the unhydrolyzed cation Me^{+z}:

$$Me^{+z} + 2H_2O \leftrightarrow Me(OH)_2^{+(z-2)} + 2H^+$$

The corresponding expression for the hydrolysis equilibrium constant is:

$$K_{12} = \frac{\left[Me(OH)_2^{+(z-2)}\right]\left[H^+\right]^2}{\left[Me^{+z}\right]}$$

These calculations can be repeated similarly for any subsequent hydrolysis products.

With these results, the concentration of each species can be calculated from the hydrolysis equilibria as follows:

$$\left[Me(OH)^{+(z-1)}\right] = \frac{K_{11}\left[Me^{+z}\right]}{\left[H^+\right]}$$

$$\left[Me(OH)^{+(z-2)}\right] = \frac{K_{12}\left[Me^{+z}\right]}{\left[H^+\right]^2}$$

The fraction of each cationic species hydrolysis product at equilibrium can then be estimated:

$$\sum species = \left[Me^{+z}\right] + \left[Me(OH)^{+(z-1)}\right] + \left[Me(OH)^{+(z-2)}\right]$$
$$\Rightarrow \sum species = \left[Me^{+z}\right] + \frac{K_{11}\left[Me^{+z}\right]}{\left[H^+\right]} + \frac{K_{12}\left[Me^{+z}\right]}{\left[H^+\right]^2}$$
$$\Rightarrow \sum species = \left[Me^{+z}\right]\left(1 + \frac{K_{11}}{\left[H^+\right]} + \frac{K_{12}}{\left[H^+\right]^2}\right)$$

$$f_{Me^{+z}} = \frac{\left[Me^{+z}\right]}{\sum species}$$

$$\Rightarrow f_{Me^{+z}} = \frac{\left[Me^{+z}\right]}{\left[Me^{+z}\right]\left(1+\frac{K_{11}}{\left[H^{+}\right]}+\frac{K_{12}}{\left[H^{+}\right]^{2}}\right)}$$

$$\Rightarrow f_{Me^{+z}} = \frac{\left[H^{+}\right]^{2}}{\left(\left[H^{+}\right]^{2}+K_{11}\left[H^{+}\right]+K_{12}\right)}$$

$$f_{Me(OH)^{+(z-1)}} = \frac{K_{11}\left[H^{+}\right]}{\left(\left[H^{+}\right]^{2}+K_{11}\left[H^{+}\right]+K_{12}\right)}$$

$$f_{Me(OH)_2^{+(z-1)}} = \frac{K_{12}}{\left(\left[H^{+}\right]^{2}+K_{11}\left[H^{+}\right]+K_{12}\right)}$$

Once these expressions are formulated, the fraction of each hydrolyzed species can be mapped out versus pH to obtain the extent of cation hydrolysis. Figure A.3 depicts this relationship for the hydrolysis of the Cr^{+3} ion.

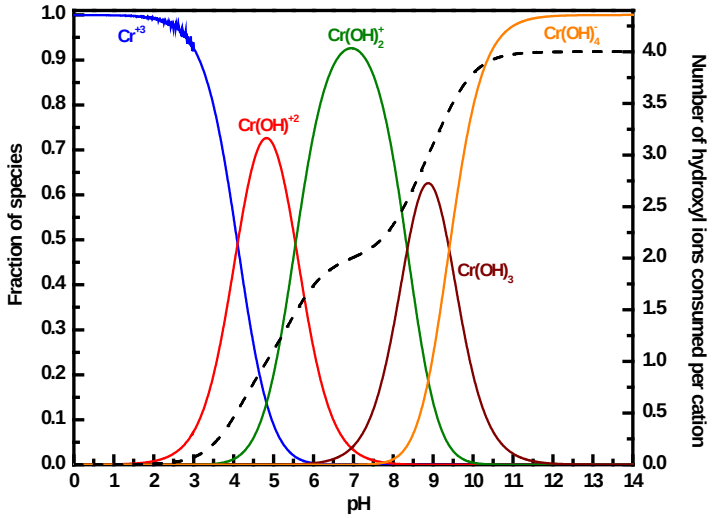

Figure A.3. Extent of cation hydrolysis as a function of pH for Cr^{+3}.

A.4. References

1. M. T. Woldemedhin, J. Srinivasan, and R. G. Kelly, *J. Solid State Electrochem.*, **19**, 3449–3461 (2015).

2. H. C. Kuo and D. Landolt, *Electrochimica Acta*, **20**, 393–399 (1975).

3. G. T. Gaudet et al., *AIChE J.*, **32**, 949–958 (1986).

4. P. Ernst and R. . Newman, *Corros. Sci.*, **44**, 927–941 (2002).

5. H. S. Isaacs, J.-H. Cho, M. L. Rivers, and S. R. Sutton, *J. Electrochem. Soc.*, **142**, 1111–1118 (1995).

6. J. Crank, *The Mathematics of Diffusion*, 2nd ed., Oxford University Press, Oxford, United Kingdom, (2004).

7. A. Turnbull, *Br. Corros. J.*, **32**, 283–290 (1997).

8. K. C. Stewart, thesis, University of Virginia, Charlottesville, VA (1999).

9. K. R. Cooper, thesis, University of Virginia, Charlottesville, VA (2001).

10. C. F. Baes Jr. and R. E. Mesmer, *The Hydrolysis of Cations*, John Wiley & Sons, Inc., New York, NY, (1976).